ISSN 2414-6056

DEW-DROP

A Scientific Journal of Meteorology and Geo-Physics

Bangladesh Meteorological Department

June 2018

Volume 5 ■ Number 1

ISSN 2414-6056

DEW-DROP

A Scientific Journal of Meteorology and Geo-Physics

Bangladesh Meteorological Department

June 2018

Volume 5 ■ Number 1

EDITORIAL BOARD

Published By
Bangladesh Meteorological Department
Agargaon, Dhaka-1207, Bangladesh
E-mail: info@bmd.gov.bd, swc@bmd.gov.bd

Simulation of Pre-Monsoon Thunderstorm over Mymensingh and its adjoining area of Bangladesh using WRF-ARW Model

Md. Joshem Uddin[1*], M. A. Samad[1], M. A. K. Mallik[2], S. M. Q. Hassan[2] and M. S. Alam[2]
[1]Department of Applied Mathematics, University of Dhaka
[2]Bangladesh Meteorological Department, Dhaka, Bangladesh

Abstract: In the present study, an attempt has been made to simulate a thunderstorm event which was occurred over Mymensingh (24.75°N, 90.40°E) on 06 May 2017 by using the WRF-ARW (Advance Research WRF) model version 3.9. The model is configured for this study by setting lat.23°N and long.90°E as central point of the domain with 250 grid point in east-west and north-south direction and Kessler Scheme as micro-physics option, Yonsei University Scheme as PBL Parameterizations, MM5 Similarity Scheme for surface layer, Unified Noah Land Surface Model as land surface model, Dudhia Shortwave Scheme and Rapid Radiative Transfer Model (RRTM) Longwave Scheme as atmospheric radiation option and Grell-Devenyi (GD) ensemble scheme as cumulus physics option. Then the model is compiled for a period of 48 hours using the 1° × 1°six hourly Global Final Analysis (FNL) data from 00 UTC of 05 May 2017 to 00 UTC of 07 May 2017 on a single domain of 10 km horizontal resolution and 38 vertical layers with 180 second history interval. Half hourly model output is visualized by Grid Analysis and Display System (GrADS). Various parameters which play important role for the formation and development of thunderstorm such as mean sea level pressure (MSLP), wind pattern at various pressure levels, surface temperature, relative humidity, amount of rainfall along with the atmospheric instability index such as CAPE, CIN and K-index is analyzed deeply and a comparison is made with the BMD observation. All of the outcomes for various parameters have been presented in graphical and tabular form.

1. Introduction

Bangladesh (10°34′ N, 26°33′E) is a land of natural calamities. Every year it faces a lot of natural disaster, particularly thunderstorm which is one of the most common disasters in Bangladesh. Most of the thunderstorms occur in March, April and May (pre-monsoon season) over Bangladesh and they are very frequent in Mymensingh and its adjoining area. From the analysis of 36 year observed thunderstorm data from 1980 to 2016 it is found that every year approximately 245 thunderstorms occur in Mymensingh and its adjoining area. During this season, the Nor'westers which are severe thunderstorms, originate in the eastern and northeastern India and Bangladesh, and mostly travel from northwest to southeast directions (Das *et. al.*, 2015). They are locally known as 'Kalbaishakhi' or the calamity of Baishakhi. Thunderstorm is associated with thunder and lightning, and accompanied by strong winds, heavy rain, and sometimes snow, sleet, hail, or, in contrast, no precipitation at all. The economic consequences and the loss of human lives due to thunderstorms is a growing concern. In recent year, Bangladesh has seen a record numbers of deaths due to lightning strike of thunderstorm during Pre-monsoon season. Thunderstorm adversely impacts agricultural production, natural environment as well as our economy. Due to this fact, study and experiment – both theoretical and practical – on the climatology of thunderstorm have become a major concern in scientific research since the last century.

Thunderstorm is a very complicated weather phenomenon. For understanding the thermodynamic features and forecasting the thunderstorm events, a huge amount of studies of thunderstorms have been made by various author. Karmakar *et al.,* (2001) analysis the spatial and temporal distribution the monthly and seasonal frequency of thunderstorm days together with the variability of thunderstorm days over Bangladesh during the pre-monsoon season using the data from1972 to 1993.According to this study, the mean thunderstorm days over Bangladesh increase significantly as the season progresses from March to May and are maximum in May. Karmakar *et al.* (2011) analyzed different modified stability indices with relation to the occurrence of Nor'wester over Bangladesh. The stability indices have been modified by considering the data at the 925 hPa pressure level. Das *et al.* (2014) conduct a coordinated field experiment on severe thunderstorm observations and regional modeling over the South Asian Region. Das *et al.* (2015) studied the characteristics of Nor'westers (severe thunderstorms) observed over northeast India and adjoining Bangladesh during the pre-monsoon season based on synoptic, Radar and TRMM observations and simulated using the WRF model. Ahasan *et al.* (2015) performed a simulation study of a thunderstorm event over Bangladesh using WRF-ARW model and concluded that the WRF-ARW model may be adopted in study of research and prediction of the thunderstorms during pre-monsoon season over Bangladesh, but it needs to do more case study. Although a huge number of studies are made on thunderstorms but it is still not possible to predict thunderstorm events over Bangladesh precisely. So we need more study on thunderstorm. In this present study, a thunderstorm

event over Mymensingh on 06 May 2017 is simulated by using Advance Research WRF (WRF-ARW) model and is also analyzed the thermodynamic features related to the development of thunderstorms over Bangladesh. The WRF-ARW model performance of capturing thunderstorms is also validated by comparing the model output with observations.

It is expected that this study will greatly impact to the forecasting of thunderstorm events in Bangladesh.

2. Event Description

For this study, a thunderstorm event has been taken for NWP study, which was occurred on 06 May 2017 over Mymensingh and adjoining area at 1530 UTC. It was a severe thunderstorm, with Northwesterly gusty wind. The wind speed at 10 meter height was 56 $Kmhr^{-1}$. 27 mm rainfall was recorded by BMD at Mymensingh on that day, and the recorded mean sea level pressure was 1006 hPa at 1500 UTC.

3. Data

The WRF-ARW model can be run by using the NCEP FNL (Final) Operational Global Analysis data or Global Forecast System (GFS) data. The NCEP FNL (Final) Operational Global Analysis data are on 1-degree by 1-degree grids prepared operationally every six hour [6]. This product is from the Global Data Assimilation System (GDAS), which continuously collects observational data from the Global Telecommunications System (GTS), and other sources, for many analyses. The FNLs are made with the same model which NCEP uses in the Global Forecast System (GFS), but the FNLs are prepared about an hour or so after the GFS is initialized. The FNLs are delayed so that more observational data can be used. Typically, FNL ingests about 10 % more observations than GFS [6]. The GFS is run earlier in support of time critical forecast needs, and uses the FNL from the previous 6 hour cycle as part of its initialization. So in the present study, the FNL Operational Global Analysis data from 05 May 2017 00 UTC to 07 May 2017 00 UTC produced by NCEP are used as the initial and lateral boundary condition. Also the observed data, recorded by Bangladesh Meteorological Department (BMD) is used to validate the model simulated results.

4. Governing Equation of WRF-ARW Model

The WRF-ARW model mainly integrates the compressible Nonhydrostatic Euler equation. The equation are formulated using a terrain following hydrostatic pressure vertical coordinate denoted and defined by

$$\eta = \frac{P_h - P_{ht}}{\mu} \quad \dots\dots\dots\dots\dots\dots\dots\dots\dots (1)$$

where, $\mu = P_{hs} - P_{ht}$ and $P_h$is the hydrostatic component of the pressure, and $P_{hs}$and P_{ht}refer to values along the surface and top boundaries, respectively. ηvaries from a value of 1 at the surface to 0 at the upper boundary of the model domain. This vertical coordinate is also called a mass vertical coordinate. Since $\mu(x, y)$ represents the mass per unit areawithin the column in the model domain at (x, y), the appropriate flux form variables are

$$V = \mu \boldsymbol{V} = (U, V, W), \qquad \Omega = \mu\eta, \quad \Theta = \mu\theta \dots\dots (2)$$

v = (u, v, w) are the covariant velocities in the two horizontal and vertical directions, respectively, while $w = \mu\dot{\eta}$is the contravariantvertical" velocity. $\theta$is the potential temperature. Also appearing in the governing equations of the ARW are the non-conserved variables $\varphi = gz$ (the geopotential), p (pressure), and $\alpha = \frac{1}{\rho}$ (the inverse density). Using the variables defined above, the flux form Euler equations can be written as

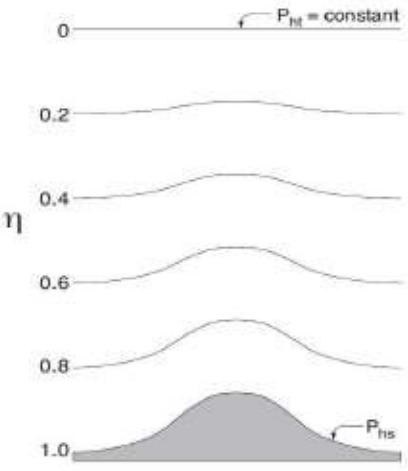

Fig. 1(i): WRF-ARW η Coordinate

$$\partial_t U + (\nabla . Vu) - \partial_x(P\phi_\eta) + \partial_\eta(P\phi_x) = F_u \dots\dots\dots\dots\dots\dots (3)$$
$$\partial_t V + (\nabla . V_v) - \partial_y(P\phi_\eta) + \partial_\eta(P\phi_\eta) = F_v \dots\dots\dots\dots\dots\dots (4)$$
$$\partial_t W + (\nabla . Vw) - g(\partial_\eta P - \mu) = F_w \dots\dots\dots\dots\dots\dots (5)$$
$$\partial_t \Theta + (\nabla . V\theta) = F_\theta \dots\dots\dots\dots\dots\dots (6)$$
$$\partial_t \mu + (\nabla . V) = 0 \dots\dots\dots\dots\dots\dots (7)$$
$$\partial_t \phi + \mu^{-1}[(V . \nabla\phi) - gW] = 0 \dots\dots\dots\dots\dots\dots (8)$$

along with the diagnostic relation for the inverse density

$$\partial_\eta \phi = -\alpha\mu \ldots\ldots\ldots\ldots\ldots\ldots\ldots\ldots (9)$$

and the equation of state in terms of Potential temperature,

$$P = P_0 \left(\frac{R_d \theta}{P_0 \alpha}\right)^\gamma \ldots\ldots\ldots\ldots\ldots\ldots\ldots\ldots (10)$$

where, $\gamma = \frac{c_p}{c_v} = 1.4$ is the ratio of the heat capacities for dry air, Rd is the gas constant ordry air, and P0 is a reference pressure (typically 105 Pascal). The right-hand-side (RHS)terms FU, FV, FW and $F_\theta$represent forcingterms arising from model physics, turbulentmixing, spherical projections, and the earth'srotation. Equation (3)-(5), (6) and (7) is referred to as the conservation of momentum, Conservation of energy and equation of continuity respectively and equation (8) represent the material derivative of the definition of the geopotential. The ARW dynamic solver solve the above equations with the inclusion of the moisture term and perturbation term. The details description of the governing equation of the WRF-ARW model is given in the reference (Skamarock *et al.*, 2005).

5. Model Description and Configuration

The Weather Research and Forecasting (WRF) model is a numerical weather prediction (NWP) model which is widely used in weather forecasting and meteorological research now a day. There are two dynamics solvers in the WRF: i) Advanced Research WRF (ARW) solver ii) Nonhydrostatic Mesoscale Model (NMM) solver. The ARW dynamics solver together with other components of the WRF system compatible with that solver is referred to as the WRF-ARW Model. Thus, itis a subset of the WRF modeling system that, in addition to the ARW solver, encompasses physics schemes, dynamics options, initialization routines, and a data assimilation package (WRF-Var). For detail information about WRF model and how to run ARW system, ARW User's Guide has the details on its operation (Ahasan *et al.*, 2015). The latest version of this model is the WRF-ARW version 3.9 which was published on July 2017. An overview of the model configuration for the present study is shown in Table 1.

Table 1: Overview of WRF model configurations Dynamics and Domain

WRF core	ARW
Data	NCEP-FNL
Number of Domain	1
Run time	48 hr
Interval	30 min
Central point of the Domain	23°N, 90°E
Horizontal resolution	10 km
Grid size	250 ×250×38
Map projection	Mercator
Integration time step	45 s
Vertical coordinate	pressure vertical coordinate
Time integration scheme	3rd order Runge-Kutta
Spatial differencing scheme	6th order centered difference
Physics options	
Microphysics	Kessler scheme
PBL Parameterization	Yonsei University (YSU) scheme
Surface layer physics	Revised MM5 scheme
Land-surface model	Unified Noah LSM
Short wave radiation	Dudhia scheme
Long wave radiation	RRTM scheme
Cumulus parameterization	Grell-Devenyi (GD) ensemble scheme

6. Results and Discussion

Various meteorological parameters such as mean sea level pressure, temperature, relative humidity, wind pattern, amount of rainfall etc., play an important role for the formation and development of thunderstorms. These parameters along with the instability index e.g., CAPE, CIN and K-index during a thunderstorm event on 06 May 2017over Mymensingh, performed by the WRF-ARW model, is analyzed deeply. A comparison with the observed data is also made for the validation of the model performance to capture a thunderstorm event over this region.

6.1. Analysis of MSLP

Mean sea level pressure play a very important roles for the formation of thunderstorm. Development of Low Pressure Area is one of most important ingredient of the formation of thunderstorm. A trough of westerly low (1006-1008 hPa) is also found by WRF-ARW model over some part of West Bengal with Rajshahi, Chuadanga and its adjoining area over Bangladesh at 1200 UTC. The MSLP of the other part of Bangladesh was varies from 1007 to 1010 hPa during this time. This trough gradually expands and produces a converging zone over the boundary area of West Bengal and Rajshahi at 1300 UTC. At 1430 UTC, MSLP in Mymensingh was high (1010 hPa) and suddenly fall from 1010 hPa to 1008 hPa in next two hour.

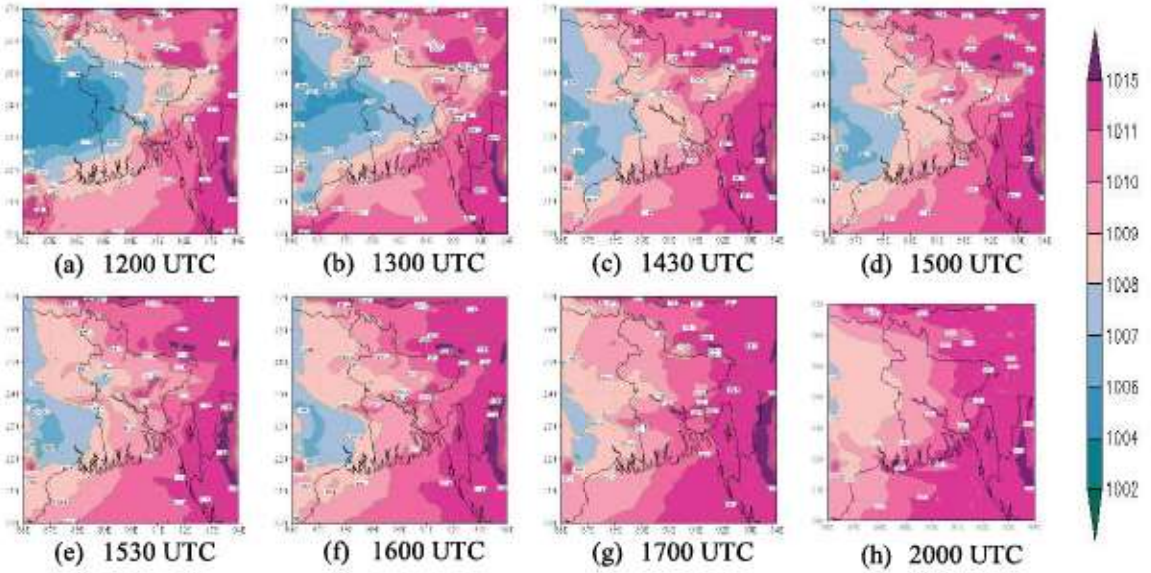

Fig. 1(ii): WRF-ARW model simulated MSLP of 06 May 2017

From 1600 UTC to 1700 UTC, simulation result shows that MSLP is continued to rise gradually from 1008 to 1011 hPa. WRF-ARW model simulated MSLP of 06 May 2017 based on the initial conditions of 0000 UTC 0f 05 May are shown in Fig. 1.

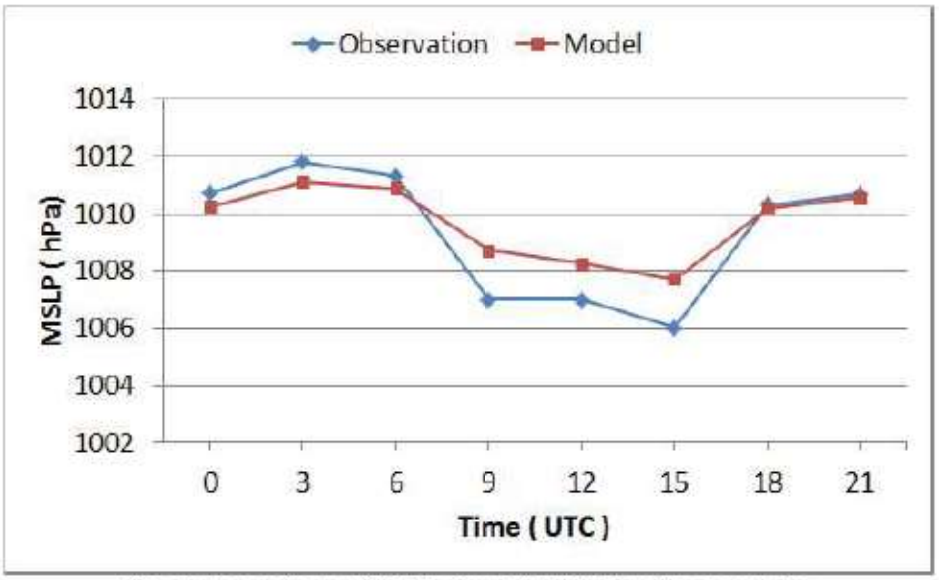

Fig. 2: Comparison of Model simulated MSLP with observation

For the validation of model simulated MSLP, a comparison is made with three hourly observed MSLP recorded by BMD, over Mymensingh on 06 May 2017. The comparison is shown in the Fig. 2. From the observed data, a sharp fall of MSLP from 1011.3 hPa to 1006 hPa is found over Mymensingh on 06 May 2017 during 0600 UTC to 1500

UTC. From the Fig. 2 it is found that the model simulated fall of MSLP is from 1010.87 hPa to 1007.7 hPa which show that the WRF-ARW model is capable to capture the sharp fall of MSLP reasonably well.

6.2. Wind Pattern and Direction Analysis

During thunderstorm event, a strong wind blows over the event area which sometimes becomes vigorous and devastating. From the model simulated wind at 850 hPa level, a conjugation of north-westerly wind and easterly wind is also found over Murshidabad (India) and its adjoining area at 1500 UTC. This conjugation of wind is responsible for the strong convection. This conjugation extends up to the western side of Mymensingh at 1600 UTC and model simulation result shows that wind speed is 25 Kmh^{-1}at that time in Mymensingh. Wind speed is gradually increased and become 50 $Kmhr^{-1}$at 1830 UTC in Mymensingh. The observed wind speed, recorded by BMD, in Mymensingh was 56 $Kmhr^{-1}$. So, from the above analysis, it is concluded that model simulated wind speed is lower than that of the observed wind speed. But the model is able to capture the strong wind speed over the event area compare to its surrounding area.

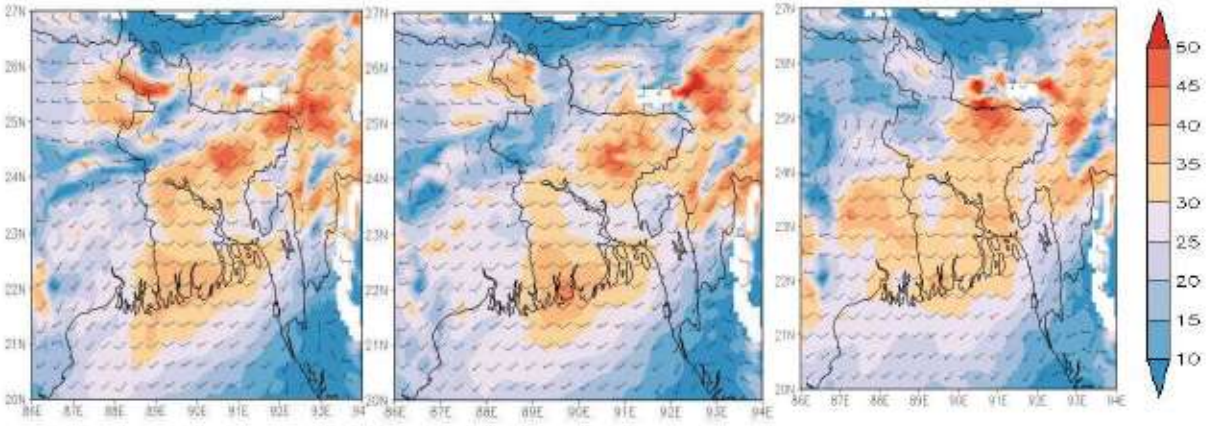

(a) 1500 UTC (b) 1600 UTC (c) 1830 UTC

Fig. 3: WRF-ARW Model simulated Wind speed and direction on 06 May 2017WRF-ARW model simulated wind speed and direction at 850 level of 06 May 2017 based on the initial conditions of 0000 UTC of 05 May.

6.3. Analysis of Relative Humidity and Rainfall

Surface level relative humidity is an essential factor for intense convection. Storm days require a sufficiently humid and deep layer in the lower and middle atmosphere. From the WRF-ARW model simulated relative humidity at 2m height, a dry-line is found in the middle part of Bangladesh at 1200 UTC which is gradually moves toward Chuadanga and it adjoining area as shown in the Fig. 4. Thunderstorms mainly occurred in the right side of the dry line. Simulation result also show that the relative humidity is 100 %in Mymensingh at 1530 UTC.

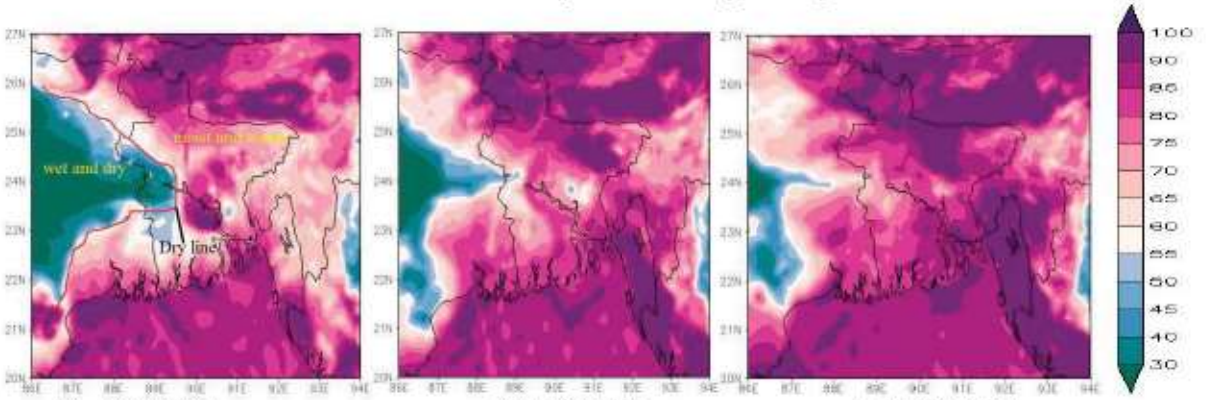

(a) 1200 UTC (b) 1400 UTC (c) 1530 UTC

Fig. 4: WRF-ARW Model simulated RH on 06 May 2017.

During a thunderstorm event a heavy rainfall is occurred and this rainfall is an important ingredient for thunderstorms. From the model output, it is found that no rain fall is simulated over Bangladesh from 0300 UTC to 0600 UTC. A heavy rainfall is simulated in the middle part of Bangladesh from 0900-1200 UTC. From 1200-1500 UTC, a low amount of rainfall is simulated to the surrounding area of Mymensingh which vary from 6 mm to 9 mm and heavy

rain fall is in just eastern part of the Mymensingh. So model shows heavy rainfall with location error. WRF-ARW model simulated Rainfall of 06 May 2017 based on the initial conditions of 0000 UTC 0f 05 May are shown in Fig. 5.

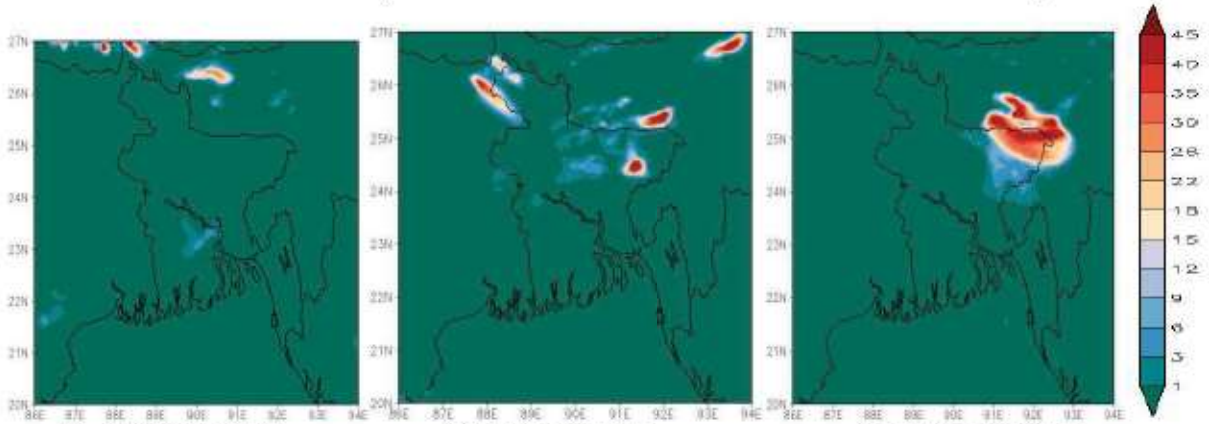

(a) 0600-0900 UTC (b) 0900-1200 UTC (c) 1500-1800 UTC

Fig. 5: WRF-ARW Model simulated Rainfall on 06 May 2017

6.4. Vertical Cross Section of Relative Humidity (RH)

From the analysis of vertical cross section of RH, a dry air of RH 50-80 % is found from 950 hPa to 850 hPa level over Mymensingh (24.75*N*, 90.40*E*) at 0800 UTC. During this time, dry air of RH less than 20 % is found over that pressure level. This condition stays almost same upto 1000 UTC. After that the RH of the lower part of the atmosphere is gradually increased with time in the vertical direction. An area of RH 50-70% is found in between 500 hPa and 400 hPa level to 90.40°E at 1500 UTC. This is an indication of cloud at this level. During this time, lower level RH is increased vertically upward compare to its surrounding region which indicate that moist air rising in the upward direction. As discussed earlier, westerly wind is blowing over this area, so this cloud gradually moves toward the eastern part of Mymensingh. From the above analysis, it is found that model capture the presence of cumulonimbus cloud over the thunderstorms events area precisely well. WRF-ARW model simulated vertical cross section of RH of 06 May based on the initial conditions of 0000 UTC of 05 May is shown in Fig. 6.

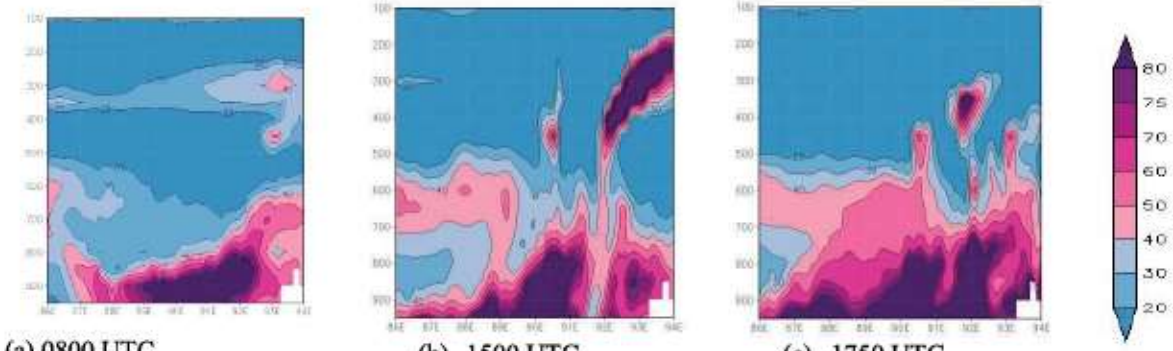

(a) 0800 UTC (b) 1500 UTC (c) 1750 UTC

Fig. 6: WRF-ARW Model simulated Vertical cross section of RH at 24.75 N on 06 May 2017

6.5. Analysis of CAPE

Convective Available Potential Energy (CAPE) is the maximum possible kinetic energy available for convection and gives an indication of tropospheric instability at a given time [9]. CAPE is calculated as the positive temperature difference between the theoretical parcel and environmental lapse rates, vertically integrated with respect to the natural logarithm of pressure, p, between the level of free convection (LFC) and equilibrium level (EL):

$$CAPE = \int_{LFC}^{EL} R_g\,(T_{ve} - T_{vp})dlnP$$

where, T_{ve} and T_{vp} are the environmental and parcel virtual temperature, R_g is the gas constant of dry air. CAPE is measured in Joule per kg (Jkg^{-1}). According to Rasmussen and Wilhelson, CAPE value at surface level greater than 1500 Jkg^{-1} is required for the formation of supper cell thunderstorm [10]. WRF-ARW model simulated CAPE value is 500-1000 Jkg^{-1} at 0600 UTC over Mymensingh. Then this CAPE value is gradually increased over the thunderstorm event area with time and CAPE value more than 2500 Jkg^{-1} is found at 1200 UTC shown in Fig. 7. This

high CAPE value is then gradually decreased with time. This is an indication that supportive CAPE value is present over Mymensingh which helps to develop a thunderstorm cell and after few hours this thunderstorms cell vanishes.

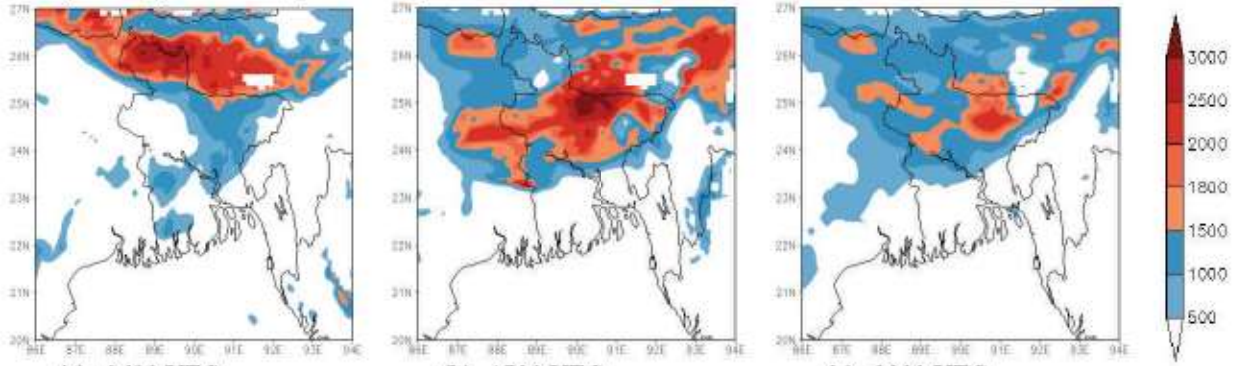

(a) 0600 UTC (b) 1700 UTC (c) 2000 UTC

Fig. 7: WRF-ARW Model simulated CAPE on 06 May 2017.

6.6. Analysis of CIN

Convective inhibition (CIN) is one of the most important factors for thunderstorm. An air parcel must have to overcome this inhibition to move to the positive CAPE region and development of deep convection. CIN value less than 50 $Jkg^{-1}$is supportive for the development of thunderstorm [11].

(a) 1100 UTC (b) 1300 UTC (c) 1800 UTC

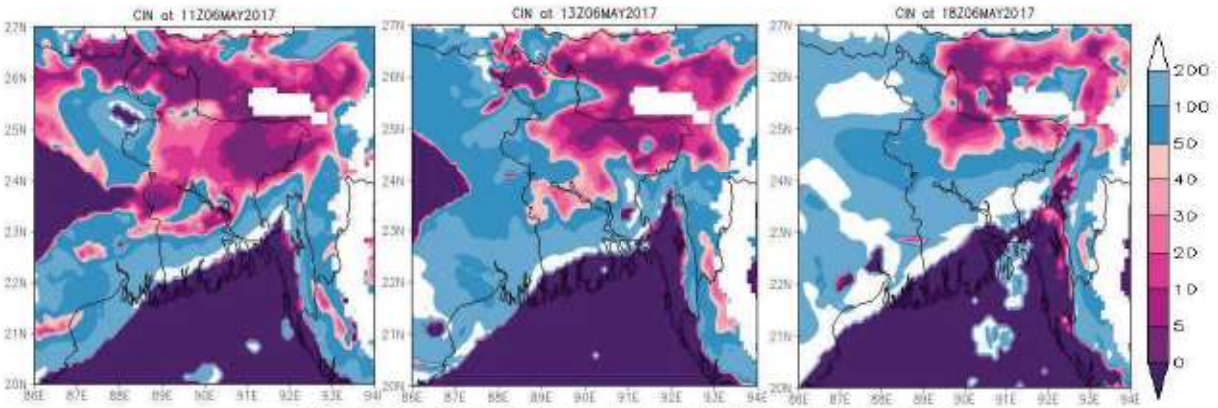

Fig. 8: WRF-ARW Model simulated CAPE on 06 May 2017.

An area of low inhibition (CIN value less than5Jkg^{-1}) at 900 hPa level is found over Mymensingh and its adjoining area at 1100 UTC which is shown in Fig. 8. This low inhibition helps air parcel to move in the positive CAPE region. Then the CIN value is gradually increased over this area with time and become more than 50 Jkg^{-1} at 1800 UTC.

6.7. Analysis of K-index

K-index is one kind of stability indices which is used to predict the severe weather events. K-index value greater than 35 is supportive for the sever convection (Litta *et al.*, 2012). The efficiency of the K-index using WRF-ARW model for the thunderstorm prediction over Bangladesh is discussed in this section. K-index values less than 35 i.e., stable atmosphere, is found over Bangladesh at 0600 UTC. K-index value gradually increases and become more than 35 at 1100 UTC in Chuadanga and its adjoining area. This high K-index value stay up to 1700 UTC over this area. During this time, k-index value more than 35 is found in Mymensingh and its adjoining area which is gradually moves toward Sylhet.

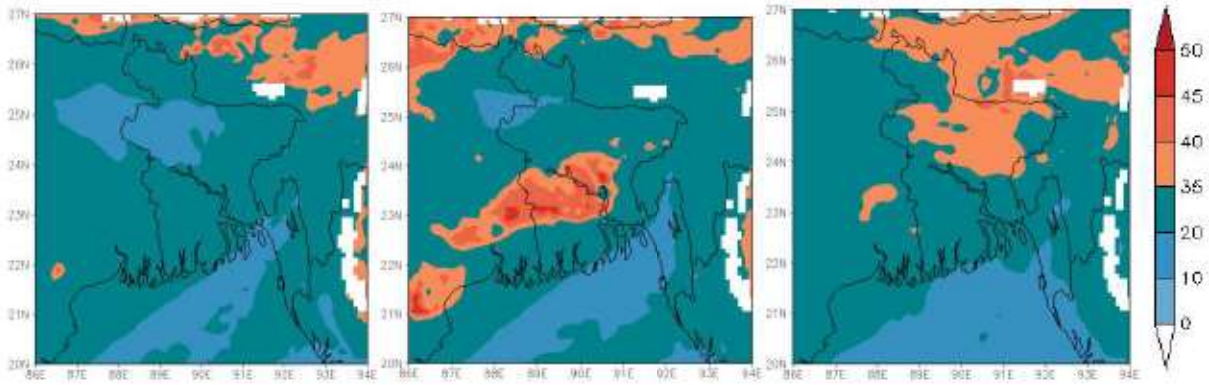

(a) 0600 UTC (b)1100 UTC (c) 1830 UTC

Fig. 9: WRF-ARW Model simulated K-index value on 06 May 2017.

From the above analysis, it is found that model simulate high K-index value (greater than 35) a few hours later of thunderstorm event in Mymensingh. So it is concluded that model can capture the K-index value few hour earlier or later of the thunderstorm events.

6.8. Analysis of Radar Reflectivity

Doppler Weather Radar (DWR) is now successfully used in the various fields including Meteorology. It is used in a wide range for the study of severe weather phenomena such as thunderstorms, tornadoes, cyclones etc. It can detect the position and strength of weather echoes as well as can measure the speed of rain or hail towards or away from the radar (Bhatnagar *et al.*, 2003). From the numerical model simulated radar reflectivity, one can easily see the details about the mesoscale and near storm scale structures such as the structure of deep convection, movement of squall line etc. (Litta *et al.*, 2012). WRF-ARW model simulated Composite radar reflectivity (dBz) on 06 May 2017 from 1500 UTC to 1900 UTC is shown in Fig. 10. From the model simulation result, dBz value more than 50, is found on the northern side of the Mymensingh at 1900 UTC which is an indication of a convective cloud over this area. This cloud is then moves toward Sylhet through the north eastern part of Mymensingh within the next two hours. From this analysis, it is found that WRF-ARW model capture the dBz value with some position error.

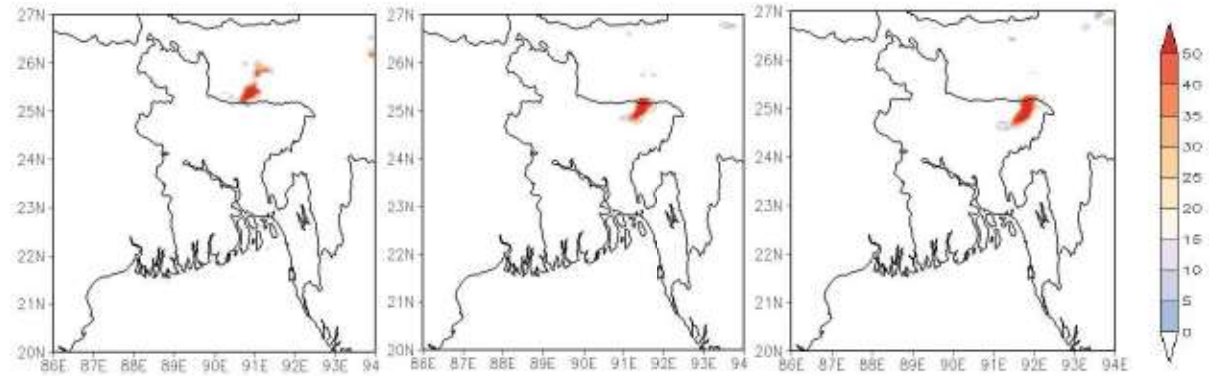

1830 UTC (b) 1930 UTC (c) 2000 UTC

Fig. 10: WRF-ARW model simulated dBz on 06 May 2017

7. Conclusion

After analyzing the various parameters during the TS events over Mymensingh on 06 May 2017, performed by WRF-ARW model for period of 48 hours, the following conclusions can be made on model performance for capturing TS events over Bangladesh.

- Model capture the sharp fall of MSLP precisely well.
- Model is capable to capture the strong wind speed over TS events area with one or two hours earlier or later at 850 hPa level compare to its surrounding area. Although this wind speed is lower than that of the observation.

- WRF-ARW model is capable to capture the rainfall in the thunderstorm events and its surrounding area.
- Model capture the rise of RH reasonably well in comparison with the observation and model can capture the Dry-line in each scheme.
- WRF-ARW Model has done well in capturing the supportive CAPE value (more than 1500 Jkg^{-1} for the occurrence of sever. Model also performs precisely well to capture CIN value and K-index value.

Finally, despite of some temporal and spatial error for capturing various parameters, it can be said that WRF-ARW model capture the thunderstorm event reasonably well. So WRF-ARW model output can be used to forecast the future TS events over Bangladesh.

Acknowledgment

At the very first, the authors would like to thank Bangladesh Meteorological Department (BMD) for their technical support to conduct this research work and also for providing the observed data. They would also like to thank NCEP for providing the FNL data to run the WRF-ARW Model.

References

Ahasan, MN and Quadir, DA and Khan, KA and Haque, MS, "Simulation of a thunderstorm event over Bangladesh using WRF-ARW model", *Journal of Mechanical Engineering*, Vol. 44, No. 2, pp.124-131,2015.

Bhatnagar, AK and Rao, P Rajesh and Kalyanasundaram, S and Thampi, SB and Suresh, R and Gupta, JP, "Doppler radar--A detecting tool and measuring instrument in meteorology", *Current Science*, JSTOR, vol. 85, no. 3, pp. 256-264, 2003.

Das, Someshwar and Mohanty, UC and Tyagi, Ajit and Sikka, DR and Joseph, PV and Rathore, LS and Habib, Arjumand and Baidya, Saraju K and Sonam, Kinzang and Sarkar, Abhijit," The SAARC STORM: a coordinated field experiment on severe thunderstorm observations and regional modeling over the South Asian Region", *Bulletin of the American Meteorological Society*, American Meteorological Society, vol. 95 no. 4, pp. 603-617, 2014.

Das, Someshwar and Sarkar, Abhijit and Das, Mohan K and Rahman, Md Mizanur and Islam, Md Nazrul, "Composite characteristics of Nor'westers based on observations and simulations", *Atmospheric Research*, Elsevier, vol. 158, pp. 158—178,2015.

Holley, DM and Dorling, SR and Steele, CJ and Earl, N, "A climatology of convective available potential energy in Great Britain", *International Journal of Climatology*, Wiley Online Library, vol. 34, No.14, pp.3811-3824,2014.

Karmakar, Samarendra and Alam, Md Mahbub," Modified instability index of the troposphere associated with thunderstorms/nor'westers over Bangladesh during the pre-monsoon season", *Mausam*, vol. 62, No. 2, pp. 205-214, 2011.

Karmakar, S.: "Climatology of thunderstorm days over Bangladesh during the pre-monsoon season", *J Bangladesh Acad Sci*, vol. 3, no. 1, pp. 103--112,2001.

Litta, AJ and Mary Ididcula, Sumam and Mohanty, UC and Kiran Prasad, S, "Comparison of thunderstorm simulations from WRF-NMM and WRF-ARW models over east Indian region", *The Scientific World Journal*, Hindawi Publishing Corporation vol. 2012,2012.

National Centers for Environmental Prediction, National Weather Service, NOAA, U.S. Department of Commerce, "NCEP FNL Operational Model Global Tropospheric Analyses, continuing from July 1999", Research Data Archive at the National Center for Atmospheric Research, Computational and Information Systems Laboratory https://doi.org/10.5065/D6M043C6, 2000.

Rasmussen, EN, "Relationships between storm characteristics and 1200 GMT hodographs, low-level shear, and stability",*Preprints of* 13^{th} *Conf. on Severe Local Stomrs, Tulsa, OK, Amer. Meteor. Soc., 1983*, 1983

Skamarock, William C and Klemp, Joseph B and Dudhia, Jimmy and Gill, David O and Barker, Dale M and Wang, Wei and Powers, Jordan G, "A description of the advanced research WRF version 2",*National Center For Atmospheric Research Boulder Co Mesoscale and Microscale Meteorology Div,* 2005.

User's Guide for the Advanced Research WRF (ARW) Modeling System Version 3.8", http://www2.mmm.ucar.edu/wrf/users/docs/user_guide_V3/contents.html.

Simulation of Heat Wave Event over Dhaka and Rajshahi Divisions using WRF-ARW Model

Md. Abdul Aziz[1*], M. A. Samad[1], M. A. K. Mallik[2], S. M. Q. Hassan[2] and M. S. Alam[2]
[1]Department of Applied Mathematics, University of Dhaka, [2]Bangladesh Meteorological Department, Dhaka, Bangladesh, *Corresponding author: aziz031du@gmail.com*

Abstract: In this study, an attempt has been made to simulate the heat wave events over Dhaka and Rajshahi divisions of Bangladesh from 19 May to 25 May 2017 using Advanced Research dynamic solver of Weather Research and Forecasting (WRF-ARW) model version 3.9. The WRF model was run for 6 days on a single domain of 10 km horizontal resolution, using six hourly Global Forecast System (GFS) datasets as initial and lateral boundary conditions. For simulation, Kessler scheme for microphysics, Yonsei University (YSU) scheme for planetary boundary layer (PBL) parameterization, Revised MM5 scheme for surface layer physics, Rapid Radiative Transfer Model (RRTM) for longwave radiation, Dudhia scheme for shortwave radiation and Kain-Fritsch (KF) scheme for cumulus parameterization were used. The model have been analyzed numerically by the Several meteorological parameters such as mean sea level pressure (MSLP), relative humidity (RH), temperature, wind pattern, rainfall and latent heat (LH), and the output is visualized by Grid Analysis and Display System (GrADS). The main objective was to assess the validity of model forecasts and sensitivity on land surface processes. To validate the model performance, model-simulated values of RH, daily maximum temperature, and MSLP were compared with BMD observed data. From the analysis it is clear that the performance of the model is good to the observations, so that for the future up-coming events of heat wave, the model can be used.

1. Introduction

Heat waves (HWs) are as the most common deadly natural disaster in the world: more than 70,000 people died as a result of the 2003 European heat wave (Robine *et al.*, 2008), according to "The Times of India"- the death due to the 1998 heat wave over India was about 2541. A heat wave is a period of excessively hot weather, which may be associated by high humidity. The definition of Heat Wave varies and which is measured relative to the usual weather in the area and normal temperatures for the season. Frich *et al.* (2002) defined Heat Wave that a heat wave occurs when the daily maximum temperature of more than five consecutive days exceeds the average maximum temperature by 5°C. Jan Kysely (2000) defined Heat Wave for Check Republic that the definition consists of three requirements imposed on a period to be treated as a heat wave: (i) T_{MAX} (daily maximum air temperature) $\geq T_1$ in at least 3 days; (ii) mean T_{MAX} over the whole period $\geq T_1$; and (iii) $T_{MAX} \geq T_2$ in each day. The threshold values were set to $T_1 =$ 30°C, $T_2 = 25$°C, in accordance with a climatological practice commonly applied in the Czech Republic which refers to the days with TMAX reaching or exceeding 30°C and 25°Cas tropical and summer days, respectively. No such definition has been developed for Bangladesh, but Bangladesh Meteorological Department (BMD) defines various types of heat waves as: when maximum temperature $36 - 38$°C → Mild Heat Wave; when maximum temperature $38 - 40$°C → Moderate Heat Wave; when maximum temperature $40 - 42$°C → Severe Heat Wave; when maximum temperature > 42°C → Extreme Heat Wave.

Heat waves have significant impacts on both ecosystems and human beings. The latest finding in the Fifth Assessment Report (AR5) of the IPCC (Pachuari *et al.*, 2014) indicates that a warming of $(1 - 2)$°C above pre-industrial levels would severely impact food production, water resources, and ecosystems, in addition to posing a moderate-to high-risk to human and natural systems. Global observed changes in daily climate extremes of temperature [5] typically show large areas and such area includes parts of south &central Asia. Frich *et al.* [2] concluded that a significant proportion of the global land area was increasingly affected by a significant change in climatic extremes during the second half of the 20th century.

Alexander *et al.* (2006) showed that annual trends in the lowest and highest daily minimum and maximum temperatures in the latter half of the twentieth century increased at many locations throughout the world. Feng Chen *et al.* (2014) showed that the Urban Heat Island (UHI) effect over Hangzhou, east China during a long-lasting heat wave which was simulated by WRF with horizontal resolution of 1 km and concluded that an average temperature increase of 0.74°C in the city center under high urbanization conditions. Das *et al.* (2007) studied variability of climate change in India and they showed that the trend of temperature was increasing over the past quarter century, but significant variations in these trends during different seasons and over different regions of India.

Some researchers research about climate changes on Bangladesh like as Zubayed Bin Rakib (2013), Bangladesh Climate Change Country Study Program (1997), BUP (1994), Mahtab (1989), Pramanik (1983), BCAS (1994) etc. and all are concluded that Bangladesh is one of the topmost countries to the unpleasant effects of global warming. The average annual temperature of Bangladesh is expected to increase by 1.4 ± 0.6°C by 2050 (IPCC, 2004; MoEF, 2008; Rakib, 2013). In the present study, an attempt has been made to simulate HW events over Dhaka and Rajshahi divisions of Bangladesh on 19 - 25 May 2017 and 19 - 25 April 2016 using WRF model, and to identify the possible synoptic conditions and reasons responsible for occurring such an event. The results of the analysis are presented, discussed and concluded in the following parts.

2. Data Used, Model Description and Methodology

The Weather Research and Forecasting (WRF) Model is a next-generation mesoscale numerical weather prediction model which schematic for both atmospheric research and operational forecasting applications, and which simulate a wide range of meteorological phenomena ranging from tens of meters to thousands of kilometers. There are two dynamical cores in the WRF system: the Advanced Research WRF (ARW) was developed and maintained by NCAR, and the NMM (Nonhydrostatic Mesoscale Model) was developed by the National Centers for Environmental Prediction (NCEP). The ARW dynamic core of WRF model (WRF-ARW) Version 3.9 has been used during the present study.

In this study, the Global Forecast System (GFS) data produced by NCEP which are used from 19 May to 24 May 2017 with 0000 UTC as the initial and lateral boundary condition. Dozens of atmospheric and land-soil variables are available through this dataset, from temperatures, winds, and precipitation to soil moisture and atmospheric ozone concentration and which is used by the operational forecasters who predict weather out to 16 days in the future. To validate the model performance, model-simulated values of RH, maximum temperature, and MSLP were compared with observational data obtained from Bangladesh Meteorological Department (BMD).

The WRF model was run on a single domain at 10 km resolution using Microphysics scheme namely Kessler scheme [16]. The configured domain for the present study is shown in Fig. 1. The Domain has 251×251 grid points in the north-south and west-cast directions respectively and which was configured to have the same vertical level of 38 unequally spaced sigma (non-dimensional pressure) levels. Bangladesh (center $23°N, 90°E$) is the main focus area of this study. The physical parameterization schemes used in this study are Yonsei University (YSU) scheme (Hong *et al.*, 2006) for planetary boundary layer (PBL) parameterization, Revised MM5 scheme (Paulsom, 1970) for surface layer physics, Rapid Radiative Transfer Model (RRTM) scheme (Mlawer, 1997) for longwave radiation, Dudhia scheme [20] for shortwave radiation and Kain-Fritsch (KF) scheme (Kain, 2004) for cumulus parameterization.

Fig. 1: WRF model domain of this study.

3. Result & Discussion

3.1 Analysis of Temperature at 2m Height

Temperature is a vital element of HW because it happens when a region experiences very high temperatures for several days and nights. Model-simulated temperature at 2m height from 19 May to 24 May 2017 at 0900 UTC based on 0000 UTC of 19 May initial conditions using the cumulus physics scheme, Kain-Fritsch (KF) are shown in Fig. 2(a-f) respectively. From the temperature analysis it is observed that on 19 May 2017, the temperature is about $34 - 38$ °C is simulated by model over the western and middle part of Bangladesh including Dhaka and Rajshahi divisions at 0900 UTC Fig. 2(a). On 20 May at the same time i.e. 0900 UTC, the temperature is about $38 - 40$ °C in Dhaka division and in Rajshahi the temperature was same. And $21 - 24$ May, the temperature is about $40 - 42$ °C is simulated by model over West Bengal and adjoining western part of Bangladesh i.e. over Rajshahi and small part of Dhaka division. For the inspection of the model performance, simulated maximum temperatures during 6 days from 19 May to 24 May 2017 at 0900 UTC were compared with the values observed by BMD. Fig. 3(a-b) shows the comparisons of maximum temperature at Dhaka and Rajshahi respectively.

From Fig. 3, it is found that model simulated temperature over both divisions overestimates the temperature compared to that of BMD observed temperature, where model shows comparatively high amount of temperature.

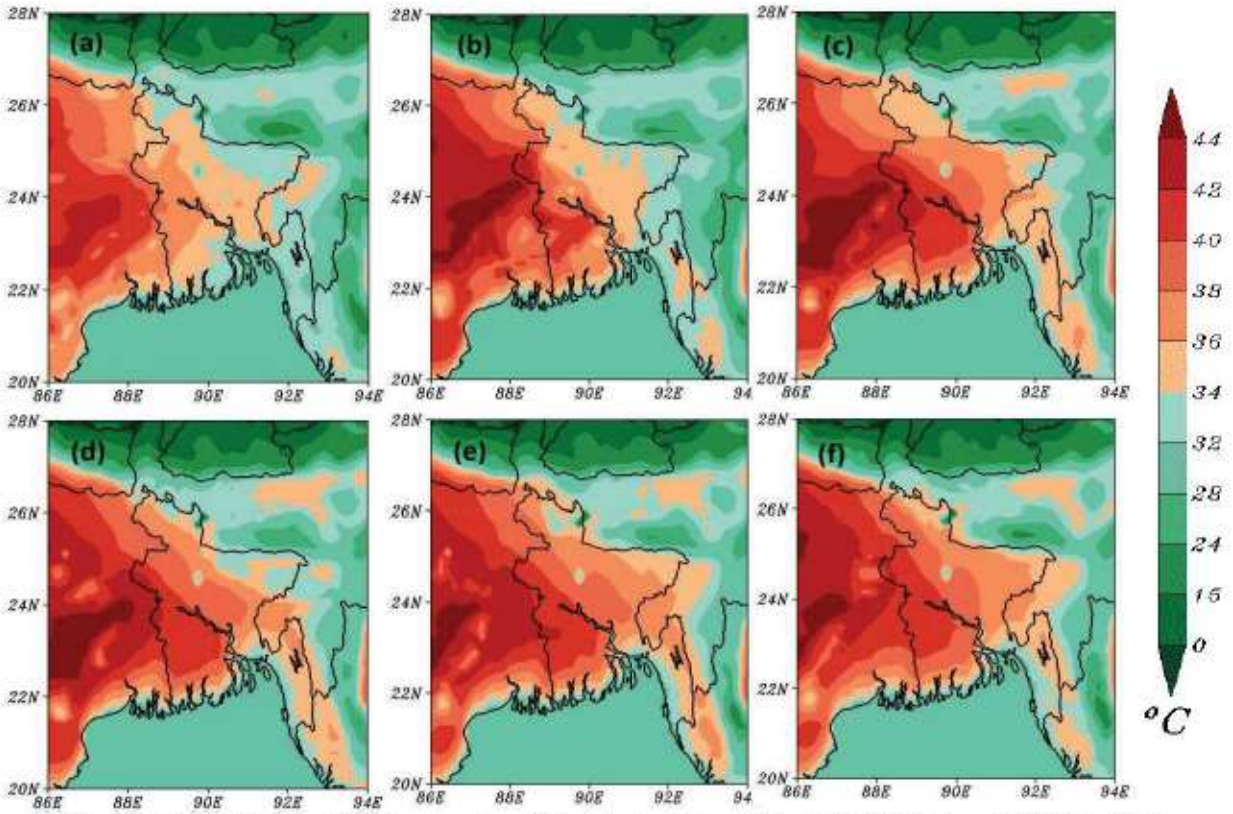

Fig. 2 (a-f): Model simulated Temperature (°C) at 2m height valid for 0900 UTC from 19-24 May 2017.

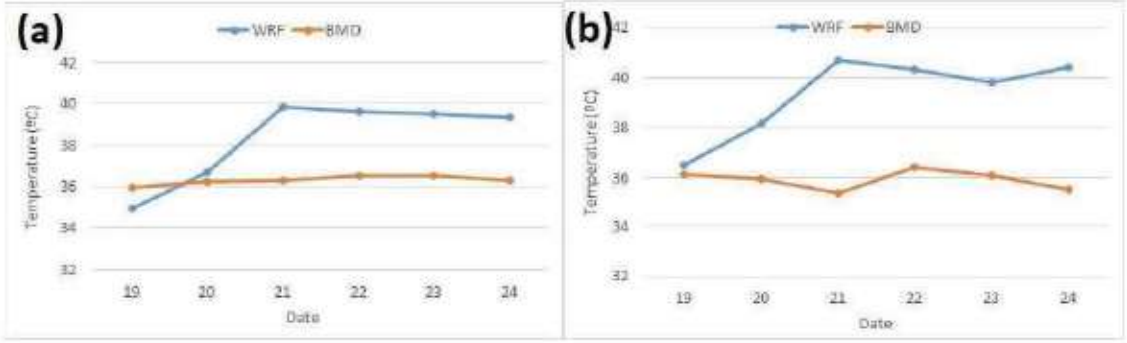

Fig. 3(a-b): Comparisons of Maximum Temperature (°C) of 19 – 24 May 2017 at Dhaka and Rajshahi division.

3.2 Analysis of Relative Humidity (RH) at 2m Height

The model simulated RH of 19 May to 24 May, 2017 at 0900 UTC for 6 days based on the initial conditions 0000 UTC of 19 May are presented in Fig. 4(a-f) respectively. The high amount of RH is an important environmental variable associated with cloud and rain formation. From the analysis of relative humidity, on 19 May, 10 – 40 % RH is found over West Bengal and Bihar, and 40 – 60 % RH is found over western and central part of Bangladesh. On 20 May the RH is increasing in Rajshahi but in Dhaka it is same as before. And from Fig. 4(c-f) the model simulated RH is found about 30 – 50 % over Rajshahi and Dhaka. For the supervision of the model performance, simulated RH (%) during 6 days from 19 May to 24 May 2017 at 0900 UTC were compared with the values observed by BMD and shows Fig. 5(a-b).

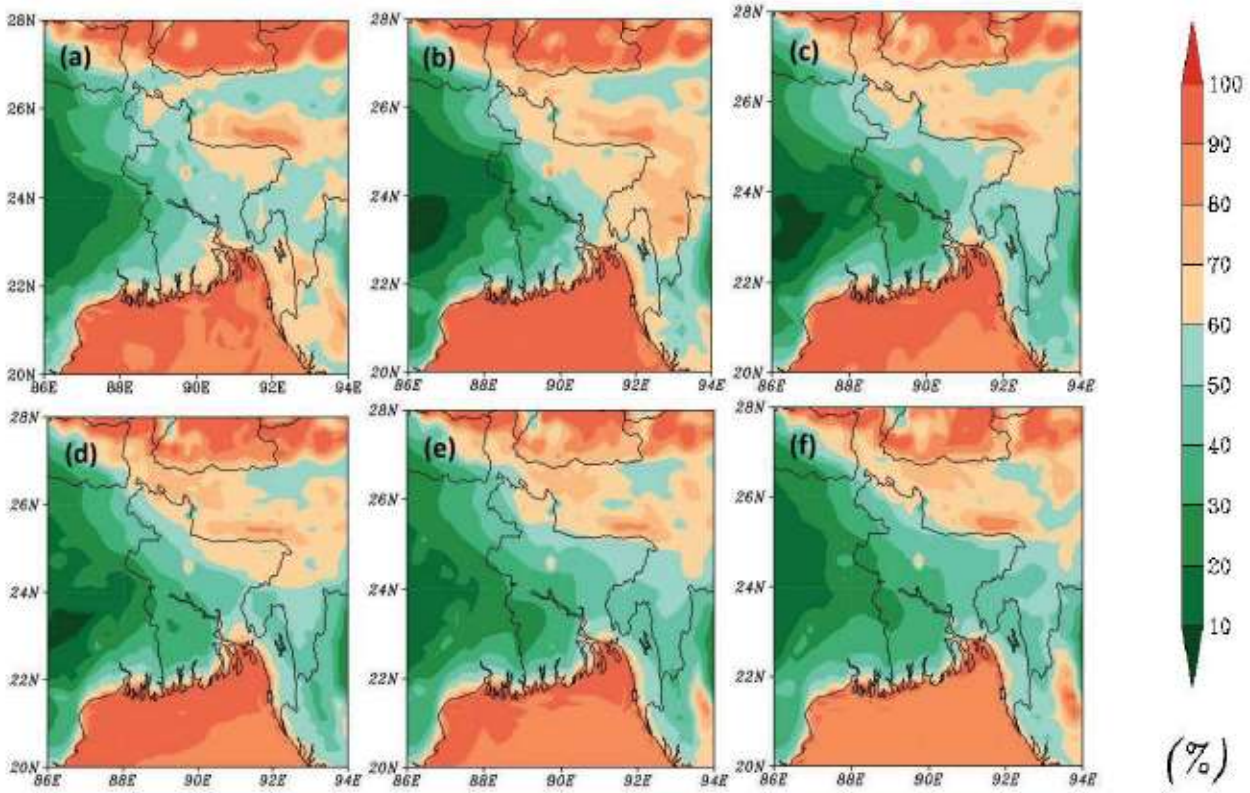

Fig. 4 (a-f): Model simulated RH (%) at 2m height valid for 0900 UTC from 19-24 May 2017.

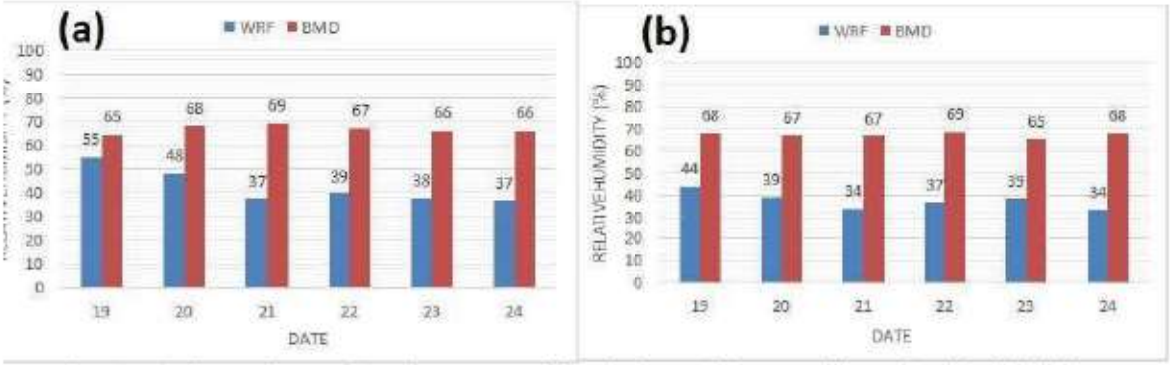

Fig. 5(a-b): Comparisons of RH between model and observed data at Dhaka and Rajshahi division respectively.

3.3 Analysis of 850, 500 & 200 hPa Levels Wind Flow

The model simulated distribution of 850 hPa, 500 hPa and 200 hPa levels wind flow (ms^{-1}) valid for 0900 UTC from 19 May to 24 May 2017 for 6 days based on the initial conditions 0000 UTC of 19 May are shown in Fig. 6(a-f), Fig. 7(a-f) and Fig. 8(a-f) respectively.

At 850 hPa level, south/southwesterly wind of speed $4-8ms^{-1}$ is simulated over Bay of Bengal whereas $2-6\ ms^{-1}$wind flow over Dhaka and Rajshahi. A divergence zone is seen over Rajshahi on 20 May where the wind speed is $2-6\ ms^{-1}$. On 21 May, southesterly wind is found over Rajshahi while southwesterly wind of speed $4-6\ ms^{-1}$is simulated over Dhaka.

At 500 hPa level, strong westerly wind of speed $15-20\ ms^{-1}$is simulated over West Bengal and adjoining part of Bangladesh including Dhaka and over Rajshahi it is about $10-14\ ms^{-1}$. On 20 May, forcible westerly and southwesterly wind of speed $15-20\ ms^{-1}$is found over Dhaka division.

At 200 hPa pressure level, strong westerly and southwesterly wind of speed $21-30\ ms^{-1}$is simulated over Bihar, Sikkim and adjoining part of Bangladesh and including small area of Rajshahi while in Dhaka the speed is $12-15\ ms^{-1}$, and during the next 5 days the westerly wind is decreasing with $9-15\ ms^{-1}$.

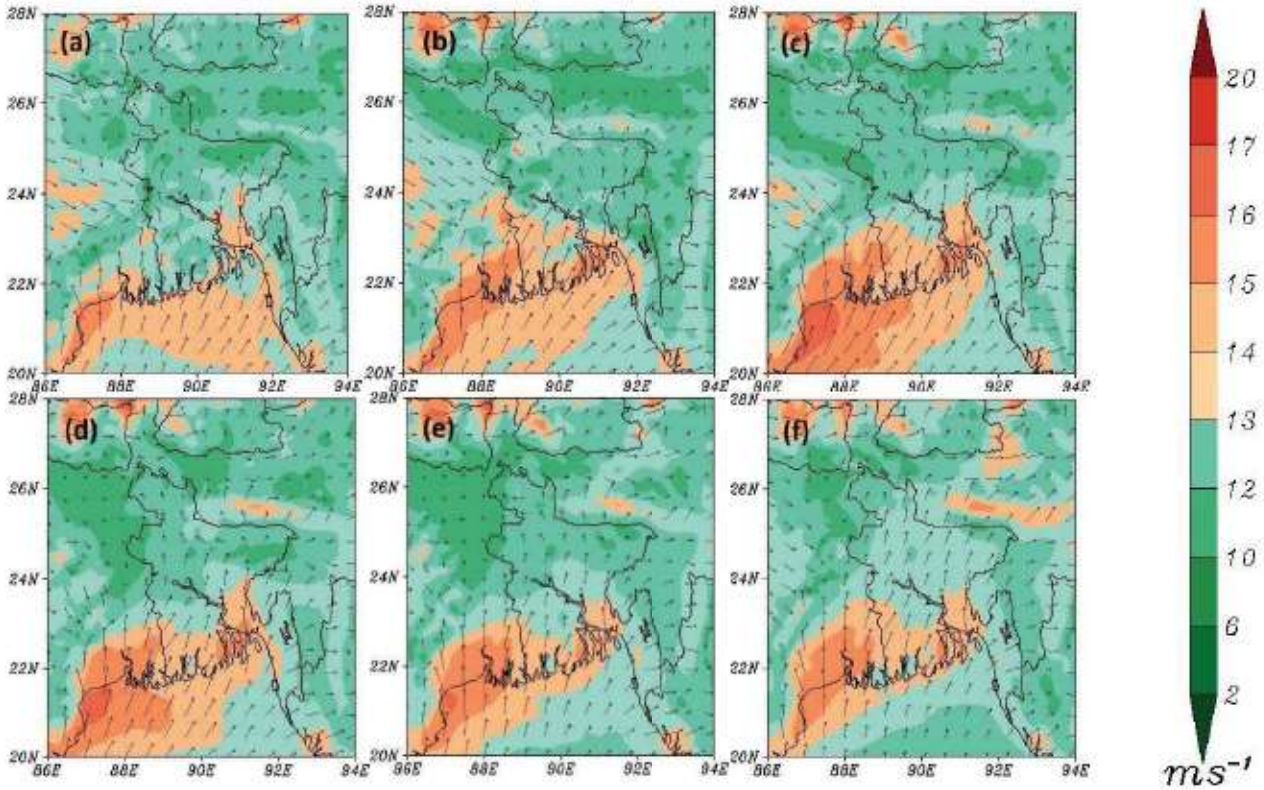

Fig. 6(a-f): Wind pattern at 850 hPa level valid for 0900 UTC of 19 to 24 May, 2017 for 6 days respectively.

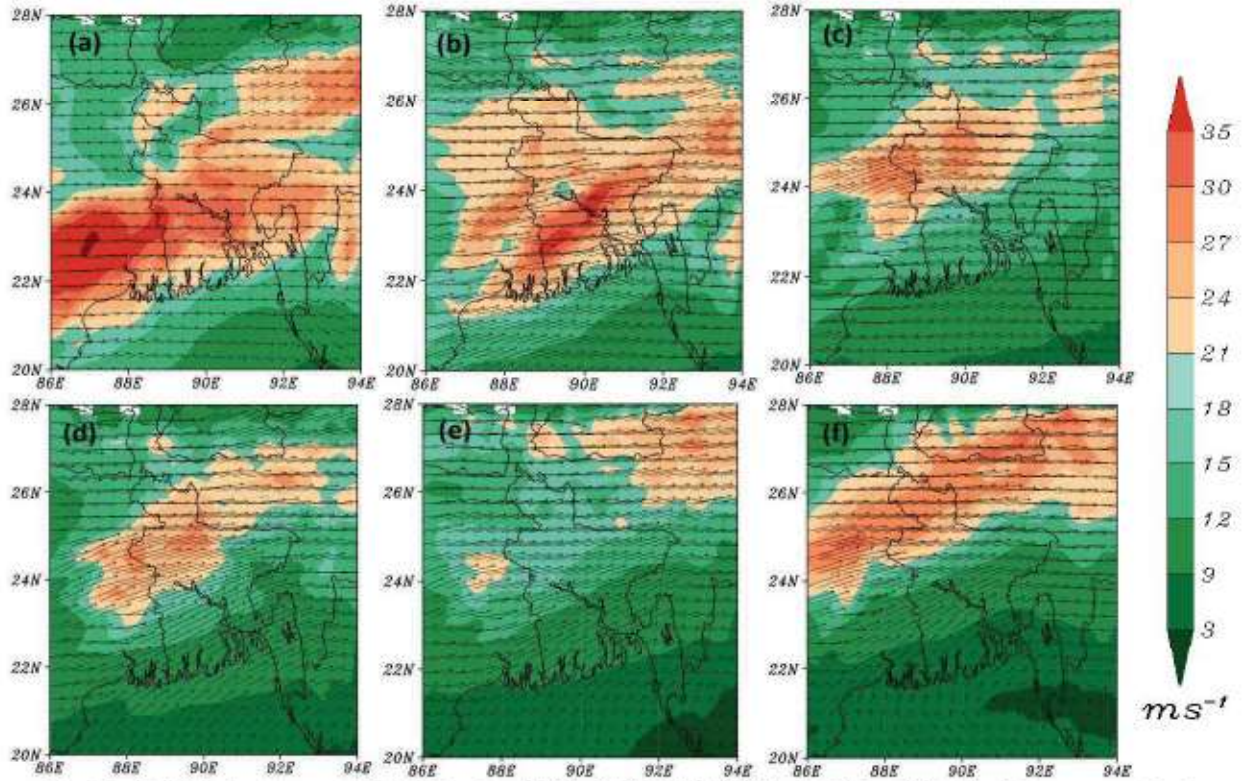

Fig. 7(a-f): Wind pattern at 500 hPa level valid for 0900 UTC of 19 to 24 May, 2017 for 6 days respectively.

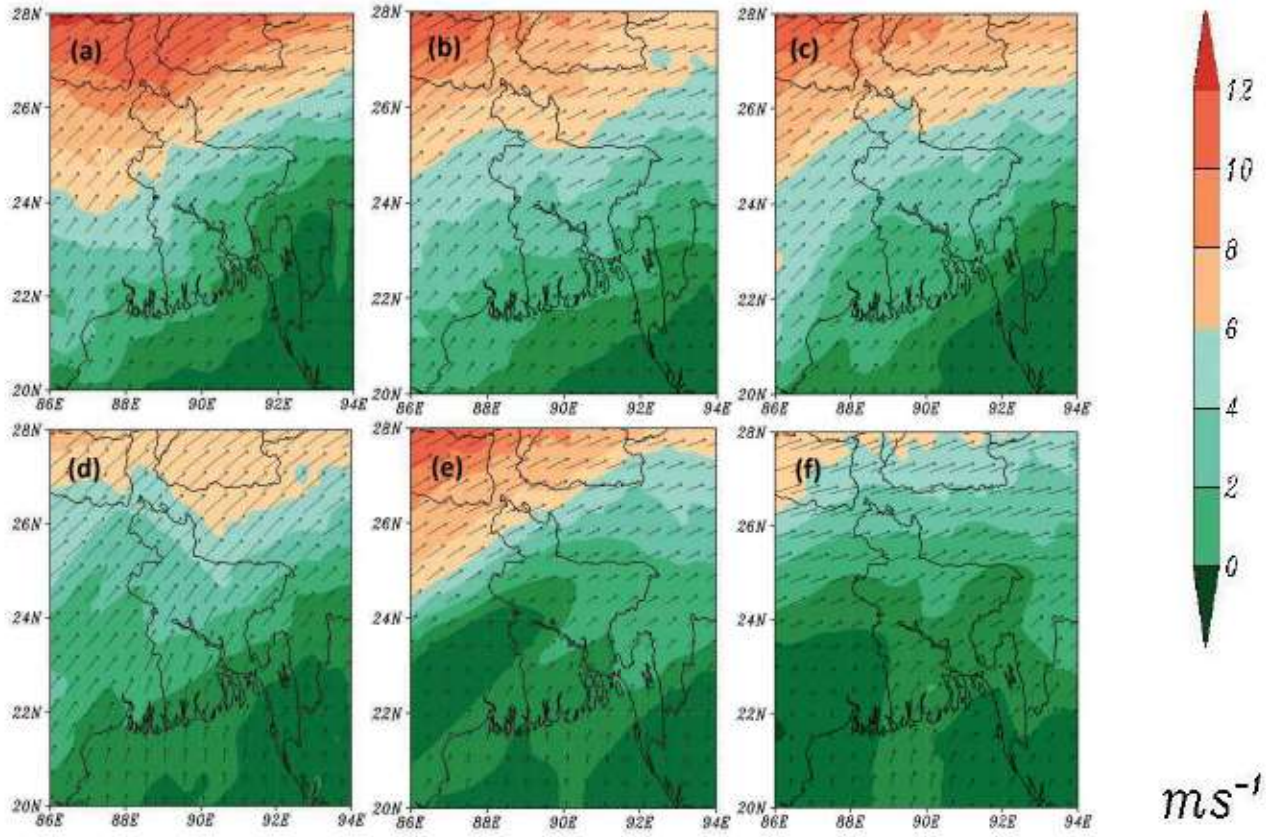

Fig. 8(a-f): Wind pattern at 200 hPa level valid for 0900 UTC of 19 to 24 May, 2017 for 6 days respectively.

3.4 Analysis of Accumulated Rainfall

The WRF model simulated accumulated rainfall distribution valid for 0900 UTC from 19 May to 24 May 2017, for 6 days based on the initial conditions 0000 UTC of 19 May are presented in Fig. 9(a-f) respectively.

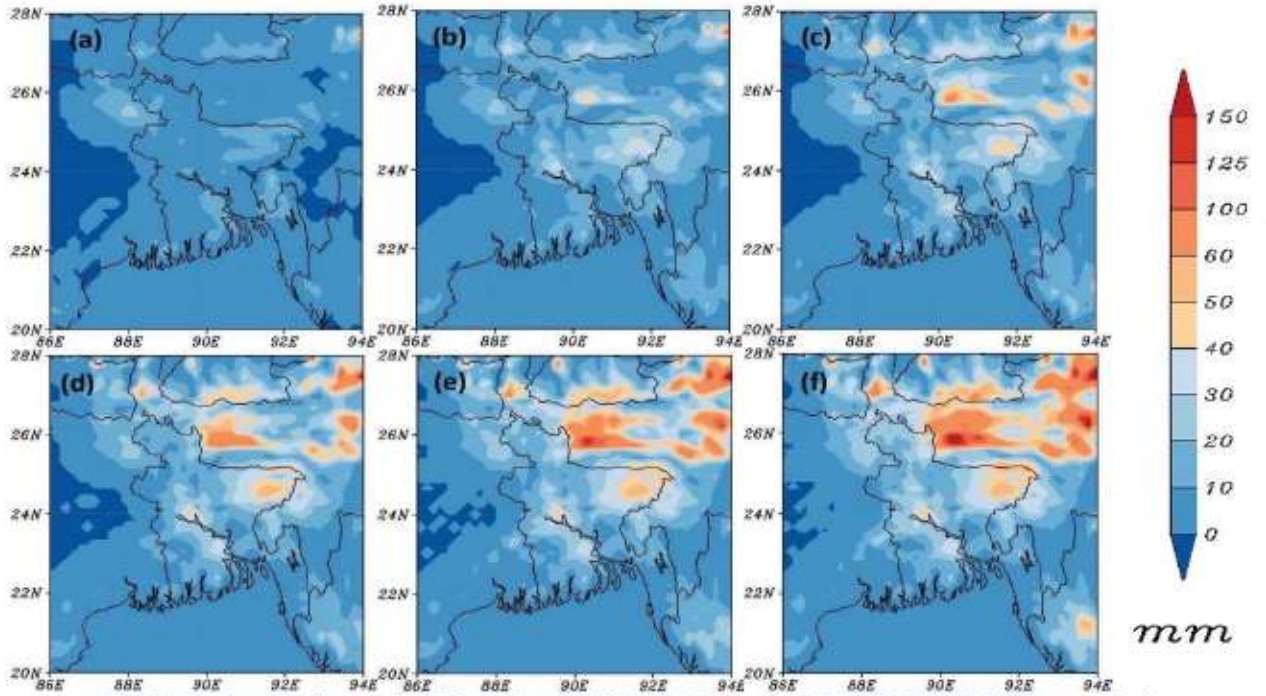

Fig. 9(a-f): Accumulated rainfall based on 0900 UTC of 19 to 24 May, 2017 for 6 days respectively.

No significant rainfall amount is simulated over Bangladesh on 19 May, $10-20\,mm$ rainfall is simulated over eastern part of Bangladesh during this period. In the next five days, total $30-50\,mm$ rainfall is found over very

small area of Dhaka. As very low amount of rainfall occurred over Bangladesh in the required time, so it is an important argument for HW continuation.

4. Conclusion

Heat wave cause enormous losses in terms of lives and human discomfort and ailments arising out of them. So forecasting of HW events over Bangladesh is really important. Therefore, this study has made an attempt to simulate the required HW event using WRF model to predict the future events more effectively.

On the basis of the present study the following conclusions can be drawn:

- WRF model captured the maximum temperature consecutively 6 days over Dhaka and Rajshahi divisions of Bangladesh although the model simulated temperature values over estimate the BMD observed temperature.
- The model simulated RH over Dhaka and Rajshahi divisions of Bangladesh underestimates the BMD observed RH.
- At 850 hpa level very low amount of wind speed is found by model and for which cause the weather was very hot.
- Approximately, no significant rainfall amount is simulated by model over Bangladesh.
- The model simulated temperature values and associated areas are sensibly well compared with the data observed by Bangladesh Meteorological Department (BMD).

Thoroughly, the analyses showed that the model performed reasonably well in capturing the required event in the face of some spatial and temporal preference. It can be concluded that WRF-ARW is a reliable model that may be used to forecast future HW events over any part of Bangladesh.

References

Bangladesh Climate Change Country Study Program, Assessment of vulnerability and adaptation to climate change. Final report, Department of Environment, Govt of Bangladesh, 1997.

BCAS-RA-Approtech, Vulnerability of Bangladesh to Climate Change and Sea Level Rise: Concepts and Tools for Calculating Risk in Integrated Coastal Zone Management; in Four Volumes (Summary report, Main reports and Institutional report), Bangladesh Centre for Advanced Studies (BCAS), Resource Analysis (RA), and Approtech Consultants Ltd., Dhaka, 1994.

BUP-CEARS-CRU, Bangladesh: Greenhouse Effect and Climate Change, Briefing Documents No. 1-7, Bangladesh UnnayanParishad (BUP), Centre for environmental and Resource Studies (CEARS), University of Waikato, New Zealand and Climate Research Unit (CRU), University of East Anglia, Norwich, UK, 1994.

C. A. Paulson, "The mathematical representation of wind speed and temperature profiles in the unstable atmospheric surface layer," Journal of Applied Meteorology, Vol. 9, No. 6, pp. 857 - 861, 1970.

E. J. Mlawer, S. J. Taubman, P. D. Brown, M. J. Iacono, and S. A. Clough, "Radiative transfer for inhomogeneous atmospheres: Rrtm, a validated correlated-k model for the longwave," *Journal of Geophysical Research: Atmospheres*, vol.102, no. D14, pp. 16663 - 16682, 1997.

E. Kessler, "On the distribution and continuity of water substance in atmospheric circulations," in On the Distribution and Continuity of Water Substance in Atmospheric Circulations, pp. 1 - 84, *Springer*, 1969.

F. Chen, X. Yang, and W. Zhu, "WRF simulations of Urban Heat Island under hot-weather synoptic conditions: The case study of Hangzhou city, china," *Atmospheric research*, Vol. 138, pp. 364 - 377, 2014.

IPCC, Intergovernmental Panel on Climate Change. Fourth assessment report Climate Change. *The Scientific Basis,* http//www.ipcc.ch/, 2007.

J. Dudhia, \Numerical study of convection observed during the winter monsoon experiment using a mesoscale two-dimensional model," *Journal of the Atmospheric Sciences*, Vol. 46, No. 20, pp. 3077 - 3107, 1989.

J. Kysely, "Changes in the occurrence of extreme temperature events," Auto report on Doctoral Thesis, Department of Meteorology and Environment Protection, Charles University, Prague, pp. 1 - 23, 2000.

J. S. Kain, "The kain-fritsch convective parameterization: an update," *Journal of Applied Meteorology*, Vol. 43, No. 1, pp. 170 - 181, 2004.

L. Alexander, X. Zhang, T. Peterson, J. Caesar, B. Gleason, A. Klein Tank, M. Haylock, D. Collins, B. Trewin, F. Rahimzadeh, *et al.*, "Global observed changes in daily climate extremes of temperature and precipitation," *Journal of Geophysical Research: Atmospheres*, Vol. 111, No. D5, 2006.

Mahtab F., Effect of climate change and sea level rise on Bangladesh. Expert Group on climate change and sea level rise, Commonwealth Secretariat, London, UK, 1989.

MoEF., Bangladesh Climate Change Strategy and Action Plan 2008. Dhaka, Bangladesh: Ministry of Environment and Forests, Government of the People's Republic of Bangladesh. 2008.

P. Frich, L. V. Alexander, P. Della-Marta, B. Gleason, M. Haylock, A. K. Tank, and T. Peterson, "Observed coherent changes in climatic extremes during the second half of the twentieth century," *Climate research,* vol. 19, no. 3, pp. 193 - 212, 2002.

Pramanik M. A. H., Remote sensing applications to coastal morphological investigations in Bangladesh. PhD dissertation, Jahangirnagar University, Savar, Dhaka, 1983.

R. K. Pachauri, M. R. Allen, V. R. Barros, J. Broome, W. Cramer, R. Christ, J.A. Church, L. Clarke, Q. Dahe, P. Dasgupta, *et al.*, Climate change 2014: synthesis report. Contribution of Working Groups I, II and III to the fifth assessment report of the Intergovernmental Panel on Climate Change. IPCC, 2014.

Robine, Jean-Marie, Siu Lan K. Cheung; Sophie Le Roy, Herman Van Oyen, Clare Griffiths, Jean-Pierre Michel, François Richard Herrmann. "Death toll exceeded 70,000 in Europe during the summer of 2003". Comptes Rendus Biologies. 331 (2): 171–178, 2008. Doi: 10.1016/j.crvi.2007.12.001. ISSN 1631-0691.

S. Dash and J. Hunt, "Variability of climate change in India," *Current Science*, pp. 782 - 788, 2007.

S.-Y. Hong, Y. Noh, and J. Dudhia, "A new vertical diffusion package with an explicit treatment of entrainment processes," *Monthly weather review*, vol. 134, no.9, pp. 2318 - 2341, 2006.

Z. B. Rakib, "Extreme temperature climatology and evaluation of heat index in Bangladesh during 1981-2010," *PRESIDENCY,* vol. 2, no. 2, pp. 84 - 95, 2013.

Modelling potential green space for Shorea robusta using Geospatial Technology: Historical review, Problems and Solution

Dhrmendra Singh[1], Avtar Singh[2], Shyamal Baran Saha[3], Md. Shahjahan Ali[4] and Md. Shamim Hasan Bhuiyan[5]

[1]Indian Institute of Remote Sensing, ISRO, Dehradun, 248001, India
[2]Forest Survey of India, Dehradun, India
[3, 4]Bangladesh Space Research and Remote Sensing Organization (SPARRSO), Agargaon, Dhaka.
[5]Bangladesh meteorological Department, E-24, Agargaon, Dhaka

Abstract: Present study has been done to find out the solution of few of the basic issues (protection of existing forest resource, Expansion of forest area, species specific site model to improve plantation practices for obtaining the maximum probability of their success, and to identify the potential area of the afforestation and reforestation) of national forestry action programme (NFAP) and greening mission of India. To identify the possible ways to support activities taken under these programmes for their success, we had used scientific input and temperament in the geo-information and space technology domain. Shorea robusta (Sal species) has been taken as the key aspect in this study as it is the dominant vegetation type of the study area and largely support the need of local habitants. In providing livelihood to them the Sal species is facing severe problem of regeneration and health which would be more severe in near future if the appropriate actions has not been taken. The output of study provided as by the models shows locations and distribution of the potential areas that could be planted, location of the potential area (eligible land) for the plantation of the Shorea robusta, and area under different land use and land cover classes. 51% of the total study area is covered under the forest. Shorea robusta habitate has been modelled with the remote sensing-based information and its integration in geographic information system using multicriteria analysis and analytical hierarchy process (AHP) to obtain the information about eligible land for the plantation of shorea robusta. Out of total 40858.58 ha, 11506.58 ha (28.16%) area has been found eligible for the afforestation purpose. Validation of the model has shown its accuracy with respect to the distribution of the shorea robusta on the suitable area of the model. Shorea robusta species map required for this was generated by the spectral angle-based species mapping method from the Hyperion Hyperspectral data with an accuracy of 77%. The suitable as well as eligible area of the study site has potential for enhancing carbon sequestration, successful forest plantation, conservation of associate species of Sal, relocation of rear, endangered and threatened (RET) species sharing similar habitat and planning sustainable utilisation of available timber and non-timber forest products (Karhi patta, put-put etc.) related to the Sal habitat.

Key words: Sal, multicriteria analysis, Analytical hierarchy process, eligible land, potential green space.

1. Introduction

Forests in India, from the ancient time, have played significant role in social, economic and religious activities by providing fresh air and water, protection of soil from degradation, greenhouse gas reduction, timber and other forest products of economic worth, and mental satisfaction in the form of ethical beliefs. Especially in case of socioeconomic growth forest and related services plays major role. Percentage contribution of Forestry Sector to GDP for the year 1992 was estimated 1.40 which has decreased to 0.9 % in the year 2010. The percentage contribution of the forestry sector to primary sector is 43.81%. The value of goods and services provided by the forestry sector is estimated about Rs. 25,984.53 crores worth. Net of maintenance, repairs and other operational costs, the gross domestic product from the forestry sector comes to Rs. 23003.43 crores. Of the gross value, some 9.27% is industrial wood, 54.21% (largest percentage) is of fuel-wood, 15.91% is NTFP, eco-tourism is of 13.85% and carbon sequestration contribute 6.76% (MOEF, 2001 NFAP Report). All the statistics are showing the importance of forest in the economy of nation.

A total of 199 Million tonnes annual Household Fuelwood Consumption in India was projected for the year 2006 (NFAP report, MOEF, 2001) which was estimated about 216.42 million tonnes for the year 2010-2011 (FSI, ISFR,

2011) and hence it is obvious to be seen some impact on the forest. The impacts of fuelwood consumption have also been assessed at local scale (Singh *et al.*, 2005) as well as global scale (Joshi *et al.*, 1995; Ravindranath *et al.*, 2000; FSI, ISFR, 2011). From the above it has been observed that the existing forests cannot continue to meet their raw material requirements, therefore it is required to have forest plantation programme in scientific manner.

The need for forest plantation was realized as early as in the mid-nineteenth century. The first attempt of organized plantation in India was a teak plantation established in 1842 at Nilambur in Kerala, southern India, with the purpose to enrich the forests (Bapat and Phulari, 1995). Investments in the forestry sector have always been very low in India relative to the large amount of revenue generated from it. The low levels of investment in the forestry sector (including afforestation and logging) in the past resulted in low production as well as in less plantation and afforestation programmes. Emphasis was put on extracting maximum revenues from the forests, and little was done to restore degraded forests. After India's independence in 1947, planned tree plantation schemes began with the commencement of the first five-year plan (1951 to 1956). Government-owned forest plantation and Laws against cutting and marketing of trees make people and farmers feared in planting and selling trees (Kerr, 1997) which was possibly a negative impact of the governmental laws in conjunction with the cutting and selling of trees.

In 1976, the report of the National Commission on Agriculture called for investment in social forestry, including farm forestry, to meet the fuel wood and small timber needs of rural people (Government of India, 1976). During the sixth five-year plan (1980 to 1985), tree plantation programmes gained considerable momentum. Expenditure on tree plantations increased dramatically, from 1 073 million rupees (US$153 million) in the course of fifth five years plan (1974 to 1979) to Rs 9 260 million (US$780 million) during the 6th five years plan (1980 to 1985) (Indian Council of Forestry Research and Education, 1999). 6 million ha of public lands, including forest lands, were utilized for tree plantations during the period 1990 to 1996, with the distribution of more than 7 000 million seedlings among the people for planting on private lands (Indian Council of Forestry Research and Education, 1999). Most of the farm forestry programmes on private lands provided subsidies to farmers (Balooni, 1991) which boost the farm forestry programme in India. WIMCO's , a Poplar raising programme on private farmlands in the states of Uttar Pradesh, Haryana and Punjab in collaboration with the National Bank for Agriculture and Rural Development (NABARD) in the early 1980s was the beginning of the involvement of a business house in raising commercial plantation with the farmers participation (Banerjee and Balooni, 1997).

With population and burgeoning growth of economy, the gap between supply and demand of timber is widening. So, it is the time to consider tree investment programmes as a serious enterprise in India and action of WIMCO possibly was the first step toward this path. On seeing the positive results of WIMCO's poplar raising programme, the National Forest Policy of 1988 says that: "As far as possible, a forest-based industry should raise raw material needed for meeting its own requirement by establishing a direct relationship between the factory and the individuals who can grow the raw material". India's success in intensifying forest plantations, in term of area, has been remarkable. A total of 23.38 million ha. area has been covered under different schemes of tree plantation up to 1997-98 which was about 3.54 million ha. before 1980. The dramatic fourfold increase has been observed during 1980s (13.51 million ha.) as compared to the before. This increase in the forest plantation area would be the effect of national forest policy of 1988. If we consider current annual rate of planting (about 1.2 million ha.) it is possible to have greater percentage area under of total forest as compared to the present 23.81% given by FSI in ISFR 2011 which is not in fact. According to the NFAP report of Ministry of Environment and Forest (MOEF), 2001 the affective area of forest plantation practices has been estimated about 11.0 million ha. which was about 40 to 50 per cent of the total recorded and reported area covered under the forest plantation since last 4 decade. The assessment was based on the survival rate, stock density and growth. The mean annual increment (MAI) of forest plantation in India varies from about 2 cu.m/ha/ yr to 8 cu.m/ha/ yr for valuable timber species and for other fast growing species like Eucalyptus respectively. This is much lower than the other countries (varies from 10 cu.m/ha/yr to 50 cu.m/ha/yr and in certatin cases over 70 cu.m./ha/yr). These statistics shows that, the performance of forest plantations in India, in term of survival and growth is poor (MOEF, NFAP Report 2001). The possible causes of the above said problems are inadequacies in site-species matching and site selection, lack of proper maintenance, poor planting stock, lack of protection (from fire, grazing, diseases and pests), unavailability of trained staff and delay in fund allocation. In way to find the solutions of the above problems National Forestry Action Programme (NFAP) was launched in 1993 with the integration and amalgamation of 26 State Forestry Action Programmes. Five inter-related basic issues have also

been identified and these are the basis of the programme structure. (1) Protect existing forest resources, (2) Improve forest productivity, (3) Reduce total demand, (4) Strengthen policy and institutional frame work and (5) Expand forest area (MOEF, 2001, NFAP Report). In the same fashion National Mission for a Green India has been started to achieve (1) Forest plantation and its extension, (2) Enhancing carbon sinks (Enhanced annual CO2 sequestration of 50-60 million tonnes by the year 2020), (3) Adaptation of vulnerable species/ecosystems and forest dependant local communities to the changing climate by the government of India (MOEF, 2011).

In view of issues given by the Ministry of Environment and Forest (MoEF) under the NFAP for the failure of the plantation and survival and poor mean annual increment in the biomass of planted species due to Inadequacies in site selection and site-species matching, it is the prime requirement to have information and models about the species habitat and their distribution pattern in term of density. These models are being used as an important tool to address issues related to the research, biodiversity conservation and management (Guisan *et al.* 2006). As habitat selection depends both on site-specific characteristics, as well as on the characteristics of the landscape surrounding a particular site (Holland, Bert & Fahrig 2004; Guisan *et al.* 2006) the scale and coverage of the data should be appropriate (Levin 1992; Mark D. S. *et al.*, 2003; Wheatley & Johnson 2009) which has been considered carefully in present study by utilizing Landsat imagery (Smith M. D., 2003, Kushwaha *et al.*, 2000, 2002,). Geographic information system became ideal tool now a days which gives promising results for habitat modelling at spatial scale with the incorporation of the satellite remote sensing information's which helps in the biodiversity conservation, afforestation, natural resource management, decision making (Lang S. *et al.*, 2005; Edenius L. 2006; Joss B. N. *et al.*, 2008; Koblera A. *et al.*, 2005; Hossain M. S., 2010; de Lamo *et al.*, 2010; Anil S.Y., 2011) etc. Taking requirement for greening mission of India and applicability of GIS in habitat suitability evaluation present study has been done to assess potential green space for *shorea robusta* in part of Doon valley which would be beneficial in solving the plantation failure problem as identified by MoEF under NFAP.

2. Materials and methodology

2.1 Study area

Area under the proposed research work is the western part of Dehradun district of Uttarakhand state extending between latitude of 30 32 11.45 N to 30 17 35.27 N and longitude of 77 34 25.55 E to 78 09 48.05 E and covering an area of about 824Km^2. The study area contributes part of lower Shiwalik with subtropical type climate and some temperate region of Mussoorie hills. It is showing varied topography from undulating hills to flat or plane area. The elevation varies from 360 meter to 2350 meter above the mean sea level. Temperature varies from less than 1^{0}C during winter to more than 37^{0}C in summer. The mean temperatures generated by the Landsat ETM+ were showing the temperature variation from 1^{0}C to 28^{0}C which was almost same as the older temperature variability (mean annual temperature 27.50C and lowest recorded temperature 1.10C) reported by Champion and Seth in 1967. Monsoon sets in by the June and rains continue until the September month. Rainfall varies from 9mm (Lowest) in November month to 731mm (Highest) in August month and rarely 1500mm too. Soil of the area exhibit wide variability in texture, colour, stoniness, moisture, organic matter content, depth, water holding capacity, and cation exchange capacity due to parental material, physiographic setup, intensity of erosion, anthropogenic activities and other environmental factors. The *Shorea robusta* species is the dominant timber species in the moist tropical climatic condition and covers large part of the forest area. Other associates are *Terminalia alata, syzygium cumini, Anogeissus latifolia, Mallotus philippensis, Lantana camara, Accasia catechu, Bauhinia variegate, Dalbergia sisso, Morraya quanigaii, Ficus bengalensis, Ficus religiosa, Lagerstroemia parviflora, Adina cordifolia, Litsea glutinosa, Grewia elastic, Clerodendrum viscosum, Glycosmis pentaphylla* etc. In the temperate region the dominant species are Quercus leucotrichophora, Quercus glauca, Quercus floribunda, *Cedrus deodara* etc. with the associates *Thuja orientalis, Cupressus torulosa, Berberis vulgaris, Rhododendron arboretum , Abies pindrow, Gravia optiva, Agev americana* etc. Sub-tropical species *Pinus roxburghii* is also present at few places. Forest type of study area includes following categories: Moist Shiwalik Sal Forest (3C/C2a), Moist Bhabar Dun Sal Forest (3C/C2b), Dry Shiwalik Sal Forest (5B/C1a), Shiwalik Chir Pine Forest (9/C1a), Northern Dry Mixed Deciduous Forest (5B/C2), Dry Deciduous Scrub (5/DSI), Lower western Himalayan Temperate Forest (CI) etc.

2.2 Materials Used

Satellite Imagery of Landsat ETM+ sensor (2009) were used for the extraction of land use land cover. Digital elevation map of ASTER (30m resolution) ware used for the extraction of Slope, Aspect and elevation strata. Soil types map were collected and geo-referenced after scanning using rubber-sheeting method in ArcGIS software (Manchanda *et al.*, 2002). Mean temperature of the study area were estimated using Landsat ETM+ data of different year (for winter season only) with the calculation, combine and average approach. The image processing and GIS software utilised in the research work are Arc GIS 9.3, ERDAS 9.2 and ENVI 4.5. Survey of India toposheet was used as a reference data. GPS device Garmin72 were used for the ground verification and surveying. Hyperion EO-1 data based *Shorea robusta* species map (Singh *et al.*, 2014) has been used for the model validation. Ancillary data regarding the requirement of the climatic conditions for *Shorea robusta* species to contribute in its better survival were collected from the older documents, studies, publications and forest plan of the forest department (Champion and Seth, 1968, forest working plan Dehradun 1998-99 to 2008-09, Singh *et al.*, 2005). Simultaneously ground data regarding the Sal suitability (soil type, Slope, Aspect, Elevation, Temperature etc. within few patches of Sal) were also collected for verifying and comparing it with the data derived from space satellite as well as older records however rainfall data (very important layer in suitability analysis) was not available. The instruments used for ground data collection were Rain gage, compass etc. Forest type map of the study area was also considered equally important as the other database and used in the modelling of the suitability after overlaying it with the LULC map.

2.3 Methodology

2.3.1 Land Used Land Cover

ERDAS Imagine and Arc-GIS 9.3, were used for the extraction of land use land cover classes. The required data for the present study were first geocoded in the common coordinate system UTM WGS 84 zone 44. The ground data have been collected by using required instrument for the purpose of comparison with the satellite driven data and formation of criteria functions and rules (table a and b). Landsat ETM+ of 2009 was used for the land use land cover extraction. The unsupervised, iterative self-organised data (ISODATA) classification approach (Ball, G. H. *et al.*, 1965) has been used for classifying the satellite imagery with the integration of visual interpretation and manual editing (FSI, ISFR 2011). ISODATA unsupervised classification approach first calculates class means evenly distributed in the data space then iteratively clusters the left over pixels using minimum distance to mean technique (Tou, J. T., 1974).

2.3.2 Habitat Suitability Modelling

As the Sal (species) is distributed from tropical to subtropical climatic conditions its ecological amplitude is very high. The rule and criteria for the habitat evaluation varies greatly as the considered ecological factors showing much variability. The sets of criteria to evaluate the habitat of the Sal (*Shorea robusta*) are given in table 1 (literature based ranges and variability) and table 2 (satellite derived information as a key factor for the species habitat suitability).

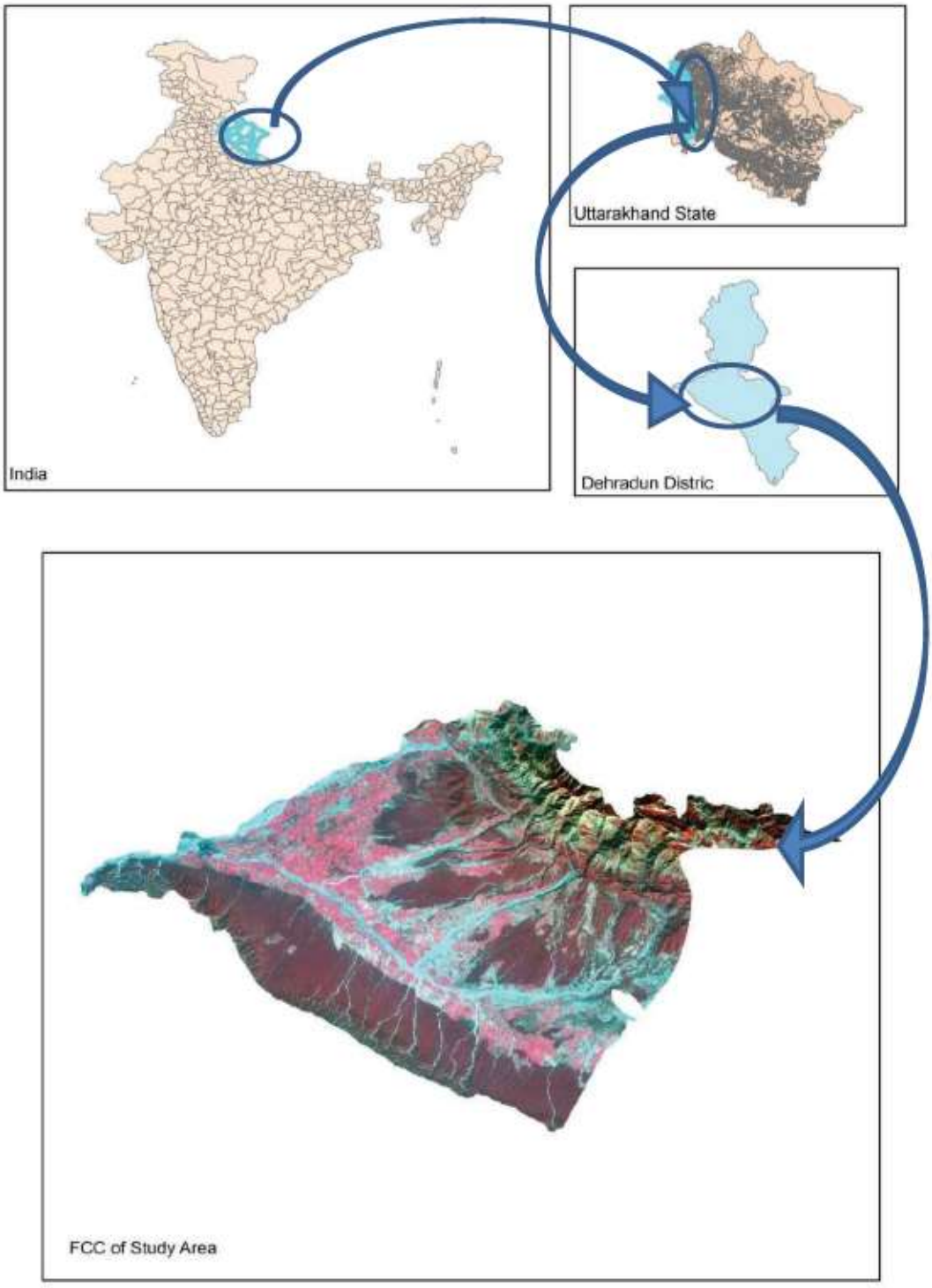

Fig.1: Showing Study Area with the FCC

2.3.2.1 Database Creation

For the modelling of Sal habitat suitability the layers and database required are as follows- Soil Type, Elevation, Slope, Aspect, Land use and Land cover map, Forest type map (FSI), Temperature (for winter season), and Rainfall map (not available for the present study). The soil type map was generated by taking reference of Manchanda *et al.* 2002. Soil type map was scanned and saved in the Geo-tiff file format. Rubber sheeting approach for the geo-

referencing has been used, taking the Landsat imagery of the study area as a reference. As the soil forms the base for any type of vegetation the soil type map has been considered most important data base in this study. Elevation map was obtained from the ASTER digital elevation model (30 meter resolution) which has been further used for the generation of the slope and aspect. Based on elevation database from satellite, ground and older records the highly suitable elevation for the Sal has been found from 400 meter to 700 meter.

Table 1: Rules/criteria for Sal habitat modelling in the part of Dehradun District from different sources.

Variation in Environmental Factors and Ecological Amplitude of *Shorea robusta* species (as per Champion and Seth, 1968, Singh *et al.* 2005, Manchanda *et al.* 2002, Forest Survey of India, 2012, Ground Survey Data, Forest working plan 1998-99 to 2008-09 & 2007-08 to 2017-18)	Slope	Aspect	Elevation	Soil Types	Temperature	Rain Fall
	<19.4^0 (some time may exceed to 45^0 or more)	All aspect	350-1500m	Alluvial, Fragmental Typic Udorthents, Loamy skeletal Typic Udorthents, Fine loamy Mollic Hapludalfs, Fine loamy Typic Argiudolls, Fine loamy Mollic/Typic Hapludalfs, Loamy skeletal Dystric Eutrochrepts, Fine loamy Typic Hapludalfs, Fine loamy Dystric Eutrochrepts, Fine loamy Mollic Hapludalfs, Fragmental Lithic Udorthents, Loamy skeletal Typic Udorthents, Loamy skeletal Dystric Eutrochrepts.	13^0-25^{0}C (may exceed more than 35^{0}C for hot area and summer months)	9mm-1500mm

The aspect in area does not have any effect on the distribution of the Sal so it has been taken same for the all suitability classes. Highly suitable temperature was varied from 13-15^{0}C, slope 2.8-10^0, forest type Moist shiwalik Sal forest (Champion and Seth, 1968, FSI, 2012).

Temperature map was generated from the Landsat TM using ERDAS imagine satellite data processing software. Thermal band 6 (10.4-12.5 μm) were used for surface temperature retrieval using following expressions given by Markham and Barker (1986).

$Ts = K2 / \ln (K1 / L6) + 1$

$K1 = 60.776$ (W/m2/Sr)

$K2 = 1260.56$ (K) and

$L6 = I\,min + (Imax - Imin / DNmax) * DNact$ (Rao *et al.*, 2009)

DNact is the actual digital number of the input pixel, Imin and Imax are the offset values, DNmax is the maximum possible digital number and L6 is the spectral radiance (it is corrected for the atmosphere, the temperature represents an estimate the ground-based radiometric temperature) (W/m2/Sr) of thermal band.

Although the rainfall data is of immense importance in this study its unavailability for the study area was problematic. However other dataset has compensated the lack of this data, principally the forest type which have been prepared by using the rainfall data as a layer with the other additional layers during the forest type mapping (FSI, 2012). All these layers have been geo-referenced in UTM WGS84 Zone 44 with reference to the Landsat Imagery for the multi-criteria analysis.

2.3.2.2 Multicriteria Analysis for Habitat evaluation

Four categories were decided to be identified in the study area namely highly suitable class, suitable class, less suitable class and not suitable class. Related database categorised and prioritized for the multi-criteria analysis (table 2). Analytical hierarchy process (AHP) method (Saaty T. L., 1977) was applied in the multi-criteria analysis to assign the weightage for each factor (Anselin *et al*., 1989). Habitat modelling of the *Shorea robusta* using different database and information's related to the key habitat factors (Kushwaha *et al*., 2002) derived from satellite platform and ground would be beneficial in the sustainable utilisation and management of this species. But the major issue is to combine all these factors and criteria together to obtain the area with the sustainability of key factors for the particular species. First of all the generated data's were divided in to the homogenous cover type. Next to this the data for the habitat modelling were multiplied with the weights derived from the Analytical hierarchy process. Addition of all these maps in the ArcGIS environment provides the desired output in the form of habitat model.

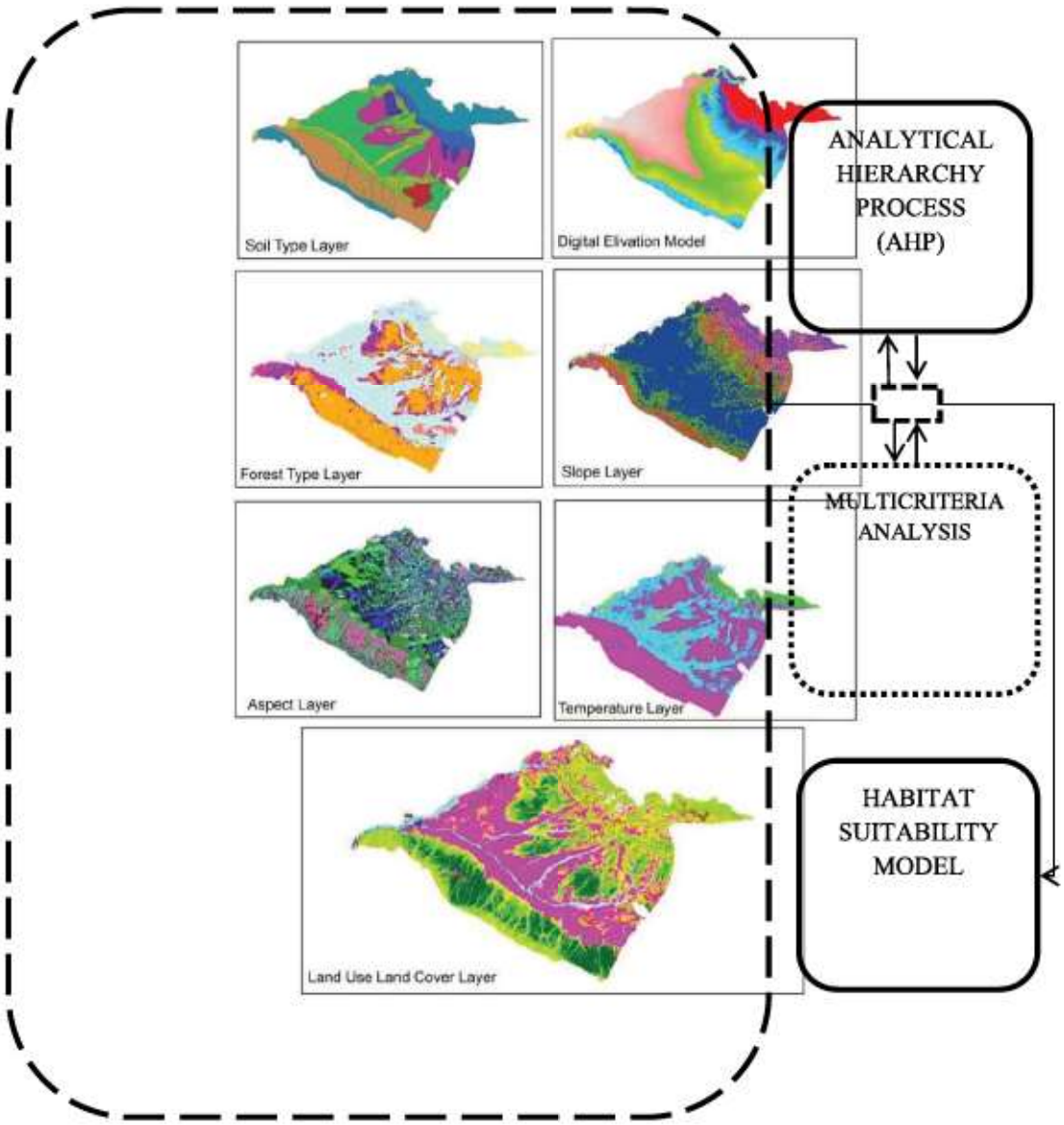

Fig. 2: Layers used for the Modelling and flowchart of methodology

2.3.2.3 Analytical hierarchy process

As our aim is to combine all these criteria and ecological factors with deferent weights, Saaty's scale of relative importance could be potential approach to derive above said purpose (Kushwaha *et al.*, 2002). Analytical hierarchy process is a theory-based decision-making approach and deals with complex, technological, socio-political and economical issues and presently best available method for multicriteria except few criticisms (Kushwaha *et al.*, 2002 Prabu S. *et al.*, 2009, Al-Harbi K. M. A. 2001). It allows both subjective and objective elements in picking up the best alternative (Prabu S. *et al.*, 2009). Firstly, all the data were arranged and prioritized according to the key factors and the best range for the species survival. Then criteria are being set by the theoretical knowledge about the *Shorea robust* habitat and saaty's measurement scale of relative importance (table 3) to obtain weight. Criteria for highly suitable and suitable class based on the slope have been taken same (table 2) as both these classes are of equal importance for the next benefit of this model.

Saaty's Measurement Scale of relative importance for Factor Prioritization

Saaty's measurement scale and the values are specified below:
1 = equal importance, 2= between equal importance and week importance, 3 = week importance, 4= between week importance and essential or strong importance, 5 = essential or strong importance, 6= between essential or strong importance and demonstrated importance 7 = demonstrated importance, 8 = intermediate values between demonstrated importance and absolute importance and 9 = absolute importance.

Table 2: Criteria and Rules for suitability classes of *Shorea robusta* on study site

Class/Factors	Soil Type	Elevation (meter)	Temperature (^{0}C) in winter	Slope (^{0})	Aspect	LULC and Forest type
Highly Suitable	Alluvial categories like Fragmental Typic Udorthents, Loamy skeletal Typic Udorthents, Fine loamy Mollic Hapludalfs, Fine loamy Typic Argiudolls	400-700	13-15	2.8-28.70	all	Forest area and cultivable wasteland, Moist Siwalik Sal Forest
Suitable	Fine loamy Typic Hapludalfs, Fine loamy Dystric Eutrochrepts, Fine loamy Mollic Hapludalfs,	700-800	15-18	Similar to the highly suitable class	all	Forest area, wasteland and forest blank, Dry Siwalik Sal Forest
Less Suitable	Fine loamy Mollic/Typic Hapludalfs, Loamy skeletal Dystric Eutrochrepts,	<400, and >800 but less than 1000	>18	<=2.8	all	Land for agroforestry, Agricultural land, other forest types
not Suitable	Other soil type present in study area	>1000	1-12	>28.70	all	Settlements, Dry River bed, water.

Table 3: AHP generated weight assigned to each layer type given in table c. Class names are arranged according to the ranking of the layers from left (1) to right (7)

Class Name	Soil Type	Elevation	Forest cover Type	Slope	Aspect	Temperature	Other LULC Classes
Weights	0.30	0.26	0.17	0.11	0.08	0.05	0.03

2.3.2.4 Model Validation

Till date the model developed by the multicriteria analysis were not validated or validated by ground method only. In the present study we had done it with the different approach which was based on the satellite gained information. The final validation of the generated Habitat Model has been done through the species map (77% accurate) generated from the Hyperion Hyperspectral Data (Singh *et al.*, 2014) using ground spectral response of the *Shorea robusta* and a valid classification algorithm the Spectral Angle Mapper (SAM). The spectral response of the *Shorea robusta* was obtained using analytical spectral device during the reconnaissance survey. Atmospherically corrected Hyperion imagery with 156 bands (spatial resolution 30m) was classified using SAM algorithm. This map was used for the validation of the habitat model taking a view in mind that highly suitable or suitable class of the model would have the similar species on the species map also.

2.3.2.5 Area estimation of potential and eligible space for planting Shorea robusta

The validated model of the shorea robusta habitat was binary coded. The code for suitable class was 1 (including highly suitable class and suitable class) and for not suitable class was 0 (including less suitable class and not suitable class). This was finally matrixes with the binary coded land use land cover (scrub, open forest, moderately dense forest, wasteland, forest blank etc. was coded as 1, rest classes were coded as 0) which provide the information about potential space and its distribution for the greening purpose. Area of the potential space for the greening mission and its percentage was analysed later.

3. Result and Discussion

3.1 Land Use land Cover

A total of 9 land use land cover class say for Very Dense Forest (VDF), Medium Dense Forest (MDF), Open Forest (OF), Scrub Forest, Non-Forest (NF), Agriculture (AG), Settlement (ST), Water and Dry River Bed were mapped in the area with an accuracy of 80% (Fig. no.3). Out of them Non-Forest, Scrub and Open Forest were considered as treatable area for the greening purpose. The areas under different classes have been given in the table 1. The percentage distribution has been given in the pi-chart (Fig. 4) which is showing that larger part of the area is covered under the forest (about 55%) and agricultural (about 28%) classes. Other classes contribute less.

Table 1: Showing area coverage under different land use/cover classes.

Lans Use Classes	Area (ha.)	Percentage Area
VDF	13432.90	16.31
MDF	15727.91	19.10
OF	16297.69	19.79
SCRUB	3652.88	4.44
AG	23383.35	28.39
ST	986.75	1.20
WATER	448.59	0.54
DRY RIVER BED	4857.87	5.90
NF	3574.43	4.34

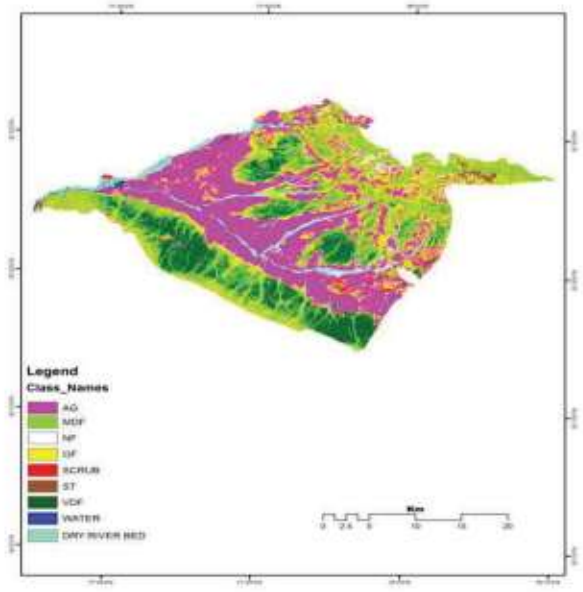

Fig. 3: Land use land cover with forest density classes

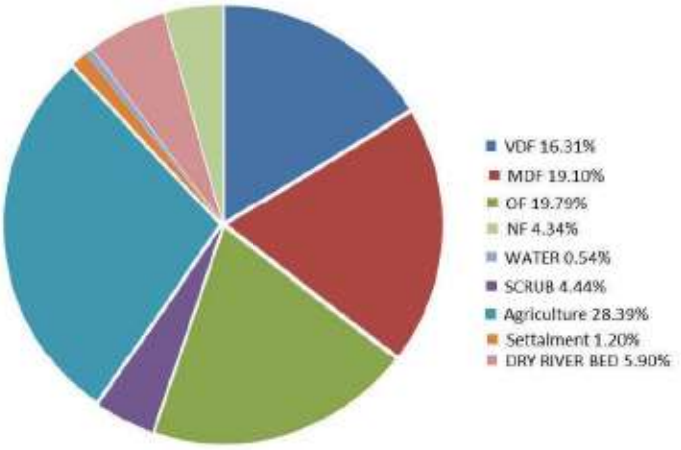

Fig. 4: Percentage area distribution of different land use/cover classes.

3.2 Habitat Suitability Map for Sal Species based on Multicriteria Analysis

Habitat suitability map (Fig. 4) of the Sal species is categories in the four classes. These are Highly Suitable, Suitable, Less Suitable and Not Suitable. Area under different suitability classes are given in table 2 and its pie chart distribution in figure 6. The highly suitable class with the suitable class were used for the estimation of area which could be used for the plantation purpose. The area under these two categories was covering about 49% of the total area. The open forest, Scrub, and non-forest area has been combined with the suitability classes (Highly suitable and Suitable categories) using matrix function which gives the potential area for the afforestation or greening, with the *Shorea robusta* species. Total area of different land use land cover classes under the suitable site were estimated and tabulated in the table 3. Total estimated area of the treatable class has given in the table 4.

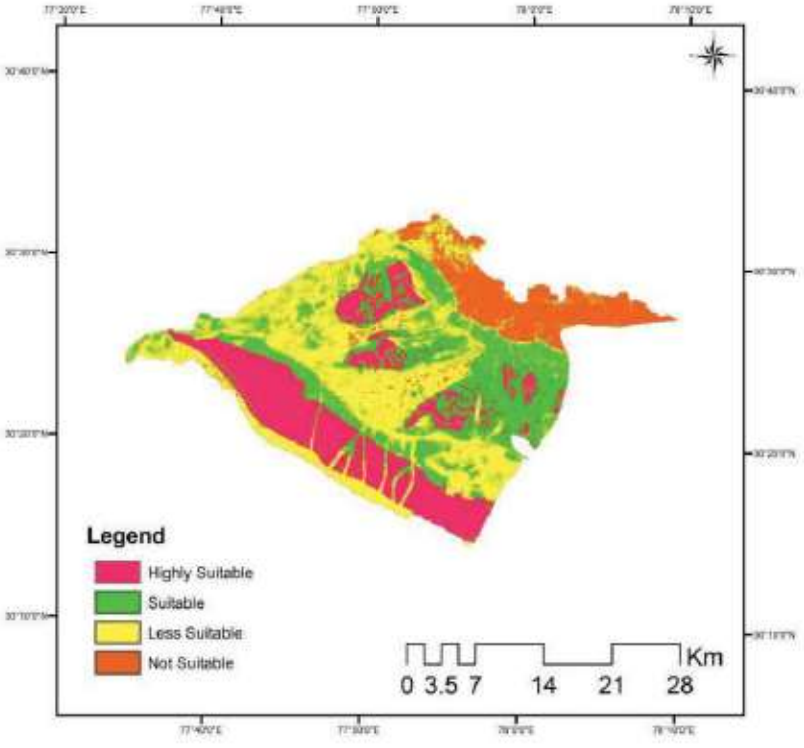

Fig. 5: Habitat Suitability Map of the *Shorea robusta* species

Table 2 Showing Area of different suitability classes in ha. with their respective percentage

Suitability classes	Area (ha.)	Percentage (%)
Highly Suitable	20821.22	25.28
Suitable	20037.73	24.33
Less Suitable	30417.57	36.93
Not Suitable	11085.83	13.46
Tatal Area	82362.36	100.00

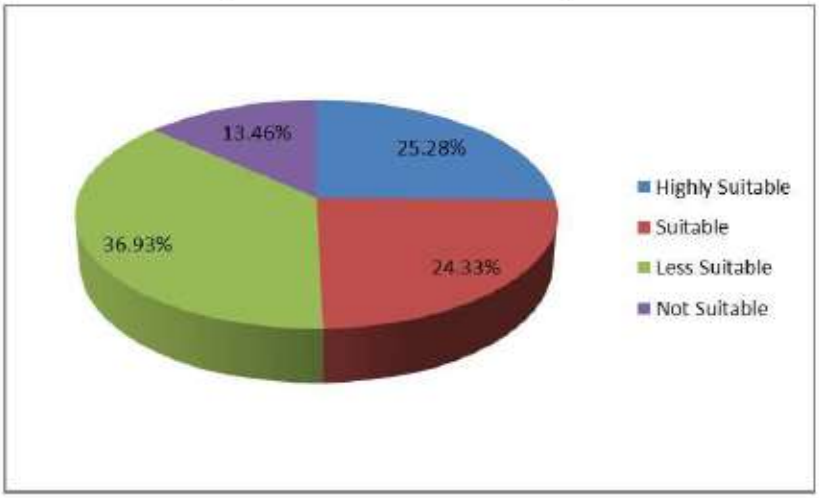

Fig. 6: Percentage area distribution of different suitability classes

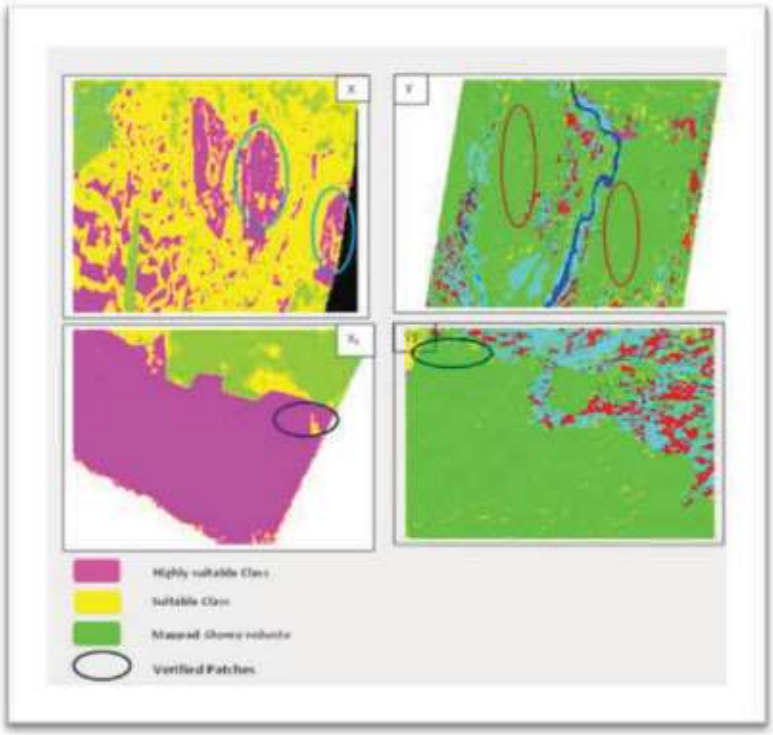

Fig. 7: Verified Habitat Model of Sal with respect to Hyperion generated Species map (X, X1 Showing Habitat Model, and Y, Y1 Showing Species map indicating same geo-location)

3.3 Model Validations

3 different patches of Habitat model those were showing high suitability (Fig.7, X and X_1) have been observed on the species map (Fig.7, Y and Y_1) derived from Hyperion EO-1 hyperspectral data in ERDAS imagine software environment using cursor location option. Highly suitable classes were showing pure patches of the *Shorea robusta* on the species map. In this way we have find that the *Shorea robusta* habitat model is valid and the final output would be effective in the plantation programmes too.

3.4 Potential Carbon sequestration site or Potential Green Space for Shorea robust species

Afforestation practices could be done on the land where the forest is of less density (open forest and scrub) or there is cultivable non forest area and these may be called as Potential Carbon sequestration site. These areas were identified using the evaluated and validated model of the *Shorea robusta* species. Total of 11506.58ha (28.16%) suitable area has been identified as the eligible land (having the properties like forest with poor density, cultivable open area, and species specific suitable environmental conditions) for the afforestation purpose out of 40858.95ha total suitable land (Fig. 7). Although the agricultural lands too, were found suitable for the afforestation with the *Shorea robusta* species in the generated habitat model, the practice is unrealistic from the legal point of view. In this case the public participation and their awareness towards the benefits of the afforestation would be the possible solution.

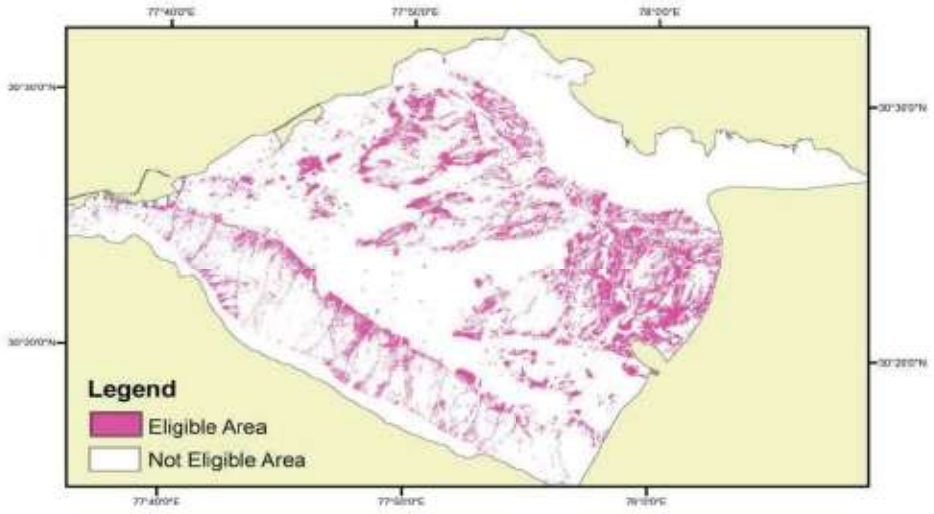

Fig.7: Eligible and not eligible area for the afforestation purpose

3.5 Plant Allocation

Total suitable or eligible area estimated as potential green space in part of Doon valley is 11506.6 ha as per the assessment of land use land cover using satellite imagery of the year 2009 and multi-criteria analysis. The estimated number of plants in this area with a gap between plants about 5 meter is 4.6 million 2 thousand 6 hundred 40 plants. The other associates of this species could be planted along with it.

4. Conclusion

The resulting maps would be used for the potential green space utilization. Simultaneously the specific species at specific site concept would increase the possibility of successful plantation practices. Another benefit of this research work is in the sustainable utilisation and management of the *shorea rpbusta* species and related forest products like karhi patta, Put-Put etc. Relocation sites for the RET species those are associated with the *Shorea robusta* species to ensure their conservation and management could also be identified and suggested as per requirement. The technology like remote sensing and geographic information system have extreme potential to identify the forestry related

problems and their solutions. Distribution map of the potential carbon sequestration site would be utilised to enhance the forest quality with respect to the coverage and density. Correct area estimation of such category would be helpful in the proper planning of the afforestation practices and valuation of the total cost for these activities. This will help in the money allocation for the afforestation purpose. Government can easily identify the area to be considered most for afforestation purpose and can estimate the cost required. Reducing greenhouse gases, efficient carbon sequestration, climate change mitigation, clean development mechanism (CDM), REDD and REDD+ are the promising areas where the products of this study could be used efficiently. So, the present research is beneficial for the society with respect to health, reduced effort and economy, simultaneously with the consideration of biodiversity conservation and climate change mitigation.

Acknowledgement

The authors place on record their sincere thanks to Director, Indian Institute of Remote Sensing, Dehradun, Dr. Sunil Chandra Forest Survey of India, Dehradun, Prof. Dr. Lakshmi Rawat, Head, Forest Ecology and Environment, Forest research Institute (Deemed University) Dehradun for their encouragement, support and guidance. We also express our gratitude to Dr. U. K. Chauhan, head Environmental Biology, APS University Rewa for her valuable encouragement. Global land cover facility, USA is gratefully acknowledged for the data products used in the study along with the other data sources.

References

Al-Harbi K. M. A. (2001). Application of AHP in project management. *International journal of project management*. Vol. 19, pp. 19-27.

Anil S.Y.; Anil S.Y.; Punam R. and Patekar, R.S. (2011)." Habitat Suitability Modeling For Great Indian Bustard (GIB) In Solapur District; A Geoinformatics Approach, ESRI India conference.

Anselin, A.; Meire P.M. and Anselin L. (1989). Multicriteria techniques in ecological evaluation: an example using the analytical hierarchy process. *Biological Conservation* Vol. 49 pp. 215-229.

Ball, G. H. & Hall, D. J. (1965) Isodata: a method of data analysis and pattern classification, Stanford Research Institute, Menlo Park, United States. Office of Naval Research. Information Sciences Branch.

Balooni K., 2000. Teak investment program an Indias Prospective. FAO corporate document repository, page 83, Vol. 51.

Balooni, K. 1991. An evaluation of social forestry programme in Himachal Pradesh. Solan, India, College of Forestry, Dr Y.S. Parmar University of Horticulture and Forestry. (M. Sc. Thesis).

Banerjee, S. & Balooni, K. 1997. Poplars replacing eucalyptus in Haryana - its ecological and economic implications. Bhopal, India, Indian Institute of Forest Management.

Bapat, A.R. & Phulari, M.M. 1995. Teak fruit treatment machine - a prototype - II. *Indian Forester*, 121(6): 545-549.

Champion H.G. & Seth S.K. (1968). A Revised Survey of the forest Types of India (Reprint, 2005), pp. 122.

Chopra K.; Bhattacharya, B. B. & Kumar, P. (2001). Contribution of Forestry Sector to Gross Domestic Product (GDP) in India. Chapter 1-6.

de Lamo, Xavier, Patenaude, Genevieve, 2010;" Mapping red squirrel (Sciurus vulgaris) habitat suitability using GIS and remote sensing techniques", Edinburgh Research Archive.

Edenius L. & Mikusiński G. (2006). Utility of habitat suitability models as biodiversity assessment tools in forest management. *Scandinavian Journal of Forest Research*. Vol 21 pages 62-72.

Government of India (1976). Report of the National Commission on Agriculture, Part IX. Forestry. New Delhi, India, Ministry of Agriculture and Cooperation.

Guisan, A.; Lehmann, A.; Ferrier, S.; Austin, M.; Overton, J.M.C.; Aspinall, R. & Hastie, T. (2006) Making better biogeographical predictions of species' distributions. *Journal of Applied Ecology*, 43, 386–392.

Holland, J.D.; Bert, D.G. & Fahrig, L. (2004) Determining the spatial scale of species' response to habitat. Bio Science, 54, 227–233.

Hossain, M. S. & Das N. G. (2010). GIS-based multi-criteria evaluation to land suitability modelling for giant prawn (Macrobrachium rosenbergii) farming in Companigonj Upazila of Noakhali, Bangladesh. Computers and Electronics in Agriculture. Vol 70, pages 172-186.

Indian Council of Forestry Research and Education (1999). Forestry Statistics India, 1996. Dehra Dun, India.

Joshi, V. & Sinha, C. S. (1995). Energy use in the rural areas of India; setting up a rural energy data base. Biomass and bioenergy. TERI, New Delhi.

Joss B. N.; Hall R. J.; Sidders D. M. & Keddy T. J. (2008). Fuzzy-logic modeling of land suitability for hybrid poplar across the Prairie Provinces of Canada. *Environmental Monitoring and Assessment.* Vol.141, pages 79-96.

Kerr, J.M. (1997). Market failures in natural resource management. In J.M. Kerr, D.K. Marothia, K. Singh, C. Ramasamy & W.R. Bentley, eds. Natural resource economics - theory and application in India. New Delhi, India, Oxford & IBH Publishing.

Koblera A.; Cundera T. & Pirnatb J. (2005). Modelling spontaneous afforestation in Postojna area, Slovenia. *Journal for Nature Conservation*. Vol. 13, pages 127-135.

Kushwaha S.P.S & Roy P.S. (2002). "Geospatial technology for wildlife habitat evaluation". *Tropical Ecology* Vol., 43(1), pp. 137-150.

Kushwaha S.P.S; Roy P.S.; Azeem A.; Boruah P. & Lahan P. (2000)." Land area change and Rhino Habitat suitability analysis in Kaziranga National park, Assam", Tigerpaper Vol. XXVII: No.2.

Lang, S. & Langanke, T. (2005). Multiscale GIS tools for site management. *Journal for Nature Conservation*. Vol. 13, pp. 185-196.

Levin, S.A. (1992) The problem of pattern and scale in ecology. Ecology, 73, 1943–1967.

Manchanda, M. L.; Kudrat M. & Tiwari A. K. (2002). "Soil Survey and Mapping using remote sensing. *International society for tropical ecology* (ISSN 0564-3295).

MOEF (2001). National Forestry Action Programme India, Forest plantation. Volume 1: status of forestry in India, Volume 2: Issues and programmes. .http://envfor.nic.in/nfap/forest-plantation.html.

MOEF (2011). National Mission for A Green India under the National Action Plan on Climate Change. pp. 1-16.

Prabu, S. & Ramakrishnan, S. S. (2009). Combined use of socio-economic Analysis, Remote sensing and GIS data for Landslide Hazard Mapping using ANN. *Journal of the Indian society of Remote Sensing*. Vol. 37, pp. 409-421.

Rao, K. H. V. D.; Singh, A. K. & Roy, P.S. (2009). Study of morphology and suspended sediment of Bhopal upper lack using spatial simulation technique and remote sensing data. *Journal of the Indian society of Remote Sensing*. Vol. 37, pp. 433-441.

Ravindranath, N.H.; Murali, K.S.; Murthy, I.K.; Sudha, P.; Palit, S. and Malhotra, K.C. (2000), ``Summary and conclusions'', in Ravindranath, N.H., Murali, K.S. & Malhotra, K.C. (Eds), Joint Forest Management and Community Forestry in India: An Ecological and Institutional Assessment, Oxford and IBH, New Delhi, pp. 279-318.

Singh, I.J.; Jugran, D.K.; Thanruma, S. & Reddy, S.R. (2005). Forest resource Assessment in mohand forest range, Uttar Pradesh Using Remote Sensing and GIS, *Journal of the Indian Society of Remote Sensing*, Vol. 33, pp. 565-574.

Singh, D., Kumar, V. and Singh S. (2014). Classifiers Ability in Targeting Species from Hyperspectral Images. Accepted for Publication in ICOL 2014 at Dehradun.

Smith M. D. & Burger L. W. Jr. (2003)." Multi-resolution approach to wildlife habitat modeling using remotely sensed imagery", Proceedings of SPIE Vol. 5153 (SPIE, Bellingham, WA).

Tou, J. T. & Gonzalez, R. C. (1974). Pattern Recognition Principles, Addison-Wesley Publishing Company, Reading, Massachusetts.

Wheatley, M. & Johnson, C. (2009). Factors limiting our understanding of ecological scale. *Ecological Complexity*, 6, 150–159.

Monsoon Rainfall Trend over Bangladesh and Tele-connection with Southern Oscillation Index (SOI) and Indian Ocean Dipole (IOD)

[1]Khadija Khatun, [2]Md. Bazlur Rashid,[3]Fahad Bin Mostafa and Md. Sanaul Haque mandal[2]
[1,3]Department of Applied Mathematics, University of Dhaka, Dhaka-1000
[2]Bangladesh Meteorological Department, Agargaon, Dhaka-1207, Bangladesh

Abstract: Monsoon rainfall patterns of all over Bangladesh as well as seven divisions of the country have been studied from 1981-2015 using non-parametric Mann-Kendall test. Changes of Rainfall variability with monthly El Nino Southern Oscillation (ENSO episode) and Indian Ocean Dipole (IOD); observed using mean ENSO and IOD index. In this research, our observation reveals, average monsoon rainfall has increased overall the country with a rate of $0.2mm/year(20mm/dec)$, 4.5mm/year at Khulna, 1.8mm/year at Chittagong, 0.24mm/year at Dhaka and 2.5mm/year at Rangpur. Each of them is statistically significant, except Dhaka division. Decreasing monsoon rainfall was over Barisal, Rajshahi and Sylhet divisions but these were not statistically significant. This study also revealed that, monsoon rainfall of all over the country and location wise were statistically significant and negative correlation with SOI index except Rajshahi and this correlation start February/march and continue at month of August. It was seen that moderate correlation southern part of Bangladesh and little bit rest part of country. Here also, observed that positive correlation with IOD index was seen at southern part of Bangladesh but no correlation with northern part of the country. This correlation starts at month of May till continue month of September. Our research project that, ENSO and IOD events may influence the future climate pattern of Bangladesh and co-inducing of these phenomena may repress their control.

Keywords: Climate of Bangladesh, Non-parametric Test, Climate Change, SOI and IOD index

1. Introduction

Climate of Bangladesh is considered by high temperature, heavy rainfall, often excessive humidity, and fairly manifested seasonal variations as well as the reversal of the wind circulation between summer and winter, which is vital part of the circulation system of the South Asian subcontinent. Bangladesh has a subtropical monsoon climate characterized by wide seasonal variations in rainfall, moderately warm temperatures and high humidity. The climate of this country can be described under four seasons:Winter or Northeast Monsoon (December – February), which is categorized by very light northerly winds, mild temperature and dry weather and clear to occasionally cloudy skies with fog over the country and the mean temperature is in the range of 18-22°C; Summer or Pre-Monsoon (March-May),the mean temperature during the summer months remains within 23-30°C, April and May are the hottest months and the highest maximum temperature ranging from 36-40°C is managed in the north-western and south-western districts; Southwest Monsoon (June-September), in this season, the surface wind changes to south-westerly/southerly direction over the southern and the central districts and to south-easterly over the northern districts of the country, rain with extensive cloud cover and high humidity are the features of this season, more than 71%of the total annual rainfall occurs in this season; Autumn or Post-Monsoon (October-November), this is the transitional season from summer monsoon to the winter, rainfall declines considerably in October and November and the dry period starts setting in over the country, only8 % of the total annual rainfall occurs in this season. The highest amount of average annual and monsoon rainfall has designed Bangladesh relative to south Asian countries; studied by SMRC (2006).

The intergovernmental panel on Climate (IPCC, 2007) said that Bangladesh may experience five to six percent increase in precipitation by the year of 2030. GCM model was studied by Nandan *et al.* (2011); which predicted that rainfall will increase by eight percent in 2050. Increase of annual and pre-monsoon rainfall of Bangladesh were also observed in the study of Shahid S. (2009), who assessed spatial patterns of rainfall trends of Bangladesh by using rainfall data of 50 years (1958-2007) recorded in seventeen rain gauge stations. In that study, spatial pattern of rainfall trends showed increase in annual, monsoon and pre-monsoon precipitation in the western part of Bangladesh, but the maximum rainfall increase was recorded in the northern part of Bangladesh by 16.45 mm/year at 99% level of statistical significance. Furthermore, Hasan *et al.* (2014) studied trend analysis of rainfall of 63 years (1949-2011) of the southeast costal part of Bangladesh; found that rainfall has increased during the time of pre-monsoon. An important increment of rainfall trend in whole Bangladesh found in the study of Ahmed Md. K. *et al.* (2016) where they used 64 years of rainfall data during1948-2012.Recently, in the study of Khatun *et al.* (2017) showed a significant increasing trend in rainfall in whole Bangladesh used rainfall data during 1981-2015.

Sea Surface Temperature (SST) of Bay of Bengal has increased and the increment of SST due to enhanced convection results the increase of rainfall all over the Bangladesh according to Kan *et al.* (2000). Singh *et al.* (2000) studied that SST of Bay of Bengal is significantly influenced by ENSO events. SST anomalies are interconnected with ENSO. Monthly and Annual rainfall trend may be significantly influenced by ENSO warm (El Nino) and Cool (La Nina) Phases.

Due to the positivity of Southern Oscillation index (SOI), the lower atmospheric pressure prevails from Australia to India but on the other side such as eastern tropical pacific-ocean prevail higher pressure (Walker and Bliss, 1932). Atmospheric circulation of Australian region becomes easterly (Glantz *et al.*, 1991) and as a result, huge volume of moisture is transported westward into the Bay of Bengal causing heavy rainfall and flood. In case of the negativity of SOI, the result will be opposite; in the upper troposphere winds in the Western Pacific are westerly and moisture is transported northward or north-eastward decreasing rainfall in Bangladesh and resulting either rain deficit or drought (Chowdhury MR, 2003).

The Indian Ocean Dipole (IOD) is well-defined by the difference in SST between two areas or poles- a western pole in the western Indian Ocean (in the Arabian Sea) and an eastern pole in the eastern Indian Ocean south of Indonesia. Similar to ENSO, IOD may have lonely connection with the rainfall in Bangladesh and its spatial region. Han and Webster (2002) and Hashizume *et al.* (2008, 2011) reported that the IOD events strongly influence flooding in Bangladesh. In the study of Ahmed Md. K. *et al.* (2016), observed that there is no tele-connection of ENSO with annual rainfall and monsoon rainfall but IOD has a connection with monsoon rainfall of western part of Bangladesh, where long term data covering period 1948-2012 were used. In the study of Khatun *et al.* (2017) showed that post-monsoon rainfall illustrated a significant positive correlation with ENSO index and negative correlation with IOD data. Mishra K. K. *et al.* (1991) has done statistical analysis on rainfall in a particular part of India. Furthermore, Sunderson M. *et al.* (1979) has been done research on pre-monsoon rainfall its variability on Bangladesh. Then (Ahsan *et al.*, 2010) has investigated the trend as well as variability of summer monsoon rainfall over whole Bangladesh.

In the present study, the variability of monsoon rainfall of Bangladesh is analyzed using thirty-five years (1981-2015) data to detect the monotonic trend and its magnitude using Non-parametric Mann-Kendall test (Mann, 1945; Kendall, 1975). Moreover, the correlation between ENSO and IOD with variability of monsoon rainfall in respect of overall Bangladesh and its seven divisions has been scrutinized by using statistical software 'R'.

2. Sources of Data

Bangladesh meteorological department (BMD) is the authentic source of these rainfall data. Monthly scales data are available in BMD. For this purpose, thirty-five years accumulation data on daily rainfall in mm are obtained from 35 rain gauges all over Bangladesh from BMD from the year 1981 to 2015. We classified the rainfall data into nine monthly sets from January to September. For the correlation, the sources of SOI and IOD data were www.cpc.ncep.noaa.gov/data/indices/soiand and

http://www.jamstec.go.jp/frcgc/research/d1/iod/e/index.html

3. Methodology

In the trend analysis, parametric and non-parametric both are used. Regression analysis methods are used for parametric purposes. Non-parametric methods offer an attractive alternative in this regard. Nonparametric models for simulating precipitation differ from the traditional methods. The Mann-Kendall test is to statistically assess if there is a monotonic upward or downward trend of the variable of interest over time. In case of monotonic upward (downward) trend means that the variable consistently increases (decreases) over time, but the trend may or may not be linear. This test can be used in place of a parametric linear regression analysis, which can be used to test if the slope of the estimated linear regression line is different from zero. The regression analysis requires that the residuals from the fitted regression line be normally distributed; an assumption not required by the Mann-Kendall test, that is, the Mann-Kendall test is a non-parametric (distribution-free) test. Each data are compared to all subsequent data. The Mann-Kendall statistics has been used where the initial value of Mann-Kendall statistics S is 0 (e.g., no trend). If x_i represent n data sets and x_j represent the data points at time j then

$$S = \sum_{k=1}^{n-1} \sum_{j=k+1}^{n} Sign(x_j - x_k)$$

Where the definition of absolute value indicates

$$Sign(x_j - x_k) = \begin{cases} 1 & \text{if} x_j - x_k > 0 \\ 0 & \text{if} x_j - x_k = 0 \\ -1 & \text{if} x_j - x_k < 0 \end{cases}$$

For $n > 8$, S follows approximately normal distribution with mean i.e. $E(S) = 0$ and the variance statistics is given by

$$Var(S) = \frac{n(n-1)(2n+5) - \sum_t^n t(t-1)(2t+5)}{18} (5)$$

Where t is the extend of any given ties. The test statistics Z_k is given by

$$Z_k = \begin{cases} \text{if } S > 0, \text{ then } \frac{S-1}{\sqrt{Var}} \\ \text{if } S = 0, \text{ then } 0 \\ \text{if } S < 0, \text{ then } \frac{S+1}{\sqrt{Var}} \end{cases}$$

$Z_k$follows a standard normal distribution. A positive and negative value of $Z_k$indicates an upward and downward trend respectively. The statistics Z_k has a normal distribution to test for either upward or downward trend at a α significance level (as usual 5%with $Z_{k_{0,025}} = 1.96$, H_0 will be rejected if the absolute value of Z_k is greater than $Z_{k_{(1-\frac{\alpha}{2})}}$ (Rejected H_0: $|Z_k| > Z_{k_{(1-\frac{\alpha}{2})}}$) where $Z_{1-\frac{\alpha}{2}}$ is the standard normal deviations and α is the level of significance for this test. The probability value (P-value) from two-tailed test using the Z_k value also can be used to test the significant trend and if the P-value is greater than significant level, the null hypothesis (H_0 : there is no trend in data series) is failed to reject. The 90% and 95% confidence level have been taken as the threshold to classify the signature of positive and negative trends for all indices considered.

Correlation is a bivariate analysis that measures the strength of association between two and the direction of the relationship, numerically measured, continuous variables (e.g. height and weight). This specific type of analysis is useful when analyst wants to establish if there are possible connections between variables. If correlation is found between two variables it means that when there is a systematic change in one variable, there is also a systematic change in the other; the variables alter together over a certain period of time. If there is correlation found, depending upon the numerical values measured, this can be either positive or negative.

In terms of the strength of relationship, the value of the correlation coefficient varies between +1 and -1. A value of ± 1 indicates a perfect degree of association between the two variables. As the correlation coefficient value goes towards 0, the relationship between the two variables will be weaker. The direction of the relationship is indicated by the sign of the coefficient; a + sign indicates a positive relationship and a – sign indicates a negative relationship. For two variables X and Y, the correlation coefficient r is calculated by the following equation

$$r = \frac{\sum_{i=1}^n (x_i - \bar{x})(y_i - \bar{y})}{\sqrt{\sum_{i=1}^n (x_i - \bar{x})^2} \sqrt{\sum_{i=1}^n (y_i - \bar{y})^2}}$$

An important property of r is that it is not affected by the change of origin or scale measurement. The shape of sampling distribution approaches to normal distribution if the number of pairs n increases. To test the correlation coefficient of population becomes zero, H_0: $\rho = 0$, then the test can be performed and the statistical test will be

$t = \frac{r\sqrt{n-2}}{\sqrt{1-r^2}} t_{n-2}; under H_0$at the 5% level of significance. The null hypothesis will be rejected whenever computed t values less than $-t_{n-2,0,05}$or greater than$t_{n-2,0,05}$

The correlation analysis of rainfall with both ENSO and IOD are performed. That is why, rainfall data should be categorized into eight spatial types, such as seven divisions and the whole Bangladesh. In this analysis, monthly rainfall has been considered.

4. Result Analyses and Explanation

Recent (1981-2015) trend of monsoon rainfall was assessed the eight categories (over Bangladesh and seven divisions) using non-parametric Mann-Kendall test. Besides, the probable response of monsoon variability with El Nino/Southern Oscillation (ENSO) episode and Indian Ocean Dipole (IOD) were observed using monthly ENSO and IOD index.

4.1 Trend in Monsoon rainfall

In this study, the trend of monsoon rainfall over all Bangladesh and spatial seven regions namely Dhaka, Barisal, Chittagong, Khulna, Sylhet, Rajshahi and Rangpur are projected. The findings from Mann-Kendal test with 5% and 10% level of significance are presented in Table1. From the table, we explore that the trend of average monsoon rainfall is increasing in Bangladesh significantly. More likely, the trend is significantly increasing at Khulna, Chittagong and Rangpur regions except Dhaka region while it is insignificantly decreasing at Barisal, Sylhet and Rajshahi regions (Table 1).The study of monsoon rainfall revealed that the average monsoon rainfall over all Bangladesh is increasing$2mm/year$,whereas these values for Dhaka, Rangpur, Khulna and Chittagong regions are $0.24mm/year$, $2.5mm/year$, $4.5mm/year$ and $1.8mm/year$ respectively (Fig. 1). In contrast, the average monsoon rainfall of Rajshahi, Barisal and Sylhet regions are decreasing at the rates $0.95mm/year$, $0.74mm/year$ and $0.84mm/year$ respectively (Fig. 2).

Table 1: Mann-Kendall test results for the presence of monotonic monsoon rainfall of Bangladesh

Regions	Tau	P value
BD	0.21	0.03*
Dhaka	-0.0084	0.47
Barisal	-0.119	0.16
Chittagong	0.15	0.10+
Khulna	0.452	0.00007*
Sylhet	-0.079	0.25
Rajshahi	-0.128	0.15
Rangpur	0.133	0.13+

+The presence of monotonic trend at 10% and *the presence of monotonic trend at 5% level of significance.

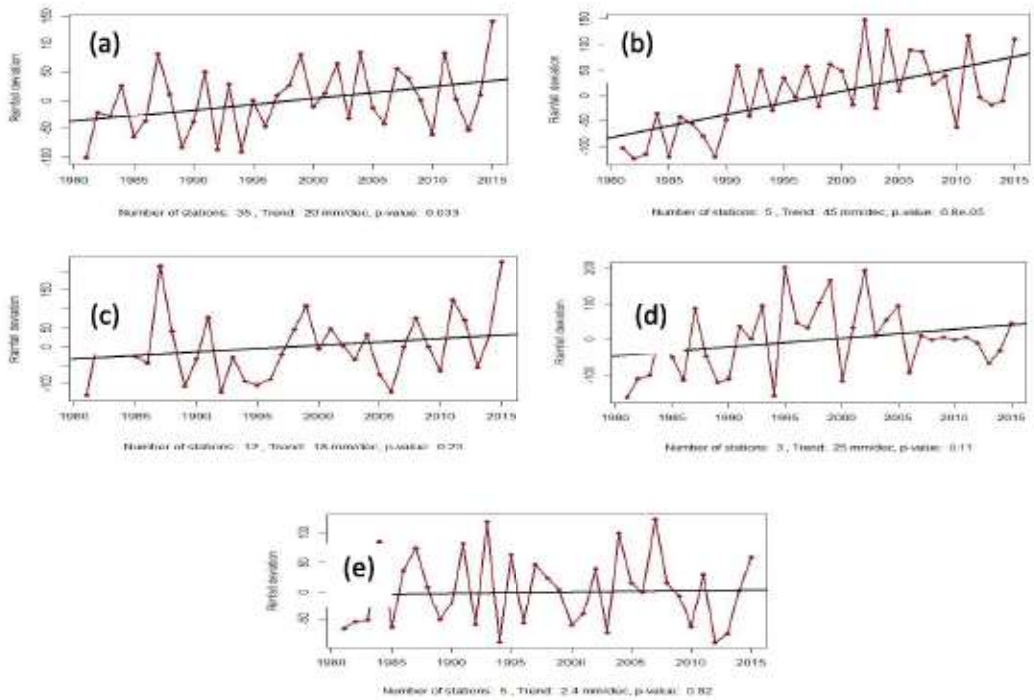

Fig. 1: Monsoon rainfall trend (a) BD, (b) Khulna, (c) Chittagong, (d) Rangpur and (e) Dhaka respectively.

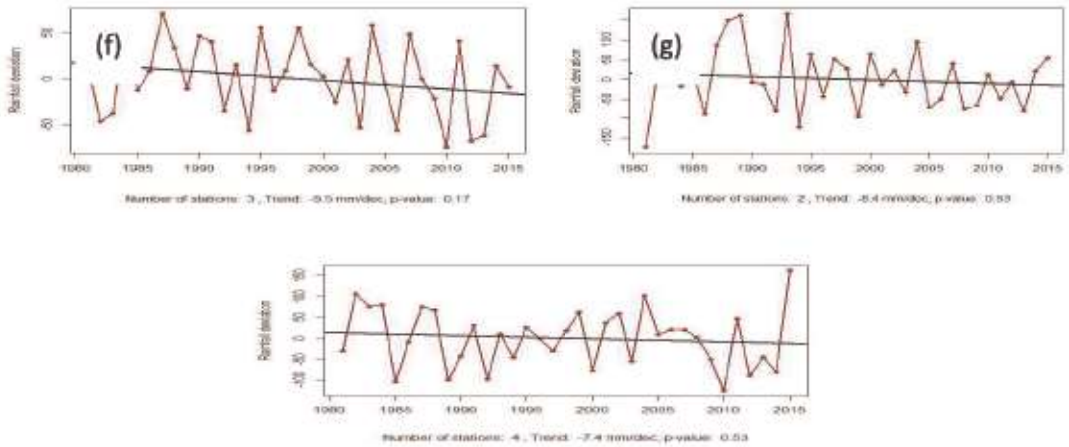

Fig. 2: Monsoon rainfall trend (f) Sylhet, (g) Rajshahi and (h) Barisal respectively

4.2 Correlation of monsoon rainfall with monthly ENSO and IOD

The observations of correlation analysis of rainfall data of overall Bangladesh including its seven spatial regions with monthly ENSO index and monthly IOD starting from January to September have been presented in Table 2 and Table 3 respectively.

Table 2: Correlation analysis of monsoon rainfall with monthly SOI for the following regions

Month	Dhaka		Sylhet		Rajshahi		Rangpur		Khulna		Barisal		Chittagong		Bangladesh	
	r	P Value	r	P Value	r	P Value	r	P Value	r	P Value	r	P Value	r	P Value	r	P Value
Jan	0.067	0.7	-0.27	0.11	0.009	0.95	-0.10	0.53	0.199	0.25	-0.07	0.69	-0.07	0.69	0.07	0.7
Feb	0.197	0.26	-0.05	0.75	0.17	0.32	0.039	0.82	0.39	0.02	-0.013	0.93	-0.001	0.93	0.25	0.14
Mar	-0.018	0.91	-0.08	0.62	-0.028	0.86	-0.03	0.86	0.288	0.09	-0.008	0.96	-0.008	0.96	0.08	0.64
Apr	-0.032	0.86	-0.13	0.42	-0.122	0.48	-0.24	0.17	0.014	0.93	-0.26	0.13	-0.25	0.13	-0.09	0.62
May	-0.27	0.11	0.07	0.65	0.015	0.92	-0.4	0.01	-0.37	0.02	-0.31	0.06	-0.313	0.06	-0.35	0.04
Jun	-0.31	0.06	-0.38	0.02	0.017	0.92	-0.16	0.36	-0.18	0.3	-0.22	0.21	-0.22	0.21	-0.29	0.08
Jul	-0.24	0.15	-0.14	0.39	0.07	0.65	0.014	0.93	-0.16	0.35	-0.35	0.04	-0.35	0.03	-0.23	0.19
Aug	-0.16	0.35	-0.08	0.64	0.05	0.73	0.005	0.97	-0.25	0.14	-0.32	0.06	-0.32	0.06	-0.2	0.23
Sep	-0.175	0.31	0.04	0.80	-0.07	0.66	0.003	0.98	-0.2	0.25	-0.27	0.11	-0.28	0.11	-0.18	0.29

Block data in presence of monotonic trend at 10% and Block and italic in presence of monotonic trend at 5% level of significance.

4.3 Correlation between rainfall and ENSO

From table 2 we observed that, monsoon rainfall of all over the country and location wise were statistically significant and negative correlation with SOI index except Rajshahi and this correlation start February/march and continue at month of August. It was seen that moderate correlation southern part of Bangladesh and little bit rest part of country.

4.4 Correlation between rainfall and IOD

Table 3reveled that, monsoon rainfall of overall country and at southern part of Bangladesh has statistically significant positive correlation with IOD index but there is no correlation with northern part of the country. This correlation starts at month of May till continue month of September. Saji and Yamagata (2001), Ajaymohan and Rao (2008) and Ashok *et al.* (2004) found interaction between IOD and Indian summer monsoon rainfall (ISMR) where data were analyzed for the period 1958-1997.

Table 3: Correlation analysis of monsoon rainfall with monthly for IOD the following regions.

Month	Dhaka		Sylhet		Rajshahi		Rangpur		Khulna		Barisal		Chittagong		Bangladesh	
	r	P Value	r	P Value	r	P Value	r	P Value	r	P Value	r	P Value	r	P Value	r	P Value
Jan	0.24	0.158	0.07	0.68	0.16	0.34	0.17	0.3	0.22	0.202	0.134	0.44	0.19	0.269	0.07	0.68
Feb	0.2	0.22	0.07	0.65	0.24	0.15	0.22	0.19	0.25	0.144	0.06	0.7	0.14	0.41	0.07	0.65
Mar	0.02	0.88	-0.23	0.17	0.06	0.71	0.077	0.66	0.37	0.02	-0.038	0.82	0.16	0.35	-0.233	0.17
Apr	0.13	0.45	-0.21	0.208	0.03	0.82	-0.008	0.96	0.22	0.19	0.088	0.61	0.19	0.28	-0.21	0.2
May	0.139	0.42	-0.18	0.27	-0.044	0.8	-0.038	0.82	0.11	0.5	0.17	0.32	0.32	0.05	0.224	0.19
Jun	0.141	0.41	-0.04	0.81	-0.055	0.75	0.08	0.64	0.22	0.18	0.38	0.02	0.47	0.004	0.4	0.02
Jul	-0.03	0.82	0.07	0.66	-0.2	0.23	-0.06	0.71	0.169	0.33	0.19	0.26	0.44	0.007	0.29	0.09
Aug	0.018	0.91	0.07	0.65	-0.18	0.28	-0.089	0.6	0.29	0.08	0.2	0.23	0.4	0.01	0.32	0.06
Sep	0.166	0.34	0.15	0.37	-0.07	0.67	-0.007	0.96	0.36	0.03	0.214	0.21	0.4	0.01	0.37	0.03
Jan	0.24	0.158	0.07	0.68	0.16	0.34	0.17	0.3	0.22	0.202	0.134	0.44	0.19	0.269	0.07	0.68

*Block data in presence of monotonic trend at 10% and Block and italic in presence of monotonic trend at 5% level of significance.

5. Conclusion

In this study, the variability of monsoon rainfall all over Bangladesh and its spatial regions have been investigated using current data. The association of monsoon rainfall indecisiveness with both monthly ENSO and IOD index has been determined also. The average monsoon rainfall showed an increasing trend at overall Bangladesh, Khulna, Chittagong, Dhaka and Rangpur regions, all are statistically significant except Dhaka region. Decreasing monsoon rainfall was over Barisal, Rajshahi and Sylhet regions but these were not statistically significant. The study also revealed that, monsoon rainfall of all over the country and location wise were statistically significant and negative correlation with SOI index except Rajshahi and this correlation start February/march and continue at month of August. It also observed that, positive correlation with IOD index was seen at southern part of Bangladesh but no correlation with northern part of the country. This correlation starts at month of May till continue month of September. It has been clear that in both cases ENSO and IOD moderate correlation southern part of Bangladesh and little bit rest part of country.

References

Ahasan MN, Chowdhury A M, Quadir D A, "Variability and trends of summer monsoon rainfall over Bangladesh", J Hydr & Meteo 7(1), 2010

Ahmed Md. K, Samsul M A, Abu Hena M Y, Monirul Md. I, "A long-term trend in precipitation of different spatial regions of Bangladesh and its tele-connection with El Nino/Southern Oscillation and Indian Ocean Dipole", Springer (TheorApplClimatol), doi 10.1007/s00704-016-1765-2, 2016

Ajaymohan RS, Rao SA, "Indian Ocean Dipole modulates the number of extreme rainfall events over India in a warming environment", J MeteoSoc Japan 86, 2008, 245-252

Ashok K, Gaun Z, Saji NH, Yagamata T, "Individuals and combined influence of ENSO and the Indian Ocean Dipole on the Indian summer monsoon", J Clim 17, 2004, 3141-3155

Chowdhury MR, "The El Nino-Southern Oscillation (ENSO) and seasonal flooding-Bangladesh", Theor Appl Clim 76, 2003, 71-88

Glantz MH, Katz RW, Nicholls N (Eds), "Tele-connection linking worldwide climate anomalies: scientific basis and societal impact", Cambridge University Press, 1991

Han W, Webster P, "Forcing mechanisms of sea level inter-annual variability in the Bay of Bengal", J Phys Ocean 32, 2002, 216-239

Hasan Z, Akhter S, Islam M, "Climate change and trend of rainfall in the south-east part of coastal Bangladesh", Europ J Sci Res10 (2), 2014, 25-39

Hashizume M, Armstrong B, Hajat S, Wagatsuma Y, Faruque AS, Hayashi T, "The effect of rainfall on the incidence of cholera in Bangladesh", Epidemiology 19, 2008, 103-110

Hashizume M, Faruque AS, Terao T, Yunus M, Streatfield K, "The Indian Ocean Dipole and Cholera incidence in Bangladesh: a time series analysis", Env Health Perspect 119, 2011, 239-244

IPCC, "Climate Change- The Physical Science Basis. Contribution of working group I to fourth assessment report of the intergovernmental panel on climate change". In: Solomon S, Qin D, Manning M, Chen Z, Marquis M, Averyt KB, Tignor M. & Miller HL. (eds). Cambridge, Cambridge University Press, 2007 (2007b)

Kendall MG, "Rank Correlation measure", Charles Griffin, London 1, 1975, 25-55

Khadija Khatun, Md. Bazlur Rashid, M A Samad, "Recent changes of precipitation over Bangladesh and it's response to Southern Oscillation Index (SOI) and Indian Ocean Dipole (IOD)", The Atmosphere (BMD), 7 (1), 2017, 90-97

Khan TMA, Singh OP, Rahman MS, "Recent sea and sea surface temperature trends along the Bangladesh Coast in relation to frequency of intense cyclone", Mar Geod 23(2), 2000, 103-116

Mann HB, "Non-parametric tests against trend", Econometrical, New York 13, 1945, 245-259

Mishra K. K (1991), "Statistical Analysis of Rainfall Data", IEC (O) Journal CV, Vol. 71.pp. 177-180

Nandan Mukherjee, Malik Fida Abdullah Khan, Bhuiya Md. Tamim al Hossain, A K M Saiful Islam, Most. Naneen Akhter & Shahriar Rahman, "A Hybrid Approach for Climate Change Scenario Generation for Bangladesh using CGM Model Results", 3rd International Conference Water and Flood Management (ICWFM), 2011

SAARC Meteorological Research Center (SMRC), "Rainfall over SAARC region with special focus on tele-connections and long-range forecasting of Bangladesh monsoon rainfall, monsoon forecasting with a limited area numerical weather prediction system", SMRC Report No-19, 2006

Saji NH, Yamagata T, "A view of the tropical Indian Ocean climate system from the vantage point of Dipole Mode events", J Clim 1, 2001, 23-45

Sanderson M, Ahmed R (1979) Pre-monsoon rainfall and its variability in Bangladesh: a trend surface analysis. Hydrological Sciences-Bulletin-des Sciences Hydrologiques 24(3): 277–282

Shahid S, "Rainfall variability and the trends of wet and dry periods in Bangladesh", Int J Climat 30(15), 2009, 2299-2313

Singh OP, Khan MTA, Rahman MS, Salahuddin M, "Summer monsoon rainfall over Bangladesh in relation to multivariate ENSO index", Mausam 51, 2000, 255-260

Walker GT, Bliss EW, "World weather V", Memor Meteo Soc 4, 1932, 53-84

Inter-relation between River Discharge and Salinity Intrusion in the coastal area of Bangladesh

Most Israt Jahan Mili[1*], K M Azam Chowdhury[1]and Md Kawser Ahmed[1]
[1]Department of Oceanography, University of Dhaka, Bangladesh
E-mail: israt.pstu@yahoo.com

Abstract: The Ganges-Brahmaputra river system have a great impact regarding river discharge toward the coastal area of Bangladesh. This riverine system is undergoing rapid ecological changes due to human activity, resulting changes in the ecosystem of coastal area of the country. In the coastal area of Bangladesh, there are 147 Upazilas under 19 coastal districts covering the eastern, central and western part. Among the 19 coastal districts, presently 12 districts are salinity affected. As there is vast coastal area along Bangladesh, present study was regarding analysis with the salinity distribution pattern in northern part of Bay of Bengal (BoB) and river discharge scenario of Ganges-Brahmaputra delta. Result reveals the higher salinity in the western and eastern coastal part rather than the central zone. This study is supported to assess the inter-relation between river discharge and salinity intrusion in the coastal area of Bangladesh and a reverse relation is found between salinity and river discharge. Analyzing with the previous study it is found that salinity intrusion in the coastal area of Bangladesh brought negative impact on agricultural crop production but it can be positive one for shrimp farming and some other fisheries production. However, this work is occupied with the river discharge of Ganges and Brahmaputra while more study should be carried out with the other rivers flowing into the BoB.

Key Words: Bangladesh, Coastal area, River Discharge, Salinity Intrusion.

1. Introduction

Bangladesh is one of the largest active deltas of the world having a flat topography with very low elevations which are larger than 10 meters from mean sea level. Eighty percent of the country is deltaic floodplains which are crisscrossed by about 230 rivers including 57 Transboundary Rivers of which 54 is shared with India and 3 with Myanmar. The river system that flows through Bangladesh is the third largest source of freshwater discharge to the world's ocean (Afroz and Rahman, 2013). Catchments area of the three major rivers system of the Ganges-Brahmaputra-Meghna (GBM) region is about 1.72 million km^2, 93% of which lies outside the country. Coastal region of Bangladesh consists of southern deltaic zones of the lower Ganges, Brahmaputra and Meghna estuary. There is a fresh and saline water interaction in the southwest coastal region of Bangladesh. Changes in tide and fresh-water flow result in the advance and retreat of the salinity limit. Under this process, during the wet season, local rainfall associated with flood flows from upland regions keeps the salinity limit near the coastline (Nobi and Gupta, 1997). But salinity starts increasing and intruding upland from the beginning of November with the cessation of the rains and consequent reduction of river flows (Pramanik *et al.*, 1987). The Ganges and its distributaries contribute the fresh water to the southwestern region of Bangladesh. The Ganges water flows are historically reducing for a long time. The human influence on surface water is one of the major reasons of water scarcity in the catchment area. After withdrawing fresh water on Farakka Barrage constructed in India started a huge area in the downstream are affected by salinity and the saline front has reached up to 240 km from the coast (Islam and Gnauck, 2007). As salinity affected coastal area of Bangladesh is increasing day by day due to fall in river discharge so, this study was aimed at to assess the inter-relation between river discharge and salinity intrusion in the coastal part of BoB covering Bangladesh. River discharge data was observed in two major rivers (Ganges and Brahmaputra) because they contribute for a large portion of freshwater flowing to BoB. These findings will help to understand the salinity distribution pattern covering the coastal area adjoining the BoB. In present scenario, increase of salinity levels in rivers and coastal region is one of the major concerns in Bangladesh. This study will help the community of coastal area to understand about salinity distribution patterns in the coast part joining with BoB. Baten *et al.* (2015) investigates in his study the impacts of salinity on agricultural crop in the interior coastal region of Bangladesh. The estimated salinity concentration of surface water was 1.3 dS/m which was 0.8 dS/m higher than the earlier estimation by ICZMP (Integrated Coastal Zone Management Plan) in 2003. Mahmuduzzaman *et al.* (2014) showed in his study the causes of salinity intrusion in the coastal belt of Bangladesh. He showed the main causes are Critical Geographical Location of the Country, Sedimentation, Sea level rise, Cyclone and Storm Surge, Tidal Flooding, Back Water Effect, Changes in Ground Water Flow etc. Afroz and Rahman (2013) presented that the diversion of water by the Farakka Barrage has introduced significant changes in the hydrology of the Ganges River system in Bangladesh. Discharge data of Ganges River for the period of 1970 to 2011 show that dry season (November–May) flow has decreased up to 82% after the construction of Farakka Barrage. Islam and Gnauck (2007) studied with the salinity level of 13 potential river Basins situated in the Ganges delta and has been asserted that 11 rivers have crossed the water salinity threshold line (43220 dS/m) in 2003.The previous average water salinity value was 54025 dS/m, whereas in their study highest

water salinity value was 69152 dS/m which is harmful and poses threats to mangrove wetland ecosystems. Islam and Gnauck (2007) represent the river discharge rate at Hardinge bridge and the discharge was 3,700 m³/sec in 1962, 1964 m³/sec in 1975, 910 m³/sec in 1980andonly 264 m³/sec in 2006. After withdrawing fresh water on Farakka Barrage constructed in India, the downstream are affected by salinity.

2. Methodology and Data Analysis

Study area for the present study was selected in the northern part of Bay of Bengal to assess salinity distribution from remote sensing data. RS (Remote Sensing) data of salinity derived from ERDDAP (Environmental Research Division Data Access Program) from April 2015 toJanuary2017 from the site of http://coastwatch.pfeg.noaa.gov. There was some lack of RS data in the central coastal zone of Bangladesh. Salinity distribution was assessed using GIS software. Along with the salinity pattern of Northern BoB, river discharge data was observed for two major rivers Ganges and Brahmaputra from 2003 to 2007 from previous study of (Hirpa *et al.* 2013). Salinity and river discharge data was combined in a graph (Fig. 5) to make comparison between them.

3. Result and Discussions

3.1 River Discharge

The river discharge of major two rivers Ganges and Brahmaputra were observed at the upstream. Peak discharge was found in the month of September for Ganges but lowest value was confined to June and December in 2003. In 2007, no significant change of river discharge was observed except highest in the month of July. Between observed two rivers, Brahmaputra has the high discharge than Ganges. Brahmaputra has the highest discharge in the month of June in 2004, whereas in 2007 the highest discharge was confined to July. Salinity distribution pattern revealed for low salinity from July to November (Fig. 1) when river discharge was high and highest salinity was found from December to June when river discharge was lower. The GBM Delta is one of the world's largest (~100,000 km²), draining land from Bangladesh, Bhutan, China, India and Nepal with many of the 147 million people living in the delta under extreme poverty. Increase of salinity levels in river and estuaries of GBM Delta is one of the major concerns in the coastal region of Bangladesh and India (Akter and Sakib, 2011). The Sundarbans mangrove wetlands and more than 27 small towns are situated in the Ganges catchment in Bangladesh. The area of Ganges-Brahmaputra-Meghna (GBM) drainage basin is 1.76 million km² of which 62% is in India, 18% in China, 7% in Nepal and 8 % in Bangladesh. The Sundarbans mangrove wetlands are the part of the Ganges delta, including extensive productive mangrove forests and major river deltas flowing into the Bay of Bengal (Islam and Gnauck, 2007).

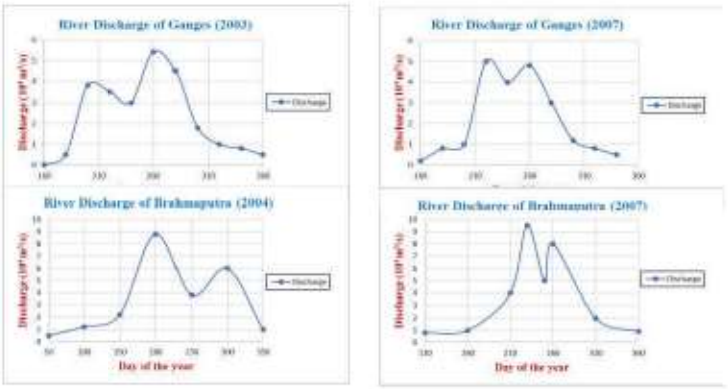

Fig. 1: River discharge ($10^4 m^3/s$) from Ganges and Brahmaputra in the year 2003, 2004 and 2007 from observed value (Source: Hirpa *et al.*, 2013)

3.2 Increasing Trend of Salinity at Mongla Port

Observed salinity pattern at Mongla Port showed an increasing trend from 2000 to 2006. Salinity increased rapidly within first three years but the rate was gradual for the next three years. Salinity distribution pattern was revealed for lower value at the central coastal part from Remote Sensing data rather than other two parts.

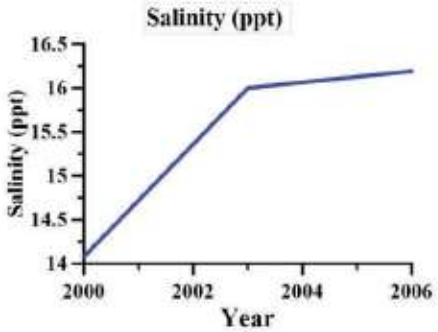

Fig. 2: Line graph showing the increasing trend of Salinity (ppt) at Mongla port from 2000 to 2006 (Source: Islam and Gnauck, 2007)

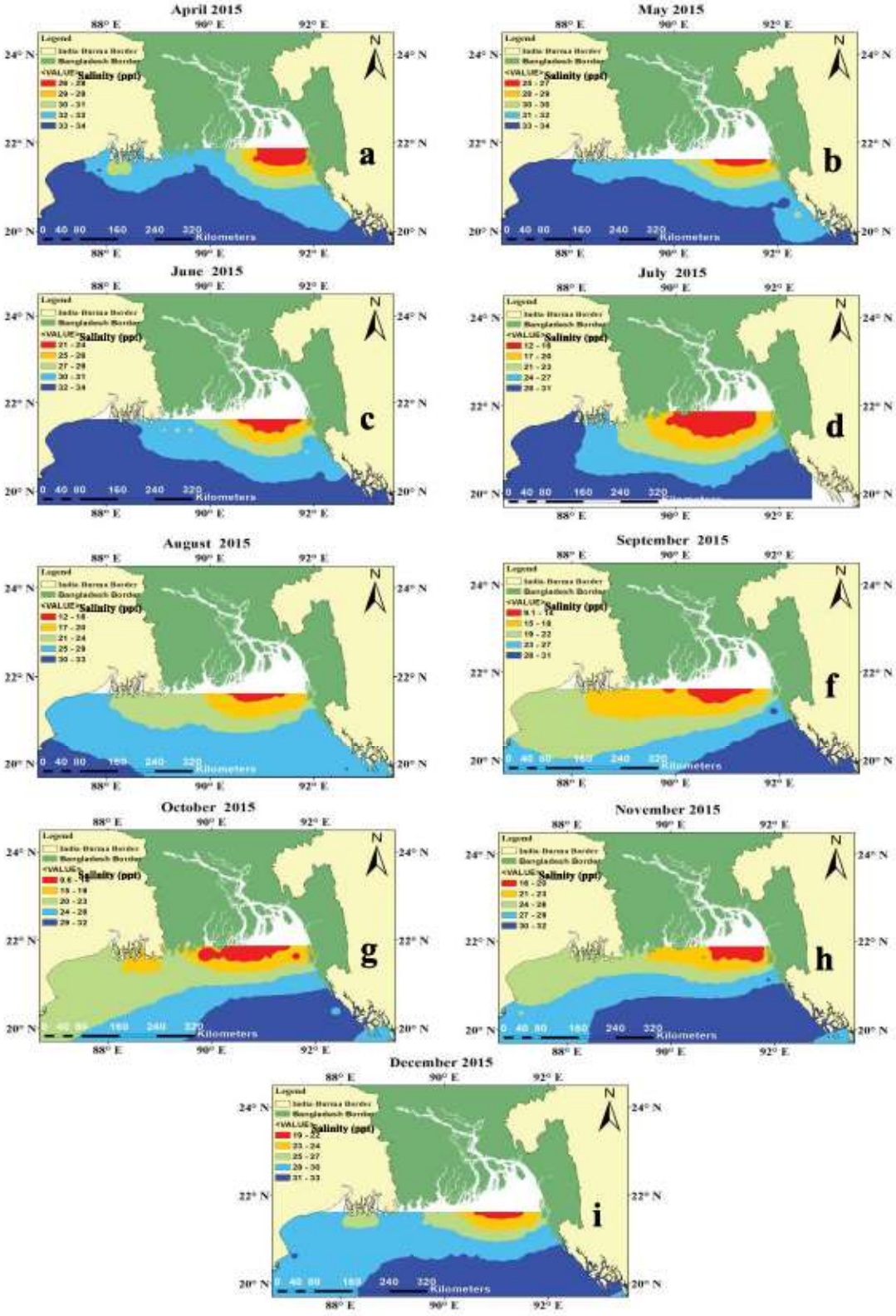

Fig. 3: Schematic diagram showing salinity distribution pattern in the northern part of BoB from April to December 2015.

3.3 Salinity Distribution in Northern Part of BoB

Remote sensing observation of salinity pattern showed that the western and eastern coastal part have higher salinity than the central area (though there some lack of RS data at central part). Highest salinity ranged from 25 – 34 ppt from December to June (Figs. 3 and 4) whereas lowest salinity ranged from 3.4 to 32 ppt from July to November (Figs. 3 and 4). Higher salinity was persisting for the months where river discharge was low and lower salinity was persisting for the months where river discharge was high (Figs. 3 and 4).

Salinity distribution in the northern part of BoB from April to December 2015 showed a range from 9.1-33 ppt (Fig. 3(a-i)). Salinity persisting higher from April to June (Fig. 3(a-c) following lowering the lowest value from July and hold up to October (Fig. 3(d-g). It increased again from November by 3ppt continuing to December (Fig. 3(h-i)). Salinity was much higher in western and eastern coastal part rather than central coastal part of BoB.

Lower salinity concentration of central part propagated to the westward gradually with the consequent months reaching its lowest value in September (Fig. 3f). Higher concentration of salinity was observed along Chittagong coast line than the western coast of Bangladesh. Salinity ranged at 3.4 – 34 ppt from January 2016 to January 2017 (Fig. 4(a-m)). At the beginning of the year the eastern Chittagong coastline was characterized by lower salinity while the western part had the higher value and central part concerning least value. But, with the subsequent increase in time the lower concentration of eastern and central part propagated to the westward resulting the lowest concentration of salinity in the west part in the month of August (Fig. 4h) and again the scenario was changed to the eastward. Central coastal part was occupied with the lowest salinity all over the year (Fig. 4(a-m)).

3.4 Comparison between Salinity and River Discharge

River discharge was near about zero from the beginning of the year and started to gradually increase from April. Brahmaputra (black line) has much higher discharge than Ganges (red line). Peak discharge for Ganges was in June while peak discharge for Brahmaputra was in August and then decreased again continuing up to the end of the year. Salinity (blue line) was higher from the start of the year when river discharge was lower and the peak salinity value was confined with the lowest river discharge of the year (Fig. 5). Lowest salinity curve was found after the consequent increase and peak value of river discharge. The same relation was also found at the end of the year where discharge was lowering and salinity started to increase. At the end of the year river discharge was lower resulting in higher salinity during this month.

3.5 Impact on Habitat

The dominant mangrove Heritierafomes and Ceriopsdecendraspecies are affected by top dying disease which is recognized as a key management concern. The Fourier Polynomial water salinity models on Sundarbans rivers are showing the cycling increasing Behavior (Islam and Gnauck, 2007). Salinity is one of the most severe environmental factors limiting the productivity of agricultural crops. Most crops are sensitive to salinity caused by high concentration of salts in the soil. As yield of crop production had been reduced due to salinity, the cost of production had gradually increased (Mahmuduzzaman *et al.*, 2014).

Agriculture production is likely to decrease as saline containing water reduces plant growth through concentrating salt in the root zone of plant and resulting in nutrients imbalance and yield loss (Baten *et al.*, 2015). The most common response of plant towards salinity is reduction in growth. In low to moderate concentration, salinity affects crop production by lowering the soil-water potential and increases concentration of salt at the root zone. Low water potential indicates that plant cannot extract sufficient amount of water from soil and maintain at very low soil-water condition. This effect is known as osmotic effect (Baten *et al.*, 2015). Bauder *et al.* (2007) argued that yield of a crop is directly linked to the quantity of water passed through it by water transpiration. When EC gets higher, less water is likely available to plants. Yield potential of plants, therefore, gets deteriorated with the increase of EC in irrigation water.

4. Recommendation

This study was carried out with the Remotely Sensed Satellite data of salinity in the coastal part of BoB where further study can be done with the measurement of in-situ data of this region. Though Satellite data provides also good results but validation can compare with in-situ measurement.

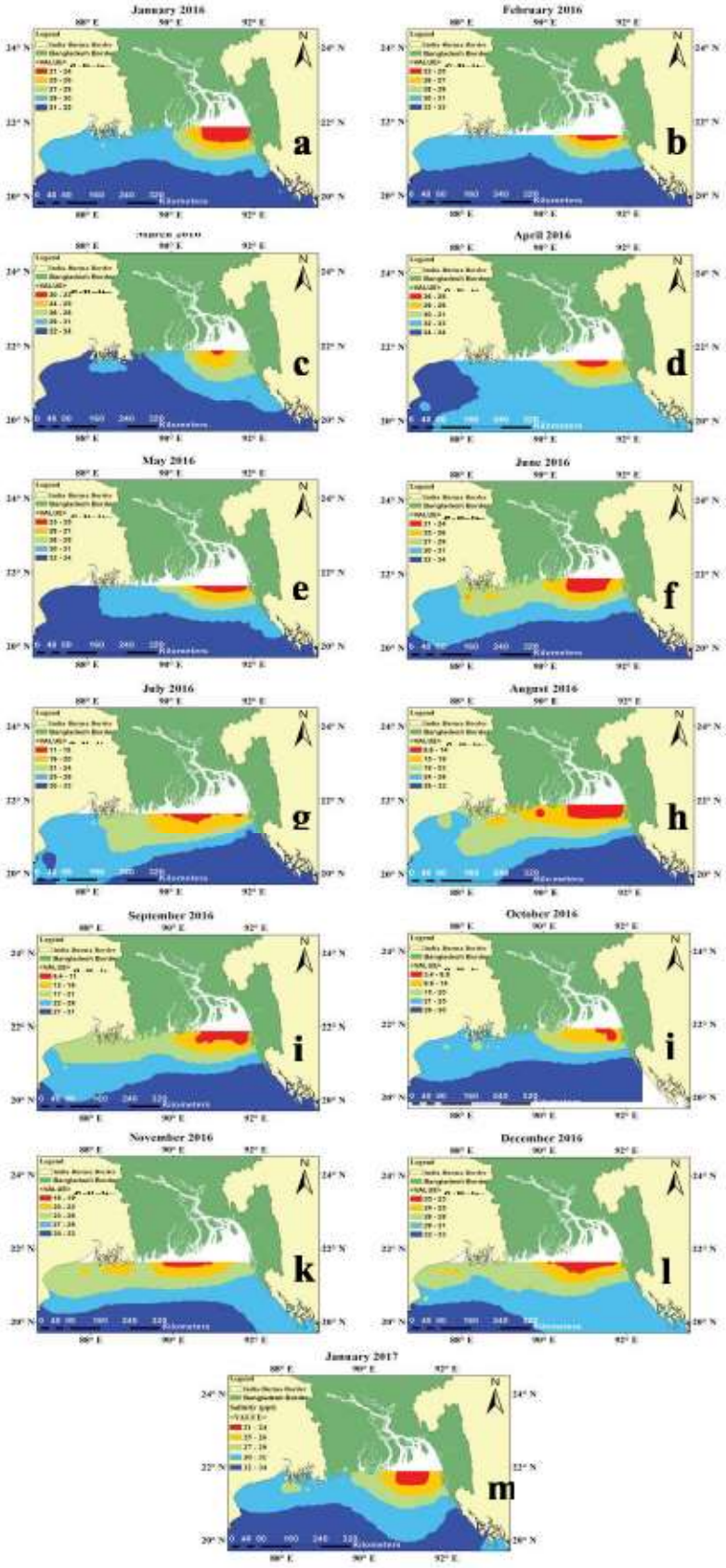

Fig. 4: Salinity distribution pattern in the northern part of BoB from January 2016 to January 2017

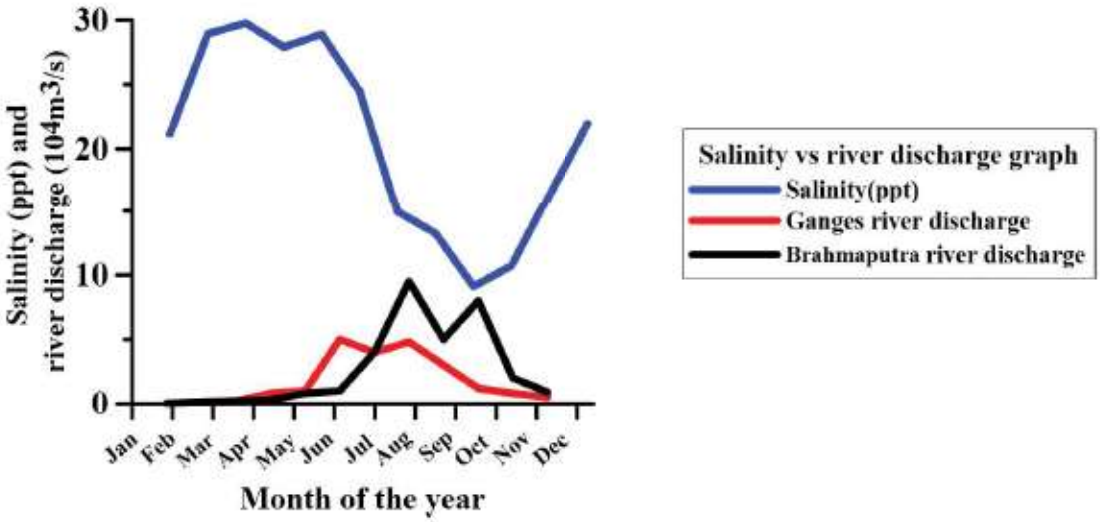

Fig. 5: Salinity (ppt) and river discharge ($10^4m^3/s$) pattern in the coastal area of Bangladesh.

5. Conclusion

Salinity in the coastal area is one of the most important environmental factors that have influence on other environmental parameters and have greater impact in controlling the ecosystem. The coastal area of Bangladesh is concerned with much higher salinity affected area than in the past and the trend is increasing day by day. The central coastal area has lower salinity level than the eastern and western coastal parts of the country. In relation with river discharge salinity was found to be higher where river discharge was lower. Peak value of river discharge was in June for Ganges and August for Brahmaputra. From the start of the year river discharge was lowest where salinity reached its peak concentration (Fig. 5). Salinity intrusion results in negative impact on some agricultural crop production. Therefore, government along with the corresponding authority should take measures on the proper monitoring in riverine system because any change in the river system may lead to hamper the coastal environment as well as to the oceanic environment.

References

Afroz R, Rahman MA (2013): Transboundary River Water for Ganges and Teesta Rivers in Bangladesh: An Assessment. *Global Science and Technology Journal*, Vol. 1, No. 1, pp 100-111.

Akter R and Sakib MN (2011): Salinity Intrusion in GBM, Institute of Water and Flood Management (IWFM), Bangladesh University of Engineering and Technology, Bangladesh.

Baten MA, Seal L, Lisa KS (2015): Salinity Intrusion in Interior Coast of Bangladesh: Challenges to Agriculture in South-Central Coastal Zone, *American Journal of Climate Change*, Vol. 4, pp 248-262.

Bauder TA, Waskom RM Davis JG (2007): Irrigation Water Quality Criteria, Crop Series Irrigation,Number.0.506.http://cospl.coalliance.org/fez/eserv/co:6315/ucsu2062205062007internet.pdf.

Hirpa FA, Hopson TM, Groeve TD, Brakenridge GR, Gebremichael M and Restrepo PJ (2013): Upstream Satellite Remote Sensing for River Discharge Forecasting: Application to Major Rivers in South Asia, *Remote Sensing of the Environment*, Vol. 131, pp 140-151.

Islam SN and Gnauck A (2007): Salinity Intrusion due to Fresh Water Scarcity in the Ganges Catchment: A Challenge for Urban Drinking Water and Mangrove Wetland Ecosystem in the Sundarbans Region, Bangladesh, www.yes, Paris.

Mahmuduzzaman M, Ahmed ZU, Nuruzzaman AKM, and Ahmed FRS (2014): Causes of Salinity Intrusion in Coastal Belt of Bangladesh, *International Journal of Plant Research*, 4(4A), pp 8-13, ISSN: 2163-2596.

Nobi N and Gupta AD (1997): Simulation of regional flow and salinity intrusion in an integrated stream-aquifer system in coastal region: southwest region of Bangladesh.*Ground Water*, Vol. 35, Issue 5, pp786-796.

Pramanik MAH, Ali A, Quadir DA, Rahman A, Shahid MA and Hossain MD (1987): Regional seminar on the application of remote sensing techniques to coastal zone management and environmental monitoring, Dhaka, Bangladesh, 18-26 November 1986, *International Journal of Remote Sensing*, Vol. 8, Issue 4.

Estimation of primary productivity using vertically generalized production model in the northern part of Bay of Bengal

Md Kawser Ahmed[1], Most Israt Jahan Mili[1*] and Muhammad Shahinur Rahman[1]
[1]Department of Oceanography, University of Dhaka, Bangladesh
E-mail: israt.pstu@yahoo.com

Abstract: The study was carried out with the estimation of primary productivity using vertically generalized production model (VGPM) in the northern part of Bay of Bengal (BoB). The model was first proposed by Behrenfeld and Falkowski in 1997 and provide good results for estimation of primary productivity in the coastal area. Productivity was estimated for four months (December, January, February and March) for five years from 2012 – 2016 using remotely sensed satellite data. Estimated primary production was ranged from 25-3500 $mgCm^{-2}d^{-1}$ over the region. Productivity was comparatively higher at the river mouth of Ganges – Brahmaputra – Meghna river system following decreasing pattern to the open part of the southward region. Among four months, February was experienced with the highest productivity varied from 65 – 3500 $mgCm^{-2}d^{-1}$. BoB receives a large freshwater influx and nutrients from the riverine system which enhance primary production in some area near the river mouth but the entire BoB remains less productive due to the strong stratified layer in the upper ocean.

Keywords: Coastal area, Primary Productivity, Remote sensing, VGPM model, BoB

1. Introduction

Productivity refers to the rate of production on a unit area basis. The total amount of solar energy converted to chemical energy by green plant is gross primary production (Mohanty *et al.*, 2014). The productivity of many coastal marine systems is limited by nutrient availability and the input of additional nutrients to these systems increased primary productivity. Coastal regions are the most productive ecosystems of the world, exemplified by the fact that coastal habitats provide feeding and reproduction ground for approximately 90% of the world's marine fish catch *(Pramanikand Mohanty, 2016)*. Productivity fuels life in the ocean, drives its chemical cycles and lowers atmospheric carbon dioxide. Nutrient uptake and export interact with circulation to yield distinct ocean regimes (Sigman and Hain, 2012). Only a fraction of the organic matter produced in the surface ocean has the fate of being exported to the deep ocean. Since nutrients are the limiting factor in algae growth, the more nutrients the more productivity. Lots of experienced, half experienced and theoretical methods have been put forward in recent decades to calculate ocean primary productivity using ocean ecological factor and chlorophyll. Besides, many discussions have been conducted on their principle, feasibilities and reliabilities. According to the VGPM model set up by Behrenfeld and Falkowski (BFM), all essential parameters can be acquired by remote sensing, which makes it possible to break away from the limit of field investigation and can acquire the large-scale distribution of ocean primary productivity rapidly. Ocean phytoplankton photosynthesis is a very complicated process and many environmental factors are involved which affect the ocean primary productivity more or less *(Guosheng et al., 2004)*.

2. Materials and Methods

2.1 Study area

Area selected for this study, is in the northern part of BoB from 89° 0' 0" E to 93° 0' 0" E longitude and 20° 0' 0" N to 23° 0' 0" N latitude. All parameters used in this model were derived from remote sensing data and weekly primary productivity pattern is shown in the result. As data were taken from satellite access there are some missing of weekly data in the coastal area.

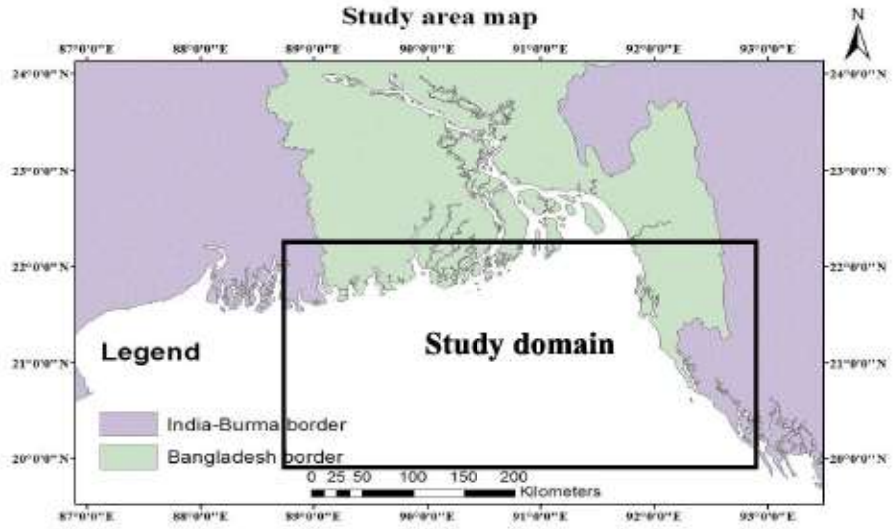

Fig. 1: Schematic diagram showing study area for estimation of Primary Productivity in the northern part of BoB.

2.2 Remote sensing (RS) data

Remote sensing data of chla have been derived from MODIS from the site ERDDAP (Environmental Research Division's Data Access Program). Chla data was taken with a spatial resolution of 4km, 8-day composite data. Data were taken for the year 2012-2016 for 4months (December, January, February, March) from the site http://coastwatch.pfeg.noaa.gov/erddap/griddap/erdMH1chla8day.graph?chlorophyll. Then data was interpolate using ArcGIS and grid was taken on $1^0 \times 1^0$. SST data derived with a spatial resolution of 4km, 8-day composite data. PAR (Photosynthetically Active Radiation) and K (490) was taken from Aqua MODIS with a spatial resolution of 4km, 8day composite data for 5 years from 2012-2016 for 4months (December, January, February, March).

2.3 Methodology of VGPM model

Original VGPM Model

VGPM (Vertically Generalized Production Model) was first proposed by Behrenfeld and Falkowski in 1997. Behrenfeld and Falkowski discovered a consistent trend in the vertical distribution of primary productivity and observed that the VGPM accounting for the trend in normalized primary productivity estimated depth integrated primary productivity well. In the VGPM model, the simplified depth-integrated primary productivity (PP_{eu}) was calculated as follows:

$$(PP_{eu}) = 0.66125 \times P^B_{opt} \times [E_0 / (E_0 + 4.1)] \times Z_{eu} \times C_{opt} \times D_{irr}$$

In the above equation, (PP_{eu}) is the primary productivity from sea surface to the euphotic depth (mg C m^{-2} day^{-1}), P^B_{opt} is the estimated optimum biomass-specific photosynthesis rate (mg C mg Chl-a^{-1} h^{-1}), E_0 is the daily sea surface PAR flux (mol quanta m^{-2}), Z_{eu} is the estimated euphotic depth, C_{opt} (mg Chl-a m^{-3}) is the chlorophyll-a concentration where P^B_{opt} is located, the sea surface chlorophyll-a concentration is used as a replacement and D_{irr} is the day length (h), which can be calculated by using the date and location of each station (Forsythe *et al.* 1995). The P^B_{opt} is very important for the estimation of primary productivity. One of the principal approaches for estimating P^B_{opt} is to define predictive relationships between P^B_{opt} and sea surface temperature by a high order polynomial equation (Behrenfeld and Falkowski, 1997). Recent studies have indicated that the sea surface temperature alone is not a sufficient indicator of P^B_{opt} variability and that the P^B_{opt} turns out to be affected by both sea surface chlorophyll-a concentration and sea surface temperature *(Kameda and Ishizaka, 2005)*. Therefore, a modified model based on sea surface temperature and sea surface chlorophyll-a concentration was established and gave good estimates in relatively high productivity areas (Kameda and Ishizaka, 2005).

According to Behrenfeld and Falkowski (1997):

P^B_{opt} is expressed by BF as a 7th order polynomial of temperature (T) as follows:

$$P^B_{opt} = -3.27 \times 10^{-8} T^7 + 3.4132 \times 10^{-6} T^6 - 1.348 \times 10^{-4} T^5 + 2.462 \times 10^{-3} T^4 - 0.0205 T^3 + 0.0617 T^2 + 0.2749T + 1.2956$$

KI modified the model based on sea surface temperature and sea surface chlorophyll-a concentration and gave good estimates in high productive area rather than P^B_{opt} was estimates in (Behrenfeld and Falkowski, 1997).

According to Kameda and Ishizaka (2005):

KI modified P^B_{opt} as follows:

$$P^B_{opt} = (0.071T - 3.2 \times 10^{-3} T^2 + 3.0 \times 10^{-5} T^3) / C + (1.0 + 0.17T - 2.5 \times 10^{-3} T^2 + 8.0 \times 10^{-5} T^3)$$

Here, T is sea surface temperature and C is sea surface chlorophyll-a concentration. This modified model varies between 1.0 and 6.0 for sea surface temperature ranging from 0 to 30 °C. E_0 is the daily sea surface PAR flux (mol quanta m^{-2}). PAR is a broadband of 400–700 nm and spectrally integrated measurement of light intensity at a given depth. In oceanography, K_{PAR} is commonly used to represent the diffuse attenuation coefficient of PAR. Previous studies have demonstrated that even for a homogeneous and well-mixed water column, the value of K_{PAR} changes significantly with depth (Morel 1988, Zaneveld *et al.* 1993, Lee, 2009). Therefore, the vertical variation of PAR at euphotic depth should be expressed as follows:

$$PAR\ (Z_{eu}) = PAR\ (0) \times e^{-K_{PAR} \times Zeu} = 1\% \times PAR\ (0)$$

Euphotic depth (Z_{eu}) is not only a water quality index of ecosystem but also an important component for depth – integrated primary productivity model. The euphotic zone refers to the region where there is sufficient light for photosynthesis to take place. Euphotic zone roughly extends to the depth where the PAR is 1% of its surface value (Kirk, 1994). Based on PAR, the relationship between the euphotic depth (Z_{eu}) and the diffuse attenuation coefficient of PAR was derived as follows:

$$(Z_{eu}) = 2\ln 10 / K_{PAR} = 4.605 / K_{PAR}$$

Referred by (*Morel and Gentili, 2004)*, PAR was regarded as a valid approximation to derive K_{PAR} and euphotic depth (Z_{eu}).In water area whose Inherent Optical Properties (IOPs) is mainly influenced by phytoplankton, the value of K_{PAR} can be estimated from remotely derived chlorophyll-a concentration (Morel, 1988). However, this chlorophyll based empirical algorithm might not be suitable in estuarine waters where the IOPs are much more complicated. Many studies have demonstrated that K_{PAR} strongly correlates with the diffuse attenuation coefficient at 490 nm [K_d (490)] (Zaneveld *et al.* 1993, Barnard *et al.* 1999) which is a standard ocean color satellite product, previously tested by the Sea-Viewing Wide Field of View Sensor (SeaWiFS) and later tested by MODIS. Based on that K_{PAR} was derived using a linear regression equation relating K_{PAR} and K_d (490):

$$K_{PAR} = a \times K_d\ (490) + b$$

Where, constants a and b value were derived by making correlation between PAR (m^{-1}) and K_d (490) (m^{-1}). The value of constant 'a' and 'b' were 1.3386 and 0.4215. Deriving the constant 'a' and 'b' value finally the equation used for (Z_{eu}) was as follows:

$$Z_{eu} = 4.605 / [1.3386 K_d\ (490) + 0.4215]$$

Day length, D_{irr} (h) was calculated according to three established models and the error were compared among three model following Forsythe *et al.*,1995.

3. Result and Discussions

Study with the primary productivity for a time period of 2011-2015 in the month of December was not revealed with a higher temporal variation rather than a few spatial variations was observed (Fig. 2(a-o)). Northern mouth of BoB that receives a large freshwater influx also with high nutrients load from riverine input matched with a higher productivity rather than southern part estimated by BFM. Photosynthesis rate was varied between 1 and 6 for the present study.

Estimated primary productivity based on VGPM model by BFM showed a higher value of productivity toward the northern mouth of BoB compared to the southern part. Estimated primary productivity in the month of December ranged from 80 to 3000 $mgCm^{-2}d^{-1}$ where, the average value was 450 $mgCm^{-2}d^{-1}$. Spatio-temporal distribution of IPP in the month of December showed a value from 80 to 500 $mgCm^{-2}d^{-1}$ covering toward the southern part whether it was frequently exceeding from 2000 $mgCm^{-2}d^{-1}$ to the northward river mouth flowing BoB. In 4th week December 2015 (Fig. (2-o)) productivity not exceed over 500$mgCm^{-2}d^{-1}$ and synchronous distribution was observed all over the area. In 2nd week February 2011 productivity frequently exceed 2000 $mgCm^{-2}d^{-1}$ to the eastward coastal area.

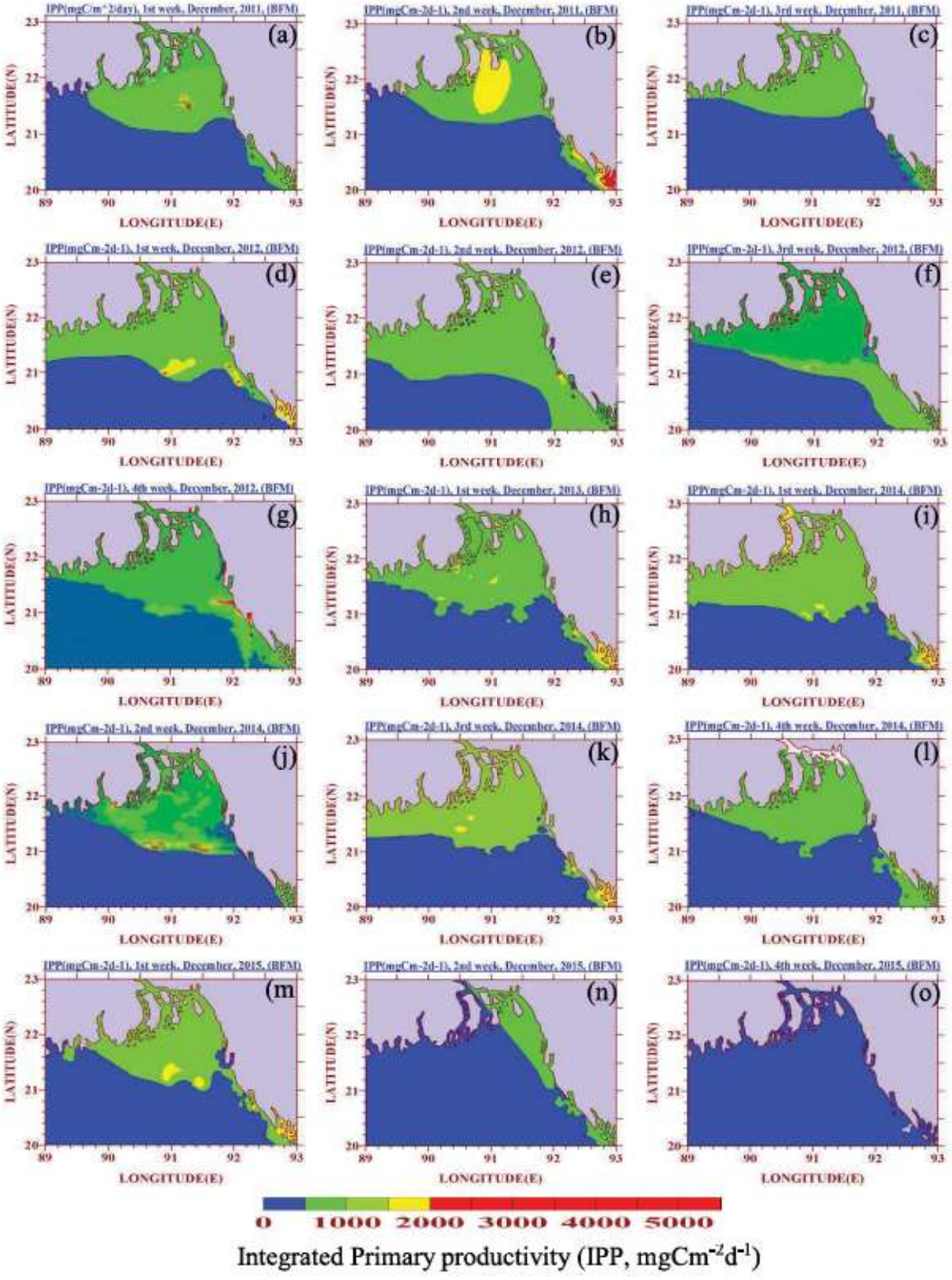

Fig. 2 Weekly Spatio-temporal distribution of estimated Integrated primary productivity ($mgCm^{-2}d^{-1}$), in the northern part of BoB based on BFM in the month of December from 2011 to 2015.

Estimated primary production in the north-eastern BoB ranged from 80 – 3000 $mgCm^{-2}d^{-1}$ by BFM in the month of December.

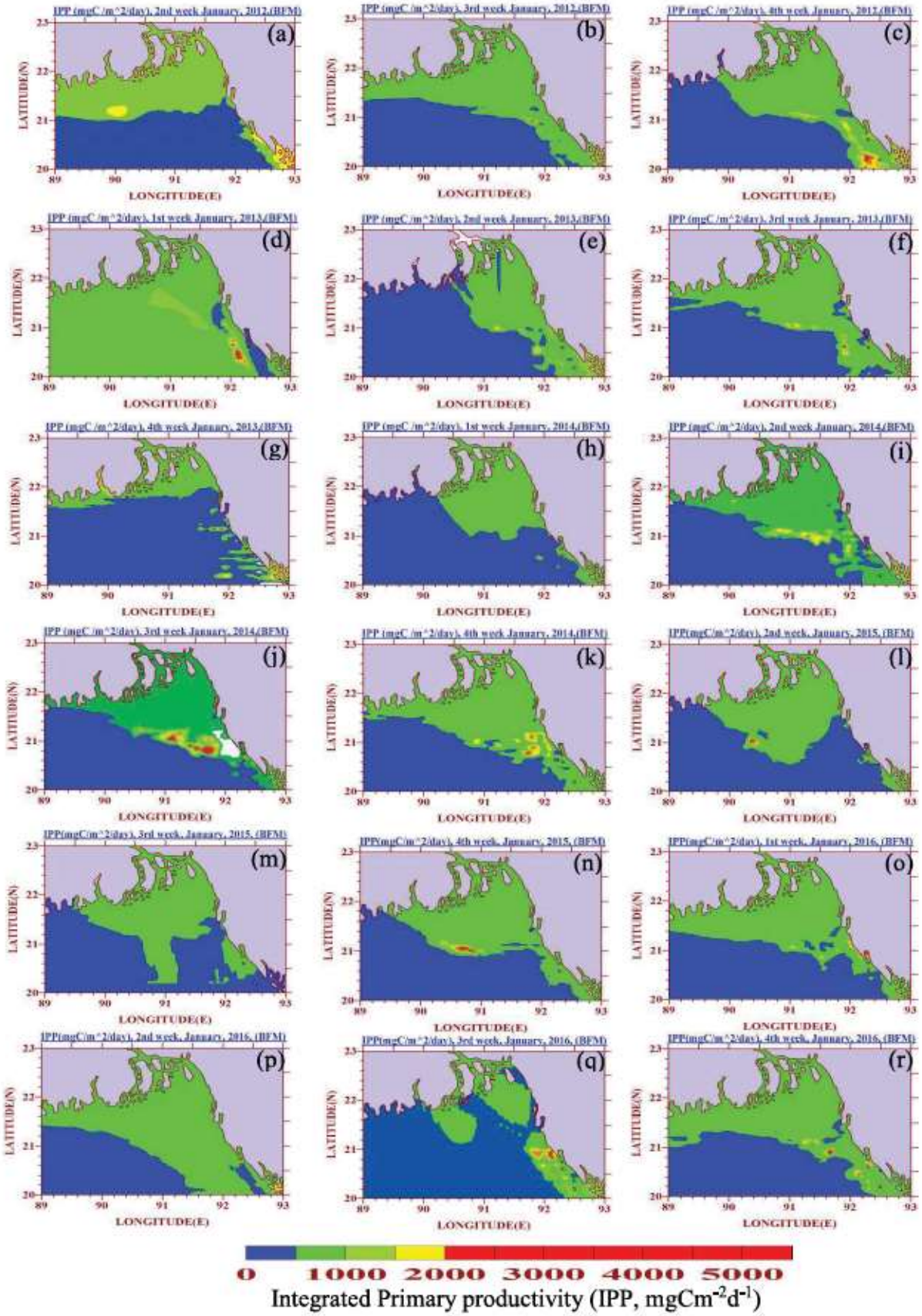

Fig. 3: Weekly Spatio-temporal distribution of estimated Integrated primary productivity ($mgCm^{-2}d^{-1}$), in the northern part of BoB based on BFM in the month of January from 2012 to 2016.

Spatio-temporal distribution of integrated primary productivity in the month of January showed a value from 35 – 2500 $mgCm^{-2}d^{-1}$ with an average productivity of 400 $mgCm^{-2}d^{-1}$ (Fig. 3(a-r)). IPP was found to be higher to the northward mouth of BoB in the month of January and that was similar type of distribution as like December but comparatively lower productivity was found in January rather than December.

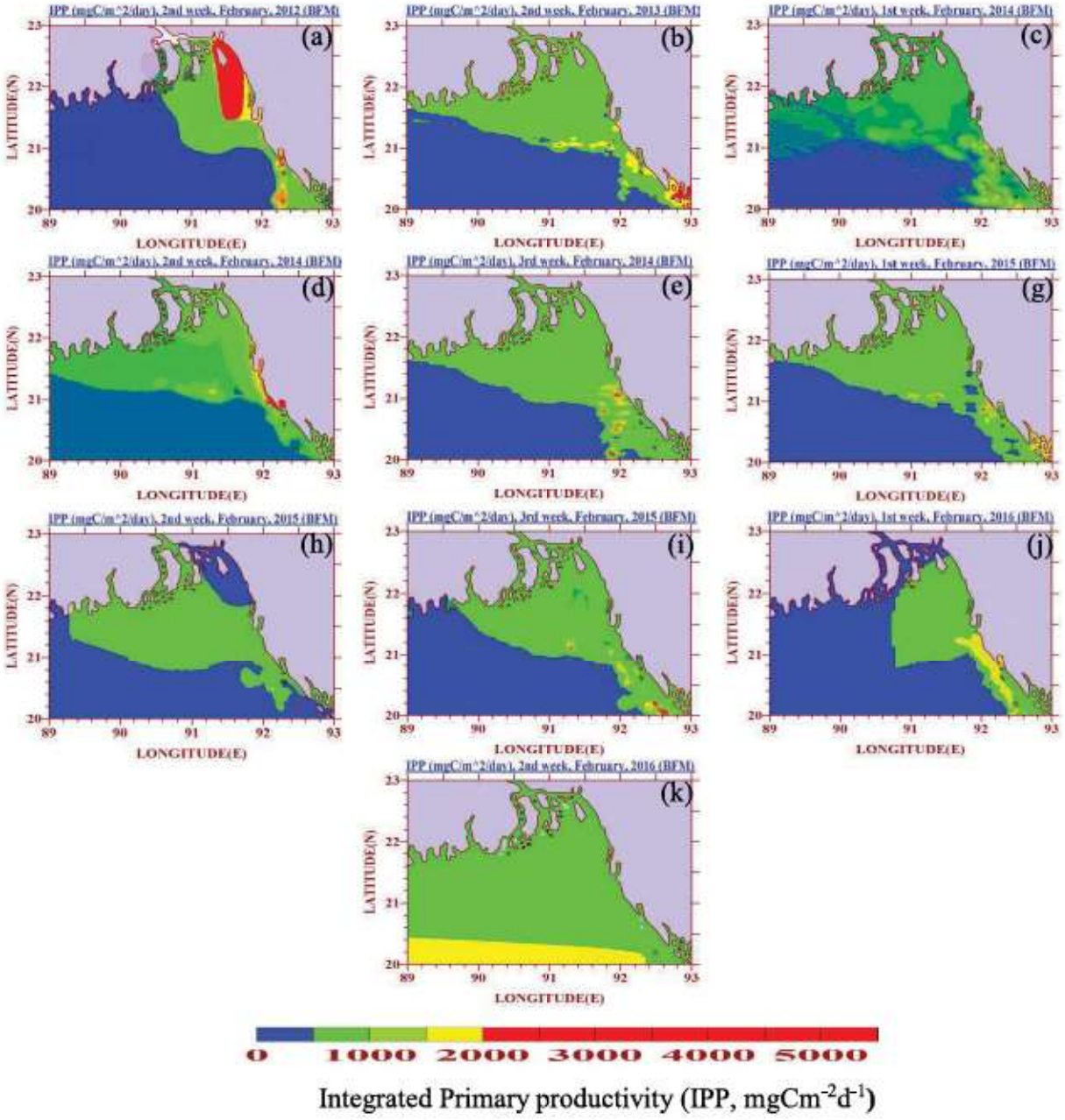

Fig. 4: Weekly Spatio-temporal distribution of estimated Integrated primary productivity ($mgCm^{-2}d^{-1}$), in the northern part of BoB based on BFM in the month of February from 2012 to 2016.

February showed the range of primary productivity from 65-3500 $mgCm^{-2}d^{-1}$ with an average estimated value of 500 $mgCm^{-2}d^{-1}$ (Fig. 4(a-k)). In general, productivity was from 0-1000 $mgCm^{-2}d^{-1}$ but frequently exceed over 1000$mgCm^{-2}d^{-1}$ in February from 2012-2016.

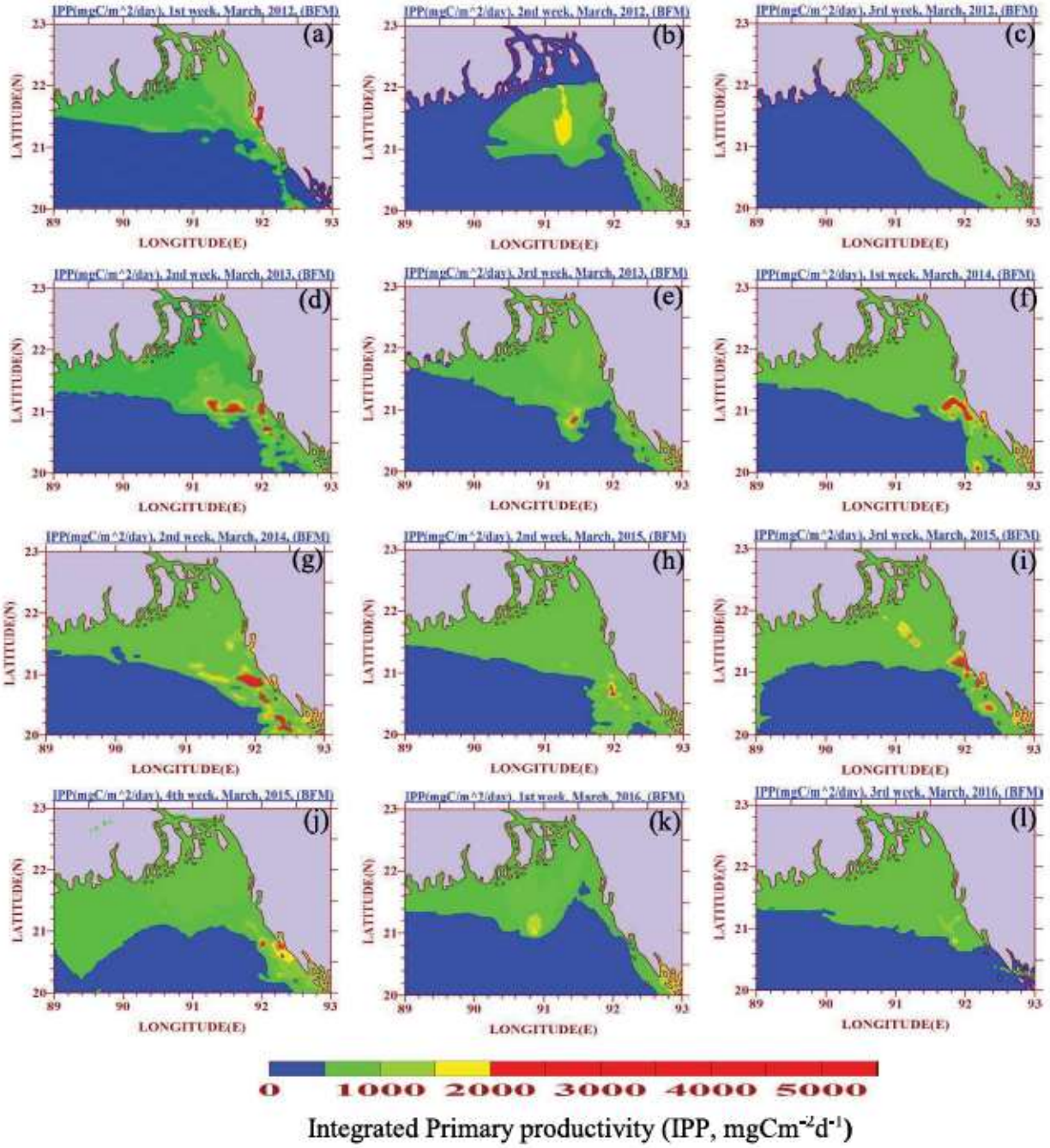

Fig. 5: Weekly Spatio-temporal distribution of estimated integrated primary productivity ($mgCm^{-2}d^{-1}$), in the northern part of BoB based on BFM in the month of March from 2012 to 2016.

Estimated IPP was ranged from 25 – 3000 $mgCm^{-2}d^{-1}$ with an average estimated value of 550$mgCm^{-2}d^{-1}$ in March by BFM model for a time period of 2012-2016 (Fig. 5(a-l)). There was no significant temporal variation rather than some spatial variation observed between the northward and southward part of the study area (Fig. 5(a-l)) in March.

In correlation matrix among the parameter of BFM showed a higher negative correlation between chlorophyll concentration and photosynthesis rate and a positive relation was found between photosynthesis rate and PAR (Table 1). Euphotic depth negatively correlated with kd490 where the depth was derived using kd490 and Kpar. Primary productivity was mainly correlated with chlorophyll concentration and photosynthesis rate (P_{opt}) in BFM model.

Table 1: Pearson Correlation matrix among the parameters derived for estimation of Primary productivity, VGPM model by BFM.

Variables	(X1)	(X2)	(X3)	(X4)	(X5)	(X6)	(X7)	(X8)	(X9)
Chlorophyll (mgm^{-3}) (X1)	1								
SST (^0C) (X2)	-0.164[a]	1							
PAR (einstein m^{-2} day^{-1}) (X3)	0.009[a]	0.035*	1						
k490 (X4)	0.131[a]	-0.129[a]	0.075[a]	**1**					
P_{opt}(photosynthesis rate) (X5)	**-0.702***	**0.469***	-0.038[a]	-0.157[a]	1				
Kpar (X6)	0.131[a]	-0.129[a]	0.075[a]	**1***	-0.157[a]	1			
Z_{eu} (euphotic depth, m) (X7)	-0.143[a]	0.143[a]	-0.060[a]	**-0.946***	0.170[a]	**-0.946***	1		
Daylength (hour) (X8)	**-0.340***	**0.553***	-0.042[a]	**-0.336***	**0.518***	**-0.336***	**0.369***	1	
Primary Productivity ($mgCm^{-2}d^{-1}$) (X9)	**0.947***	-0.125[a]	0.009[a]	-0.074[a]	**-0.676***	-0.074[a]	0.065[a]	-0.251[a]	1

a = Absolute correlation values below 0.291 are not statistically significant *(*Neto *et al., 2015)*
***** = Absolute correlation values above 0.291 are statistically significant

Graph 1 Average IPP with standard deviation estimated by VGPM model of BFM in northern part of BoB

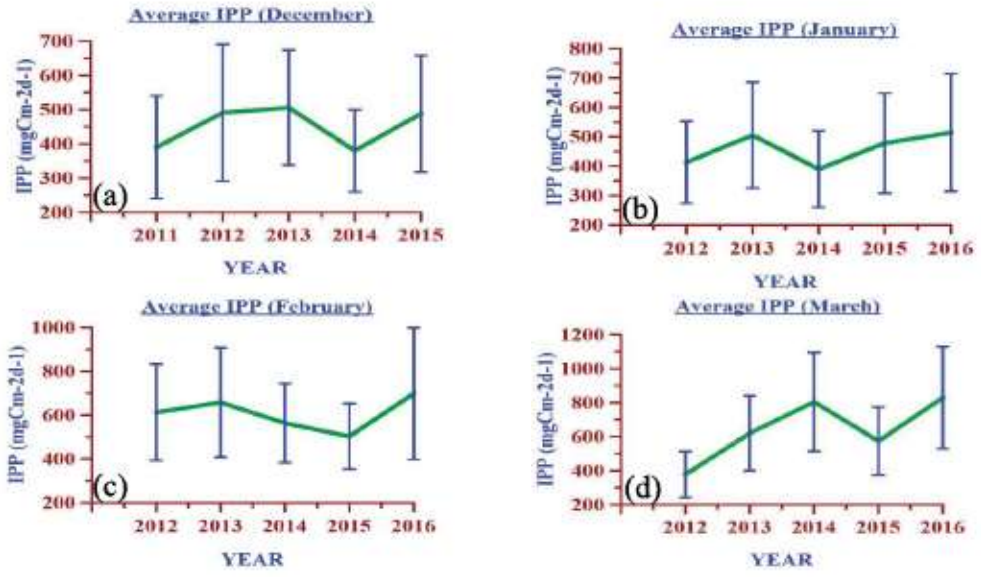

Fig. 6: Estimated intra-seasonal average integrated primary productivity ($mgCm^{-2}d^{-1}$) based on VGPM of BFM in northern part of BoB.

A lower value of average IPP was found in March, 2012 and the peak value was also governing with March 2016 when IPP estimated by VGPM of BFM (Fig. 6d). There was a significant decrease in concentration of productivity in 2014 for December and January (Fig. 6(a-b)) and in 2015 for February and March (Fig. 6(c-d)).

4. Conclusion

The study area was characterized with lower productivity to the southward open part of BoB and frequently occurring higher concentration in some area. The unique physical characteristics of BoB influence primary production all over the area. Due to lack of oceanographic in-situ data in this region and survey cost, use of RS data and estimation is followed to study about different physico-chemical features of this area and also provide good results with historic data. Applying BFM model to estimate primary productivity in the northern part of BoB provides acceptable results under this study.

References

Barnard AH, Zaneveld JRV and Pegau WS (1999): In situ determination of the remotely sensed reflectance and the absorption coefficient: closure and inversion. Applied Optics, Vol. 38, Issue 24, pp. 5108-5117.

Behrenfeld MJ and Falkowski PG (1997): Photosynthetic rates derived from satellite-based chlorophyll concentration. Limnology and Oceanography, Vol. 42, Issue 1, pp 1-20.

Forsythe WC, Rykiel Jr EJ, Stahl RS, Hsin-i Wu and School field RM (1995): A model comparison for daylength as a function of latitude and day of the year. Ecological Modelling, Vol. 80, Issue 1, pp. 87-95.

Guosheng Li, Ping G, Fang W and Qiang L (2004): Estimation of ocean primary productivity and its spatio-temporal variation mechanism for East China Sea based on VGPM model. Journal of Geographical Sciences, Vol. 14, Supplement 1, pp. 32–40.

Kameda T and Ishizaka J (2005): Size-Fractionated Primary Production Estimated by a Two-Phytoplankton Community Model Applicable to Ocean Color Remote Sensing. Journal of Oceanography, Vol. 61, pp. 663 – 672.

Kirk JTO (1994): Light and photosynthesis in aquatic ecosystems. Cambridge University press.

Lee Z (2009)KPAR: An optical property associated with ambiguous values. Journal of Lake Sciences, 21(2): 159-164.

Mohanty SS, Pramanik DS and Dash BP (2014): Primary Productivity of Bay of Bengal at Chandipur in Odisha, India. International Journal of Scientific and Research Publications, Volume 4, Issue 10, ISSN 2250-3153.

Morel A (1988): Optical modeling of the upper ocean in relation to its biogenous matter content (Case I waters). Journal of Geophysical Research, volume 93, Issue C9, pp. 10749 – 10768.

Morel A, Gentili B (2004): Radiation transport within oceanic (case 1) water. Journal of Geophysical Research, Vol.109,C06008,doi:10.1029/2003JC002259.

Neto JLR and Fragoso CR, Malhado ACM, Ladle RJ (2015): Spatio-temporal Variability of Chlorophyll-A in the Coastal Zone of Northeastern Brazil. Estuaries and Coasts, Volume 38, Issue 1, pp 72–83.

Pramanik DS and Mohanty SS (2016): Seasonal variation of primary productivity of Bay of Bengal at Chandipur-on Sea, Odisha. International Journal of Fisheries and Aquatic Studies, 4(2): 331-336.

Sigman DM and Hain MP (2012): The Biological Productivity of the Ocean. Nature Education, Vol. 3, Issue 6.

Zaneveld JRV, Kitchen JC and Mueller JL (1993): Vertical structure of productivity and its vertical integration as derived from remotely sensed observations. Limnology and Oceanography, Vol. 38, Issue 7, pp. 1384-1393.

Thermal inversion, Mixed Layer Depth (MLD) and Barrier Layer Thickness (BLT) variability and associated fluorescence pattern during winter in the Northern Bay of Bengal

Kazi Belayet Hossain[1], Md Kawser Ahmed [2], Abdullah-Al-Hasan[3], Sultan Al Nahian[4], Rupak Loodh[5], Seema Rani [6] and K M Azam Chowdhury [8]

[1,3,4,5,6] Post-graduate student, Department of Oceanography, University of Dhaka, Bangladesh.
[2] Professor, Department of Oceanography, University of Dhaka, Bangladesh.
[8] Lecturer, Department of Oceanography, University of Dhaka, Bangladesh.
*Author for correspondence: hossain_kb@ymail.com

Abstract: The Bay of Bengal is the unique and largest bay in the world. Freshwater flux like runoff and rainfall can enhance stratification in the Bay of Bengal (BOB) through the formation of a barrier layer, which can lead to the formation of a temperature inversion. Because of excessive freshwater intrusion in the bay mixed layer is always shallower than barrier layer on the other hand during winter there are less wind-stress which also cause less mixing in the water column. For calculating Thermal inversion, MLD, BLT and ILD, CTD data collected from 23 stations in the fishing ground of northern Bay of Bengal during January 18 to February 11' 2016. MLD (max 25m) in the entire ground was low whereas BLT (max 40m) was high, Thermal inversion was observed near the eastern coast. Fluorescence was maximum in the sub-surface in the entire stations except in station 1 where fluorescence was maximum in upper region and in station 2 where maximum fluorescence was in the bottom, because of upwelling in station 1 which pumped up the nutrient and chlorophyll to the surface and downwelling in station 2 which pumped down the nutrient and chlorophyll on the bottom, this phenomena is called subsurface chlorophyll Maxima (SCM), in this study SCM showed below 20m. The vertical plot of the CTD data showed perfect scenario of downwelling in eastern zone of Bay of Bengal.

Key word: Physical Oceanography, Bay of Bengal, Fishing ground, CTD, MLD, BLT, ILD, Sub-surface chlorophyll maxima, Upwelling and Downwelling.

1. Introduction

The Bay of Bengal (BOB) is a semi-enclosed tropical basin which is situated in the northeastern part of the Indian Ocean; it is the largest bay in the world. The unique feature of the Bay of Bengal is the large seasonal freshwater pulse, which makes the waters of the upper layers less saline and highly stratified. This seasonal freshening is brought about by the excess precipitation over evaporation (2 m/yr, Prasad, 1997; Gill, 1982) and also by the freshwater influx from the adjoining rivers (1.625×10^{12} m^3/yr, Subramanian, 1993). Climatology of cumulative river discharge (m^3/s) during July-October period from Ganges (130×10^{10} m^3/s), Brahmaputra (150×10^{10} m^3/s) into the Bay of Bengal (Global Runoff Data Center, Germany) especially in the shelf zone of Bangladesh or the northern part of Bay of Bengal. Mixed layer (ML) is a layer where is turbulence generated in the ocean by the wind, convective cooling, breaking waves, current shear, and other physical processes creates a surface layer characterized by uniform to near-uniform density, active vertical mixing and high dissipation (Wijesekera and Gregg, 1996).

Mixed layer Depth (MLD)is a depth where mixed layer is observed. Jayu Narvekar, and S. Prasanna Kumar (2006) mentioned in a study that, north of 15^0 latitude at the BOB, MLD is Shallow (~ 20m) throughout the year, which means that in any season low saline water influences MLD in the northern bay. They also mentioned that by prevailing circulation, the winter freshening from rain and river discharge is advected to offshore. This result shows a strong stratification, even in winter (4^0C) cooling of SST is unable to cause convective mixing. Pankajakshan Thadathil *et al.* (2007) mentioned another cause responsible for intense mixing namely horizontal advection in the surface layer. He also described that, MLD in the BOB remains shallow because of the fresh water brought in this region through Ekman drift.

Isothermal Layer depth (ILD) is defined as a vertical column of water having a constant temperature with depth. It varies with the change of seasons. Thadathil *et al.* (2007), Rao and Sivakumar, (2003), Kara *et al.* (2003), Sprintall and Tomczak (1992) defined ILD as depth top of the thermocline, is the depth at which temperature drops by 1^0C from the SST. This is a simple definition where temperature is decreasing downward in ocean water column. The Barrier layer (BL) in the ocean is a layer of water separating the well-mixed surface layer from the thermocline.

Barrier Layer Thickness (BLT) is a layer between ILD and MLD, if we measure the ILD and MLD value then we can easily calculate the BLT. Vinayachandran, P. N (2002), define BLT as the layer difference between ILD and MLD, which has which has strong salinity stratification and weak (or neutral) temperature stratification..PankajakshanThadathil *et al.* (2007) at his study on BOB, mentioned that to understand the mechanism of BLT, it is important to comprehend the mechanism of MLD and ILD. If MLD is determined by thermal stratification caused by net heat flux, then both MLD and ILD become almost equal and results a very thin BL (Girishkumar, M, S.; 2013). Thadathill also mentioned that strong wind will deepen the MLD and resist forming thick BLT.

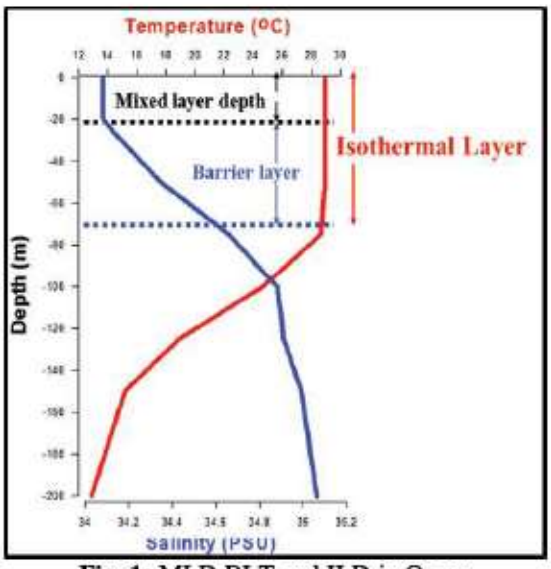

Fig. 1: MLD BLT and ILD in Ocean

The depth profiles of phytoplankton pigments in the Bay of Bengal are generally characterized by a subsurface chlorophyll maximum during winter (Madhu *et al.*, 2006). Sub-surface Chlorophyll Maxima (SCM) is define as when there is sufficient sunlight and nutrient contain in subsurface phytoplankton gradually maximize their population in the subsurface this phenomena is called SCM. According to N.V Madhu (2006), during winter the chlorophyll maxima occurred in the upper layer of the euphotic zone or subsurface layer (< 20m).

2. Material and Methodology

The study area was between latitude $20^0 - 21.5^0$ N and longitude $89.5^0 - 92^0$ E. Total number of the stations are 23 from in 19 different days. Among them 15 stations are from South patches, 2 stations are from South of south patches, 4 stations on the Middle ground and 2 stations on the Swatch of No Ground. It took 26 days to cover these stations. Total distance run 181 nautical mile or 334 km. Study area covered almost entire fishing ground area about 16000 sq. km (Figs. 1, 2, 3 and 4).

2.1 Hydrographic Data

Temperature, salinity and density were measured from the in situ observation by a Sea-Bird Electronics CTD Machine (SBE 19 plus V2). Fluorescence and turbidity was measured by WET Labs ECO-FLNTU sensor attached with the CTD machine. Measurement was done by the help of Agro Food – 4, a fishing trawler with 42m length and 11m wide and 13m height of Sea Resource Company Ltd. Depth of each stations were determined by SIMRAD Sonar. Vertical plot of Temperature, Density, Salinity, Turbidity and Fluorescence (Figs. 6, 7, 8) and vertical contour of Temperature, Density and Salinity (Fig. 9) are generated from Golden Software "Grapher 2" and "Surpher 8". MLD, BLT and ILD was calculated using MATLAB 2015a.

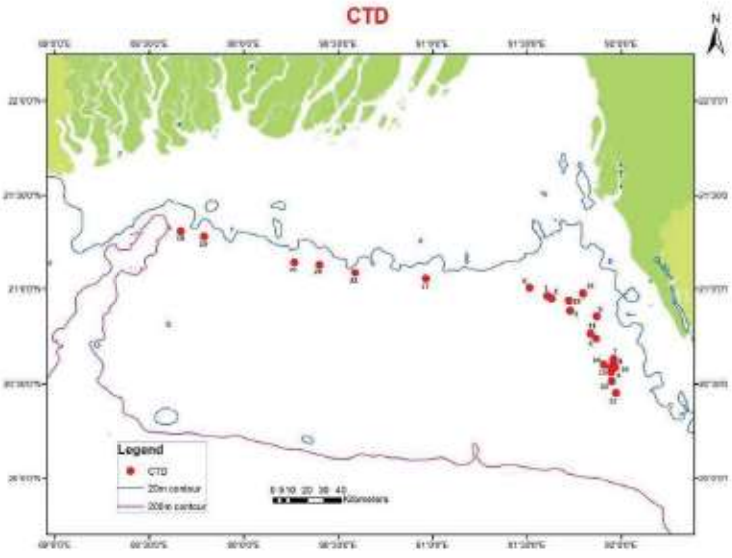

Fig. 2: Study area, CTD Measurement stations are the red dots

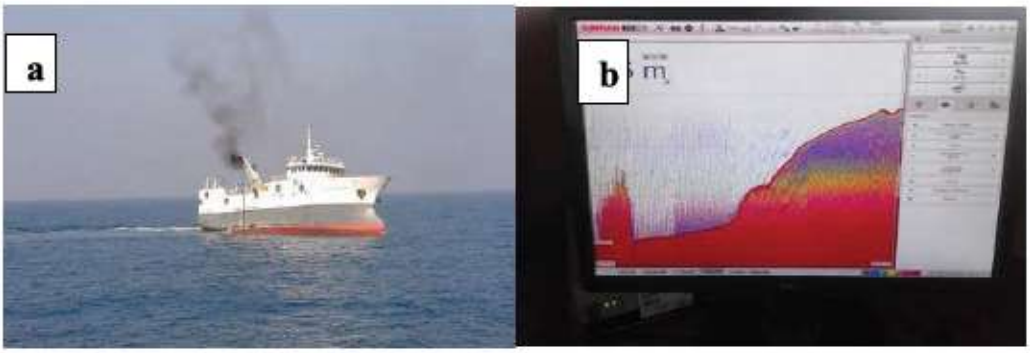

Fig. 3: (a) Agro food – 4 fishing trawler, and (b) SIMRAD sonar

2.2 Methodology

2.2.1 Selection of MLD

There are many studies conducted by different authors in order to find out the best way for MLD selection in BOB. Density (sigma-t) and temperature (^{0}C) have been taken as the base for selecting MLD. The depth at which density increase by 0.2 kg/m^3 plus temperature changes by 0.8 ^{0}C both from the surface were taken as criteria for determining the MLD.

Fig. 4: CTD Machine (SBE 19 Plus V2)

2.2.2 Selection of ILD

Different methodologies are exist for selecting ILD in the BOB. Schematics of MLD and BLT in the Bay of Bengal in the case of no thermal inversion (Fig. 5(a)) and ILD is calculated as the depth where temperature changes by 1oC from surface value, in Fig. 5(b) temperature profile with surface layer inversion and circle and star represents top and base of the inversion layer respectively and ILD is calculated as the depth where the temperature increases by 1oC from surface value, in Fig. 5(c) ILD is selected as the depth where temperature drops by 1^{0}C from surface value, in Fig. 5(d) ILD is selected as the depth where temperature at the base of the inversion layer is equal to the temperature at the top of the inversion layer. In this paper ILD is selected at as the depth of the top of the thermocline, is defined as the depth at which temperature changes by 1°C from SST (Fig. 5). This method hold good result in normal condition but does not hold good result during winter when Bay of Bengal experiences large scale thermal inversion (Thadathil *et al.*, 2007).

2.2.3 Selection of thermal inversion

During winter Bay of Bengal experiences large scale of thermal inversion. For thermal inversion ILD is selected as the depth where temperature at the base of the inversion layer is equal to the temperature at the top of the inversion layer (Fig. 5d).

2.2.4 Selection of BLT

Finding out BLT was rather straight forward. It was determined by subtracting MLD from ILD. Same criteria were used to determine the barrier layer thickness throughout the study.

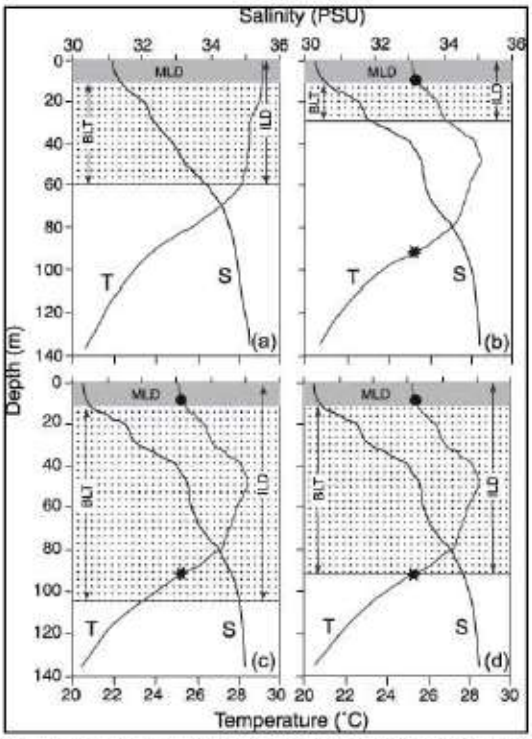

Fig. 5: Different methods of calculating ILD (Thadathill *et al.*, 2007)

3. Result and Discussion

MLD in the entire ground was low whereas BLT was high. Maximum BLT was 48m (Station 5) and minimum was 0m (Station 7). BLT was zero in station 7 because on that point depth wasn't fully covered. There were some stations where BLT is lower than MLD those stations are 6, 15, 19 and 22. There were some stations where BLT is lower than MLD, those stations are 6, 15, 19 and 22. There were some stations where BLT is lower than MLD, those stations are 6, 15, 19 and 22. MLD was minimum (1m) in station 9, 10 and 14 as in these stations fresh water is overlaid by saline water for which upper density and salinity became very low. It happened because of during low tide, estuarine low density water flow moved toward the sea and the measurement of these stations were done during low tide. Maximum MLD is 25m in station. Thermal inversion has also been observed in the fishing ground. Criteria of thermal inversion was applied in 11 stations among them 6 stations showed exact inversion (station 6, 8, 14, 15 18 and 19) and the rest of the 5 stations showed opposite of thermal inversion (station 4, 9, 16, 20 and 23), criteria of thermal inversion was applied in these 5 stations as no other criteria of calculating ILD were able to calculate. Thermal inversion was occurred near the coast. A table below is showing the thermal inversion status in different stations 3.

Table 1: Thermal inversion status in different stations

SI	Station No.	Latitude North	Longitude East	Thermal inversion starts from the depth (m)	Thermal inversion ends in the depth (m)
1	4	20.55955	91.945083	8	27
2	6	21.00685	91.51295	13	18
3	8	20.614917	91.957133	8	20
4	9	20.8575	91.8684	1	8
5	14	20.5996	91.90735	1	20
6	15	20.582983	91.9455	11	17
7	16	20.977667	91.797	4	7
8	18	21.3085	89.665333	7	21
9	19	21.279933	89.789183	10	14
10	20	21.131333	90.3995	10	25

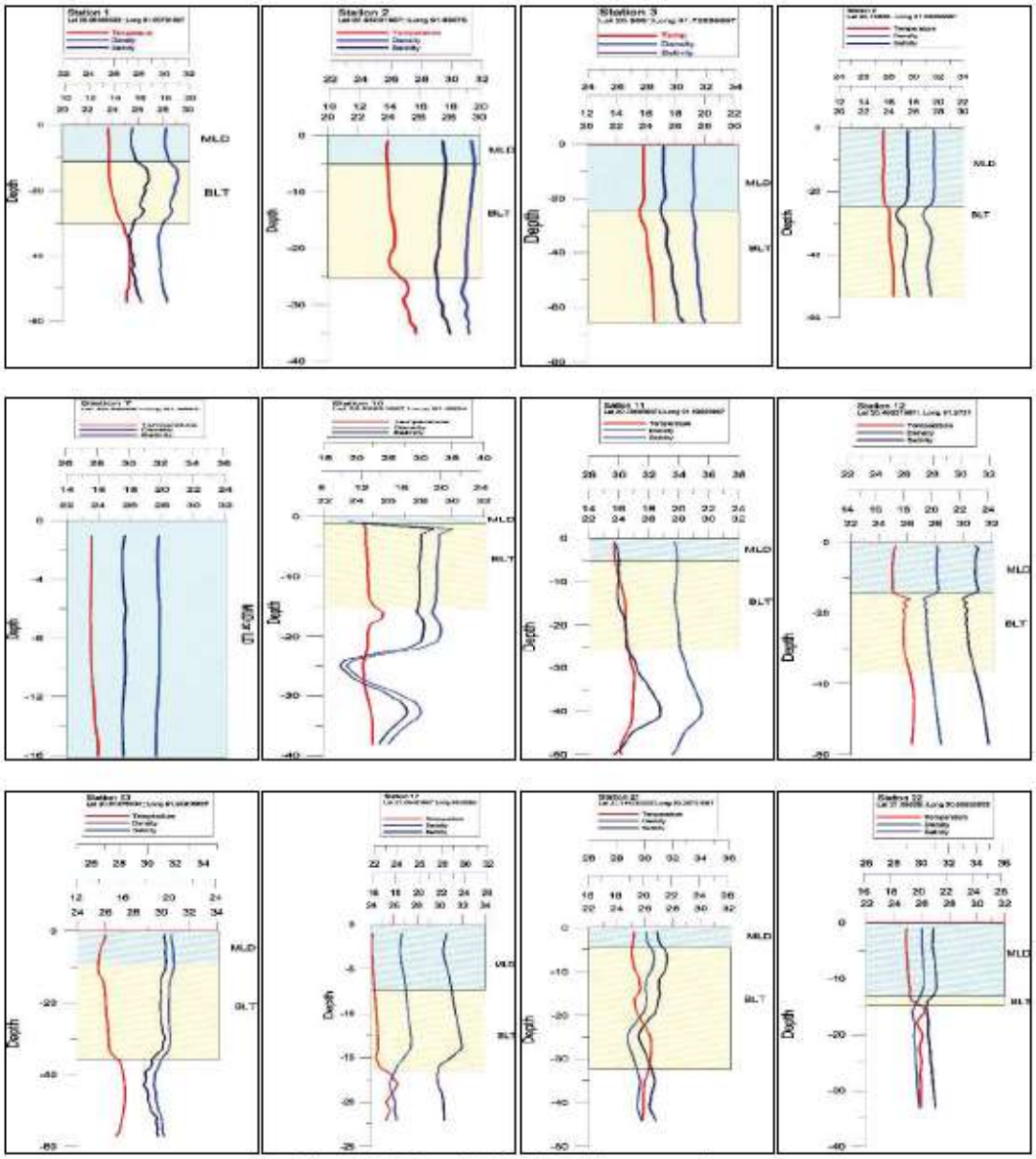

Fig. 6: MLD and BLT in Different stations

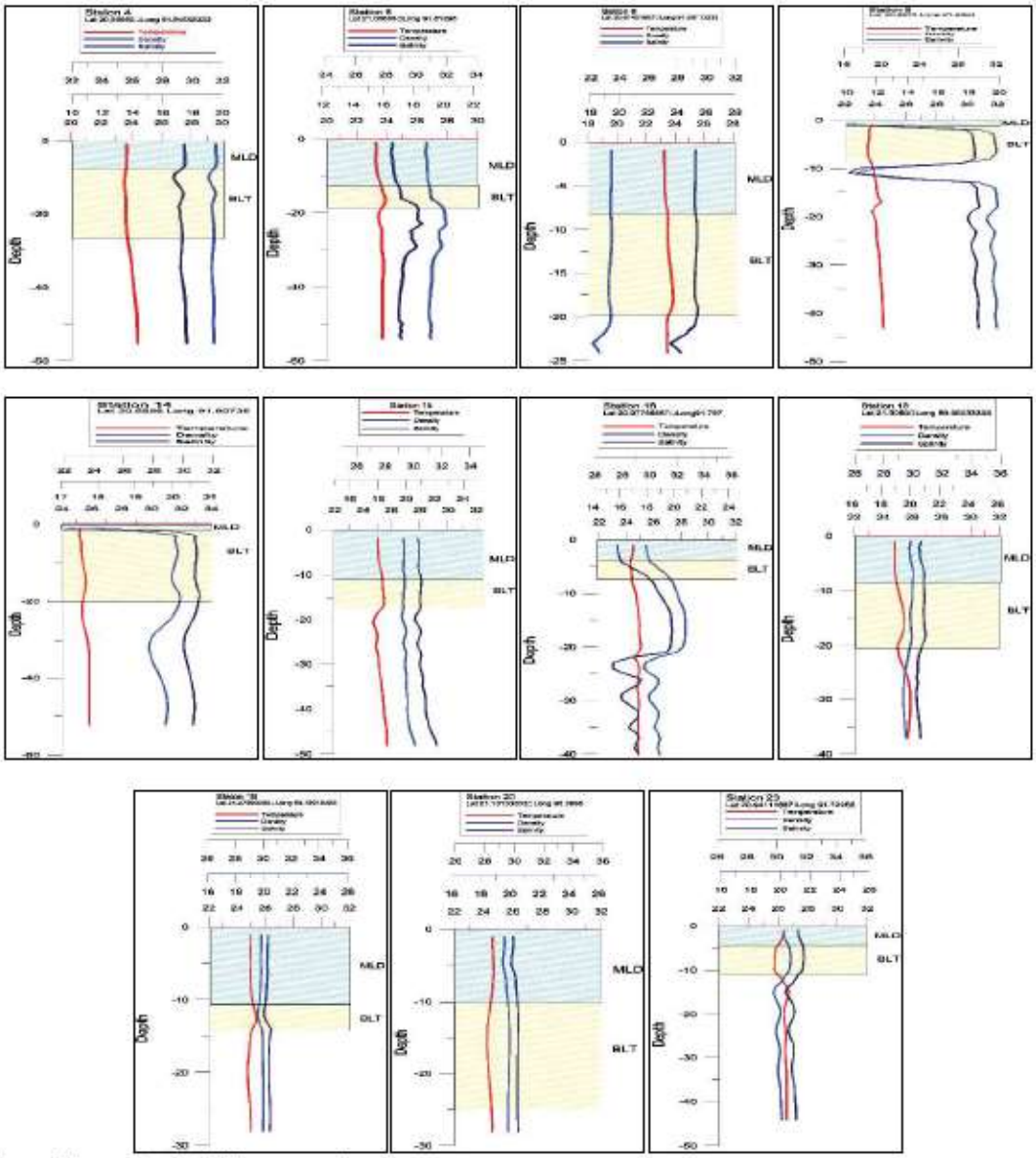

Fig. 7: Thermal inversion in different stations

Fluorescence was maximum in the sub-surface in the entire stations except in station 1, where fluorescence was maximum in upper region and in station 2 where maximum fluorescence was in the bottom because of upwelling in station 1 which pumped up the nutrient and chlorophyll to the surface and downwelling in station 2 which pumped down the nutrient and chlorophyll on the bottom. Maximum fluorescence was in the subsurface layer (<20m) because in every case fluorescence was trapped in the barrier layer. As we know that the water in barrier layer is highly stagnant it doesn't mixed with any other region of the water column, so when the phytoplankton community entered in the barrier layer it gets trapped and increasing with sufficient Photosynthetic Active Radiation (PAR) and nutrient which results subsurface chlorophyll maxima.

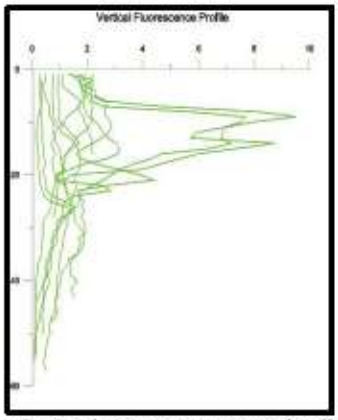

Fig. 8: Fluorescence Pattern in all stations

The vertical contour of the CTD data from 89 to 92°E, where downwelling pattern was observed in 91° to 91.5°E. (3.2 (a-c)). On that region water column of low density and salinity which appeared like something pumping down this water in to the bottom. The other region didn't show any upwelling and downwelling because of limited data on that particular region.

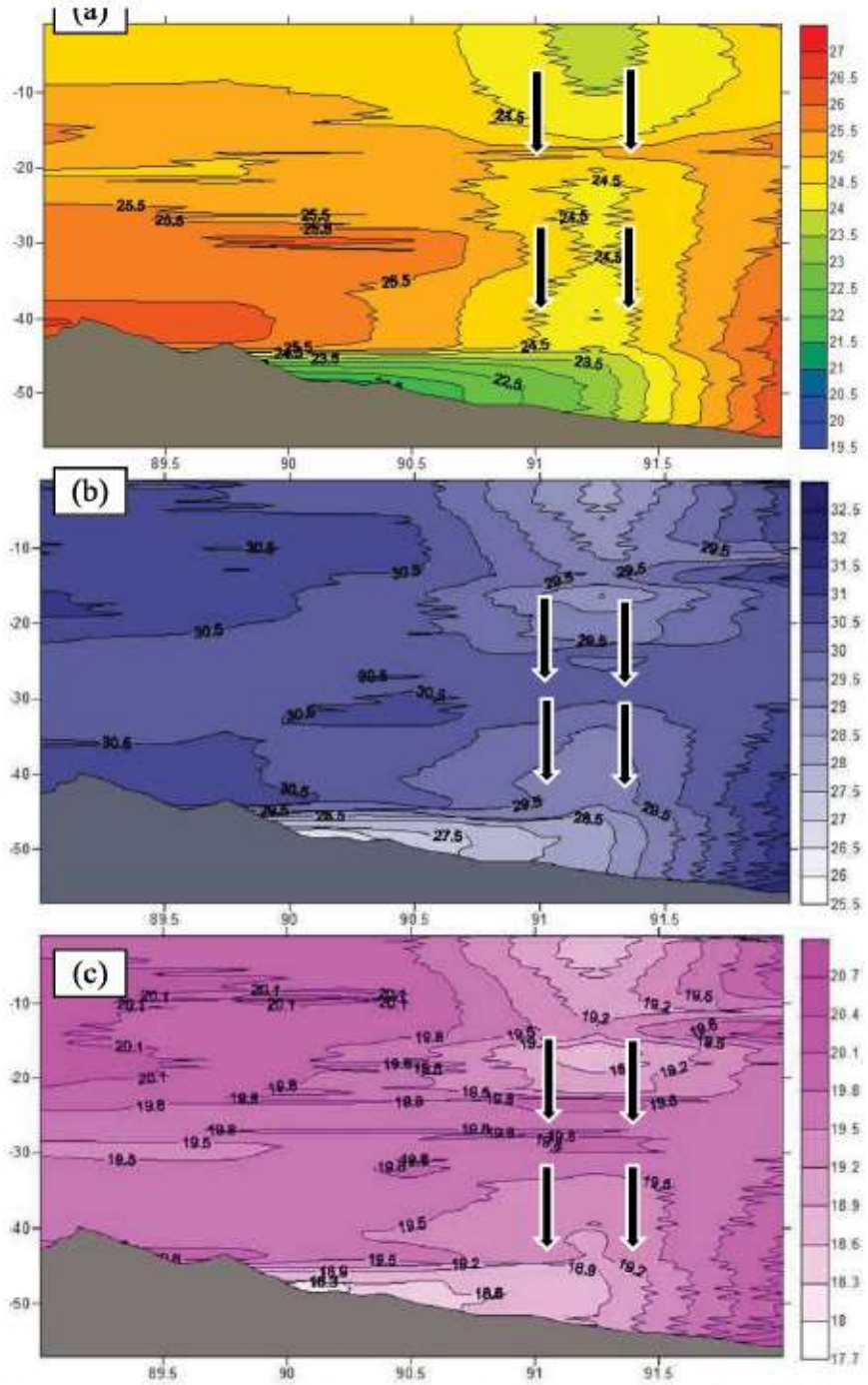

Fig. 9: Vertical contour of (a) Temperature, (b) Salinity and (c) Density, in this figure black arrow shows that downwelling was occurred on the region between 91 to 91.5^{0}E.

4. Conclusion

Bay of Bengal is highly influenced by MLD, BLT and thermal inversion. Excessive fresh water discharge from different river systems like Ganges-Brahmaputra and others, a layer of fresh water remains entire region all the year and during winter there is less wind stress in the Bay of Bengal which causing shallow MLD and thick BLT. Thermal inversion occurs near the coast of Bay of Bengal during winter. Another feature showed in the Bay that maximum Fluorescence found in the subsurface which clearly indicate the term sub-surface chlorophyll maxima (SCM) is often occurred in the Bay of Bengal.

Acknowledgement

Author wishes to thank Mr. Syed Arif Azad, Director General, Directorate of Fisheries and Mr. Nasiruddin Mohammad Humayun, Director, Department Marine Fisheries, Directorate of Fisheries, People's Republic of Bangladesh for arranging deep sea fishing vessel for collecting samples and CTD measurement in the fishing ground.

References

Gadgil, S., P. V. Joseph, and N. V. Joshi, (1984): Ocean-atmosphere coupling over monsoon regions, Nature, 312, 141-143, 1984.

Girishkumar, M, S., M. Ravichandran, and M, J. McPhaden (2013): Temperature inversions and their influence on the mixed layer heat budget during the winters of 2006—2007 and 2007—2008 in the Bay of Bengal, J. Geophys. Res. Oceans, 118, doi:10.1002ljgrc20192.

Kara, A. B., Rochford, P. A., and Hurbun, H. E. (2003): Mixed layer depth variability over the global ocean, J. Geophys. Res, 108, 3079, doi: 10.1029/2000JC000736, 2003.

Nuncio, M., Prasanna Kumar, S., (2012): Life cycle of eddies along the western boundary of the Bay of Bengal and their implications. J, Mar. Syst. 94, 9-17.

Narvekar, J. and S, Prasanna Kumar (2014): Mixed layer variability and chlorophyll a biomass in the Bay of Bengal, Biogeoscienoes, 11, 3819-3843, 2014.

Narvekar, J., S. Prasanna Kumar. (2006): Seasonal variability of the mixed layer in the central Bay of Bengal and associated changes in nutrients and chlorophyll, Deep-Sea Research I, 53, 820-835.

N.V. Madhua, R. Jyothibabu, P.A. Maheswaran, Vijay John Gerson, T.C. Gopalakrishnan, K.K.C. Nair (2006). Lack of seasonality in phytoplankton standing stock. *Continental Shelf Research, 26*, 1868 - 18883.

Prasad, T.G (1997): Annual and seasonal mean buoyancy fluxes for the tropical Indian Ocean. Current Science 73, 667—674.

Prasanna Kumar, S., and T. G. Prasacl (1999), Formation and spreading of Arabian Sea high salinity water mass, J. Geophys. Res, 104, 1455—1464.

Prasanna Kumar, S,Narvekar, J, Nuncio, M, Kumar, A, Ramaiah, N, Sardesai, S, Gauns, M, Fernandes, V, and Paul, J, (2010): Is the biological productivity in the Bay of Bengal light limited?, Curr. Sci, 98, 1331-1339, 2010.

Subramanian, V. (1993): Sediment load of Indian Rivers. Current Science 64, 928—930.

Rao, R. R., C.K., Naqvi, S.W.A., Kumar, M.D., Varaprasad, S.J.D., Jayakumar, A., George, M.D., Singbal, S.Y.S., (1994): Hydrochemistry of the Bay of Bengal: possible reasons for a different water-column cycling of carbon and nitrogen from the Arabian Sea. Marine Chemistry 47, 279—290.

Sprintall, J. and Tomczak, M. (1992): Evidence of barrier layer in the surface layer of the tropics. J. Geophys. Res, 97, 7305—7316, 1992.

Thadathil, Pankajakshan (2007), Observed seasonal variability of barrier layer in the Bay of Bengal, J. Geophys. Res, 112, 002009, doi:10.1029/2006J0003651.

Vinayachandran, P. N. (2002), Observations of barrier layer formation in the Bay of Bengal during summer monsoon, J. Geophys. Res, 107(C12), 8018, doi: 10.1029/ 2001 J0000831, 2002.

Wijesekera, R. W., and M. C. Gregg, 1996: Surface layer response to weak winds, westerly bursts, and rain squalls in the western Pacific warm pool. J. Geophys. Res., 101, 977–997.

Study of severe thunderstorm and associated rainfall in Bangladesh during pre-monsoon season

Md. Abdul Mannan[1]*, Farzana Rahman[2], Shamsuddin Ahmed[1], Md. Abdul Mannan Chowdhury[3], Samarendra Karmakar[4] and Md. Moniruzzaman[2]

[1]Bangladesh Meteorological Department, Agargaon, Dhaka
[2]Department of Geography and Environment, Jagannath University, Dhaka
[3]Geography and Department of Physics, Jahangirnagar University, Savar, Dhaka
[4]National Oceanographic and Maritime Institute (NOAMI), Dhaka, Bangladesh
Corresponding author: mannan_u2003@yahoo.co.in, mamannanbmd2015@gmail.com

Abstract: Bangladesh is a disaster prone country. Severe thunderstorms (STS) are one of the major disasters in Bangladesh. STS are responsible for the development and formation of many severe weather phenomena like heavy rainfall. Attempt has therefore been made to know the inherent properties of STS for better prediction of heavy rainfall associated with this. It is found that the atmospheric condition became unstable in the afternoon period in the dates when STS occurs in the late hours of the day; the magnitude of LI, SI, KI were much higher than average value and the magnitudes of PW became 30 mm and above. The magnitudes of the thermodynamic indices recorded at 0000UTC from Radiosonde observations are not always representing the instability condition of the day. They are limited with time and location. This problem may be resolved through simulation using WRF-ARW model. Simulation of the events indicates the evolution of CAPE, KI, TTI, SWI and PW with the progress of the day became the favourable for TS occurrence with high amounts of rainfall. Simulated rainfalls were higher than observation at some part but it is less than observation at other part. RMSEs of simulated rainfall at BMD station locations for selected outer domain (D1) and inner domain (D2) are 19.9 and 21.3 mm. But RMSEs of model rainfall with station rainfall of 30 mm or more are 29.2 and 29.3 mm.

1. Introduction

Bangladesh is a disaster prone country. Almost every year, the country experiences disasters of one kind or another such as tropical cyclones, storm surges, thunderstorm (TS), coastal erosion, floods, and droughts causing heavy loss of life and property and jeopardizing the development activities (Ali, 1999). Thunderstorms are responsible for the development and formation of many severe weather phenomena. Thunderstorms, and the phenomena that occur along with them, pose great hazards to populations and landscapes. Damage that results from thunderstorms is mainly inflicted by downburst winds, large hailstones, and flash flooding caused by heavy precipitation. Stronger thunderstorm cells are capable of producing tornadoes and waterspouts (Gomes *et al.,* 2006). In Bangladesh, thunderstorms occur in all seasons of pre-monsoon, monsoon and post-monsoon are characterized by strong surface wind generally from 40 to 100 miles per hour and accompanied by heavy rain and often destructive hail with lightning (Ferdousi *et al.,* 2014).

Thunderstorm (TS) is a major form of convectional rainfall over Bangladesh. The pre-monsoon season comprises the months of March to May when most of the severe thunderstorms (STS) occur in Bangladesh (Karmakar, 2001). It is a violent, short-lived weather disturbance that is associated with lightning, thunder, dense clouds, heavy rain or hail, and stronggusty winds. Moisture sources of the Bay of Bengal and the crisscross river system in Bangladesh, the topographic features in the north and east help to form STS during pre-monsoon and post-monsoon (October-November) seasons. Apart from local TS, some of them that over from Choto Nagpur, West Bengal and northeastern states of India also move towards Bangladesh and creates havoc. Annual death rate of TS is almost 0.09% in Bangladesh (2008).

Karmakar (2001) has studied on the spatio-temporal distribution the monthly and seasonal frequency of TS and the variability of TS days over Bangladesh during the pre-monsoon season using the data of 1961-2008.It was found that the mean TS days increases significantly from March to May and the mean monthly and seasonal TS days are maximum over Sylhet, Jashore, Faridpur, Rajshahi, Chattogram and Cox's Bazar regions having the highest frequency over Sylhet region. Robert *et al.* (2007) examined the changes in STS environment frequency during the 21stcentury caused by anthropogenically enhanced global radiative forcing. They opined that STS comprise an extreme class of deep convective clouds and produce high-impact weather such as destructive surface winds, hail, and tornadoes.

Mannan *et al.* (2016) explained that TS are frequent in the months of pre-monsoon, monsoon and post-monsoon seasons in Bangladesh. They also identified that the frequencies of TS are the highest in May followed by April during pre-monsoon months. They identified that TS frequencies are the maximum in the northeastern part of

Bangladesh. It decreases towards southwest. TS frequencies are less in the southeastern and northwestern parts of Bangladesh. TS are mostly associated with rainfall but there is very limited research on rainfall connected with TS. As such a comprehensive study of STS and its associated rainfall in Bangladesh during pre-monsoon season has been taken into consideration.

Mannan *et al.* (2017) studied on the heavy rainfall event with severe thunderstorm occurred on 31 March 2016 through numerical simulation using WRF-ARW model. It was found that the model fairly simulates the event. But the most suitable simulation has been found for Kain-Fritsch cumulus parameterization (CP) with WDM5 and Tiedtke with WDM5microphysics (MP) schemes. It was also found that the Standard Error of Estimation (SEE) for the predicted rainfall amounts for this case are the lowest and are 14.2 and 14.4 mm respectively for selected outer domain D1 and inner domain D2.

2. Methodology

For understanding the variability of TS days and TS frequency available record from 35 stations of Bangladesh Meteorological Department (BMD) are collected and utilized. To understand the thermodynamic features six selected STS recorded during 2017 are- (i) 10 March, (ii) 19 April, (iii) 22 April, (iv) 24 April, (v) 15 May and (vi) 30 May 2017. Thermodynamic indices of Showalter Index (SI), Lifted index (LI), K-Index (KI), Convective Available Potential Energy (CAPE) and Convective Inhibition Energy (CINE) and precipitable water (PW) on the event days, their preceding and subsequent days are collected and analyzed. The magnitudes of SI, LI, KI, CAPE, CINE and PW of the event days are compared with the selected average value found from the earlier studies.

Table 1: WRF Model and Domain Configuration

Dynamics	Non-hydrostatic
Number of domain	2
Central points of the domain	Central Lat.: 22.5°N, Central Lon.: 90.0°E
Horizontal grid distance	30 km and 10 km
Integration time step	60 s (for domain1 and domain 2)
Number of grid points	X-direction 100 points, Y-direction 104 points (for domain 1) X-direction 88 points, Y-direction 94 points (for domain 2)
Map projection	Mercator
Horizontal grid distribution	Arakawa C-grid
Nesting	Two way
Vertical co-ordinate	27 sigma levels up to 100 hPa
Time integration	3rd order Runge-Kutta
Spatial differencing scheme	6th order centered differencing
Initial conditions	Three-dimensional real-data (FNL: 1° × 1°)
Lateral boundary condition	Specified options for real-data
Top boundary condition	Gravity wave absorbing
Bottom boundary condition	Physical or free-slip
Diffusion and Damping	Simple Diffusion
Radiation scheme	Dudhia for short wave radiation/ RRTM long wave
Surface layer	Monin– Obukhov similarity theory scheme
Land surface parameterization	5 Layer Thermal diffusion scheme
PBL parameterization	Yonsei University Scheme (YSU) scheme

The event occurred on 10 March 2017 has been simulated using WRF-ARW (v3.8) model with the grid resolution of 30 km for outer domain and 10 km for inner domain. The coverage area of model domain is 12-30°N and 80-100°E. The topography in the model is obtained from USGS land covers data set. NCEP data are provided at every 6 hrs as initial and boundary conditions, CP and MP schemes are Kain-Fritsch and WDM5. The model is run for 24 hours starting from 0000 UTC of 10 March 2017. Details of the WRF Model set up are given in Table 1. The parameters of SI, LI, KI, CAPE, CINE and PW are extracted for understanding the dynamical feature of the system. Non-convective and convective rains are taken out for comparing with the observed rainfall. Simulated rainfall at BMD station locations for the selected CP and MP are compared with the observed rainfall at the same locations Root Mean Square Error (RMSE), Mean Absolute Error (MAE) and BIAS using equation 1(a-b).

$$RMSE = \sqrt{\frac{1}{N}\sum_{i=1}^{N}(F_i - O_i)^2} \quad \text{.....(1a)}$$

$$MAE = \frac{1}{N}\sum_{i=1}^{N}|F_i - O_i| \quad \text{.....(1b)}$$

Where, F_i denotes the forecast (or simulated) value and O_i denotes the observed value of any parameter.

3. Analysis

3.1 Thermodynamic condition

The magnitudes of thermodynamic indices considered under this study during the selected dates, previous as well as following days of the selected dates are given in Table 1. The indices are described as per dates of occurrence separately:

Table 1: Magnitudes of the indices at Dhaka on TS occurrence dates including previous and next day

Date	SI		LI		KI		CAPE		CINE		PW	
	00 UTC	12 UTC	00 UTC	12 UTC	00 UTC	12 UTC	00 UTC	12 UTC	00 UTC	12 UTC	00 UTC	12 UTC
09.03.17	-	-	-	-	-	-	-	-	-	-	-	-
10.03.17	0.93	-	-0.65	-	31.7	-	143.7	-	-133	-	36.36	
11.03.17	3.14	-	4.47	-	28.1	-	0	-	0	-	36.9	-
18.04.17	3.99	-1.17	-5.81	-3.58	9.3	37.0	1288	928.3	-99.9	-33	30.84	48.51
19.04.17	-0.68	4.83	-3.11	-2.94	34.1	31.0	969.3	733.9	-44.7	0	46.99	60.95
20.4.17	-	-3.8	-	-3.09	-	37.1	-	336.5		179		50.78
21.4.17	-2.94	-5.16	-4.19	-3.66	25.70	33.7	697.2	501.0	-101	-222	47.5	51.65
22.04.17	-3.8	-3.06	-2.17	1.55	35.7	41.5	228.3	0	-214	0	54.97	56.29
23.04.17	-3.95	-	0.59	-	37.6		20.16	-	-472		51.1	-
24.04.17	-4.25	-4.85	0.61	-0.46	38.0	37.5	0	8.51	0	-358	46.09	50.48
25.04.17	0.27	3.26	-3.54	-9.02	32.7	25.5	935.5	3775	-198	-52.4	43.42	42.48
14.04.17	5.09	-0.33	0.81	-2.40	27.1	36.7	25.97	2101	-1554	0.0	38.70	57.54
15.05.17	-2.14	-5.56	0.19	-5.28	36.7	34.3	0	1299	0	-41.6	51.08	49.67
16.05.17	4.15	-	1.44	-	31.4	-	0	-	0		41.98	-
29.05.17	-	-0.68	-	-4.82	-	38.2	-	1804	-	-9.6	-	72.2
30.05.17	1.27	-1.12	-0.53	-1.66	37.6	39.6	224.5	273.1	-106	0	65.71	73
01.06.17	-2.39	-	-4.66	-	39	-	1856	-	-15.4	-	66.77	-

a. 10 March 2017: SI, LI, CAPE were not favourable but KI and PW were favourable and their magnitudes were higher than the climatological average in the morning of the event day.

b. 19 April 2017: The magnitude of SI was negative from the afternoon of 18 April to morning of 19 April. But the magnitude of LI was negative during 18-19 April. KI was high during afternoon of 18-19 April. CAPE was slightly lower and CINE was also lower. PW was high during afternoon of 18-19 April.

c. 22 April 2017: The magnitude of SI was negative during morning of 21-22 April. But LI was negative during 21 April to afternoon of 22 April. KI was slightly high during afternoon of 21-22 April. CAPE was slightly lower but CINE was negative. PW was high during afternoon of 21-22 April. This situation indicates that all of the stability parameters (except CAPE) were supportive for the event.

d. 24 April 2017: The magnitude of SI was negative in the afternoon of 23-24 April but LI was negative on 24 April. KI was high on 24 April. CAPE and CINE were low. PW was high during morning of 24-25 April. The situation was suitable for the event.

e. 15 May 2017: The magnitude of SI was negative during afternoon of 14-15 May. But the magnitude of LI was negative during both afternoon of 14 and 15 May. KI was slightly high during morning of 15 May. CAPE was high

during the both afternoon of 14-15 May but CINE was lower. PW was high during afternoon of 14-15 May. This situation indicates that all of the stability parameters (except CAPE) were suitable for the event.

f. 30 May 2017: The magnitude of SI was negative during afternoon of 29-30 May 2017. But the magnitude of LI was negative during afternoon of 29-30 May. KI was high during afternoon of 29-30 May. CAPE was slightly high during the afternoon of 29 May but low on 30 May. On the other hand, CINE was also low. PW was high during afternoon of 29-30 May. This situation indicates that the stability situation (except CAPE) was favorable for the event.

3.1.1 Comparison with the climatological normal situation

The average magnitude of LI for the TS occurrence in Bangladeshis -0.2 (Yamane *et al.*, 2010) but LI is found much lower than this value (Fig. 1) for maximum numbers of the selected events. The magnitudes of LI are found negative for the events which occurred during afternoon at Dhaka station which indicates that lower troposphere was sufficiently unstable during these dates. But lower troposphere is found stable at 0000UTC during the occurrence dates. This situation indicates that though the lower troposphere was stable in the early hours of the day but it becomes unstable with the progress of time due to some other meteorological conditions as an essential condition for the event.

This situation can be resolved through numerical simulation. The average magnitude of SI during the days of TS in Bangladesh is 0.8 (Yamane *et al.*, 2010). Analysis reveals that the magnitudes of SI are close to zero during a few numbers of dates but it is much lower during other dates (Fig. 2). The magnitudes of SI are found negative for the events which occurred during afternoon period but it is found positive or close to zero during the dates in which TS occurred during early hours of the day. This situation indicates that lower troposphere was sufficiently unstable before the occurrence as it becomes stable after the event occurred. The average magnitude of KI during the days of TS is 27.6 (Yamane *et al.*, 2010) but the magnitude of KI is found larger than this in more numbers of days (Fig. 3).

The magnitudes of KI are also higher during morning and afternoon period. It indicates that the lower troposphere had sufficient moisture contents during these days. The average magnitude of CAPE is 1363 (Yamane *et al.*, 2010) but the CAPE is found lower than this (Fig. 4) in all of dates. This situation indicates that the signature of CAPE was not sufficient for the occurrence of TS but with the progress of the day CAPE evolved which was essential for the occurrence of TS. The average magnitude of CINE is 322 (Yamane *et al.*, 2010) but the CINE is found lower than this (Fig. 5) in all of the selected dates. This situation also depicts the stable condition of the lower troposphere.

Fig. 1: Comparison of observed LI during thunderstorm days with the average LI

Fig. 2: Comparison of observed SI during thunderstorm days with the average SI

Fig. 3: Comparison of observed KI during thunderstorm days with the average KI

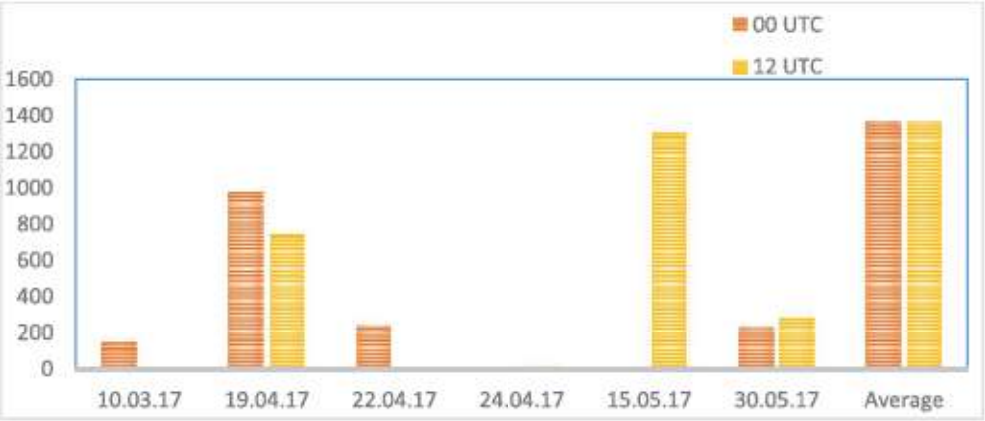

Fig. 4: Comparison of observed CAPE during thunderstorm days with the average CAPE

Fig. 5: Comparison of observed CINE during thunderstorm days with the average CINE

3.2. Rainfall associated with thunderstorm

On 10 March 2017, higher amounts of rainfalls were recorded over southeastern, south-central parts and their adjacent area. The highest amounts of rainfall of 90, 60 and 51 mm are recorded at Kutubdia, Cox's Bazar and Madaripur respectively.

On 19 April 2017, higher amounts of rainfalls were recorded over southeastern part and their adjacent area. The highest amounts of 72, 47 and 39 mm rainfall were recorded at Kutubdia, Cox's Bazar and Sandwip respectively.

On 22 April 2017, higher amounts of rainfalls were recorded over southwestern and southeastern parts and their adjacent areas. The highest amounts of 49, 46 and 38 mm rainfall were recorded at Mongla, Chandpur, Feni respectively.

On 24 April 2017, higher amounts of rainfalls were recorded over northeastern and adjoining central part. The maximum amounts of 25, 17 and 14 mm rainfall were recorded at Rajarhat, Sylhet and Gopalganj respectively.

On 15 May 2017, higher amounts of rainfalls are recorded over central part and its adjacent areas. The maximum amounts 90, 70 and 69 mm rainfall were recorded at Dhaka, Tangail and Ishurdi respectively.

On 30 May 2017, higher amounts of rainfalls were recorded over northeastern, southeasternparts and their adjacent areas. The maximum amounts of 177, 173 and 138mm rainfall were recorded at Netrokona, Chattogram and Sandwip respectively.

Spatial distribution of average rainfall recorded during these selected dates is depicted in Fig. 6. It indicates that central, northeastern and southeastern parts are most prone to rainfall associated with TS.

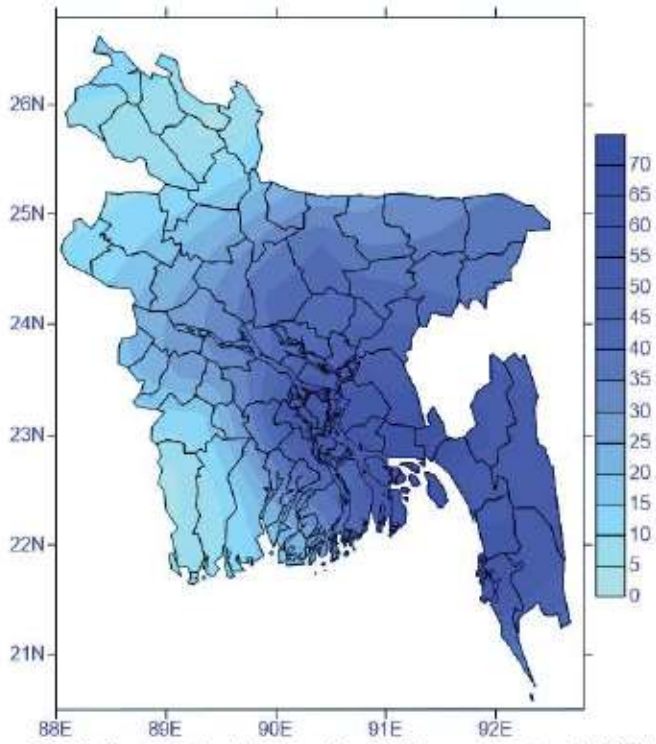

Fig. 6: Spatial distribution of rainfall associated with STS in Bangladesh during pre-monsoon season of 2017

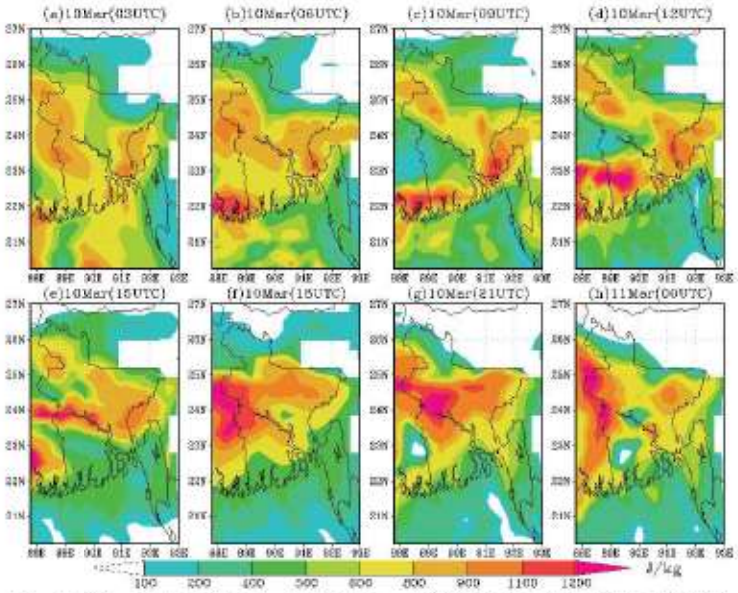

Fig. 7: Simulated CAPE at 925 hPa at (a) 0300, (b) 0600, (c) 0900, (d) 1200, (e) 1500, (f) 1800 (g) 2100 of 10 March 2017 and (h)0000 of 11 March 2017

3.3 Numerical Simulation

3.3.1 CAPE and CINE

Simulation reveals that quiet strong CAPE was over central Bangladesh and adjoining western part of Bangladesh during early hours of the day. The patches of CAPE shifted towards east over Bangladesh and at the same time its strength increased during late hours of the day. A strong signature of CAPE originated again over western part of Bangladesh in the early night of 10 March 2017, which then intensified, enlarged and moved eastwards during the remaining period of the day. The successive position of the CAPE field is depicted in Fig. 7.

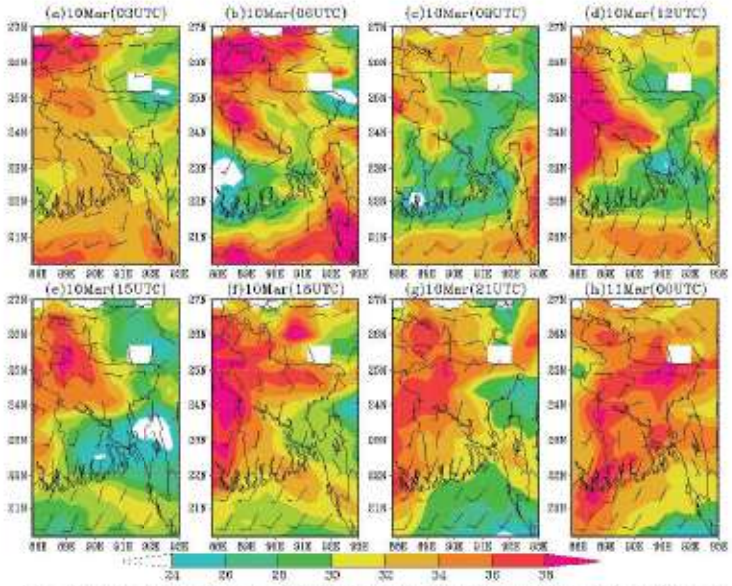

Fig. 8: KI at 925 hPa at (a) 0300, (b) 0600, (c) 0900, (d) 1200, (e) 1500, (f) 1800 (g) 2100 UTC of 10 Marchand (h) 0000 UTC of 11 March 2017

CINE and its spatio-temporal distribution depicts that the signature of CINE weakens over central Bangladesh and adjoining western part of Bangladesh during early hours of the day. The patches of strong CINE shifted towards east over Bangladesh and at the same time its strength decreased during late hours of the day. A strong signature of weak CINE originated again over western part of Bangladesh in the early night of 10 March 2017, it then weakened, enlarged and moved eastwards during the remaining period of the day. The behavour of CINEis found completely opposite of CAPE.

3.3.2 K Index, Total Totals Index, SWEAT Index, Maximum wind and Perceptible Water

Development of 3-hourly KI is depicted in Fig. 8. Signature of high KI value over northwestern part of Bangladesh is observed during morning hours of the day. But strong signature of KI is found to evolveover western part at 1200UTC which then shifted and enlarged and covered during the next successive hours of the day. The maximum magnitude of KI is found to vary between 36-40 Jkg^{-1} over the most intense KI zone.

Evolution of intense TTI is found over the northwestern part of Bangladesh in the beginning hours of the day. It is seen to expand, intensify and progressand covernorthern part during the remaining period of the day. The maximum TTI is found to reach 50 and it's above over northwestern and adjoining northern part of Bangladesh (Fig. 9).

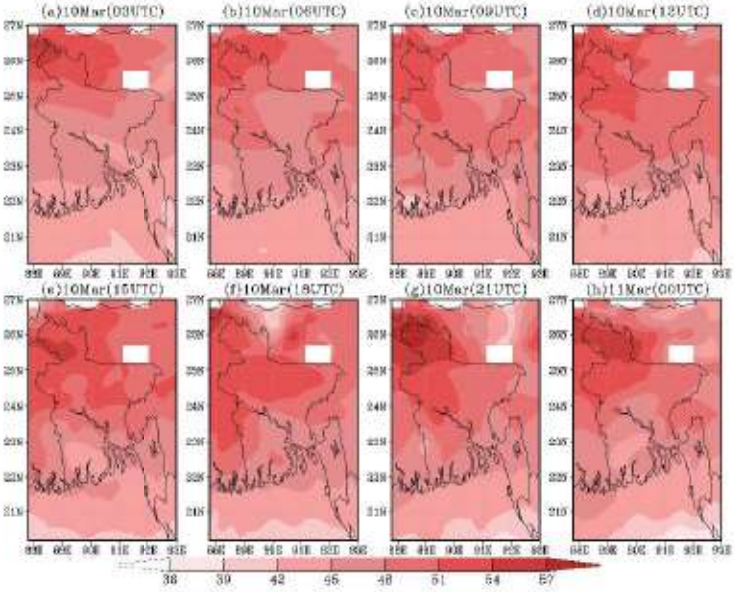

Fig. 9: TTI at (a) 0300, (b) 0600, (c) 0900, (d) 1200, (e) 1500, (f) 1800 (g) 2100 of 10 March and (h)0000 of 11 March 2017

Evolution of SWI and its spatial distribution is given in Fig. 10.

It is observed that the strong existence of SWI is observed first over northwestern part at 1500 UTC, it then expanded and strengthened over the same area. Strong signature of SWI is co-located over the simulated rainfall zone. Magnitude of SWI is found to lie with the range of 400-550 Jkg^{-1} over northwestern part of Bangladesh. Following the thermodynamic indices, model simulates high winds over Rangpur division at 03, 06, 12, 15, 21UTC with the

maximum wind speed of 25-30 km/hr. Signature of precipitable water (PW) is found to evolve over northern and southeastern parts. The patch of PW is found to move eastward during successive hours for domains D1 and D2 (Fig. 11).

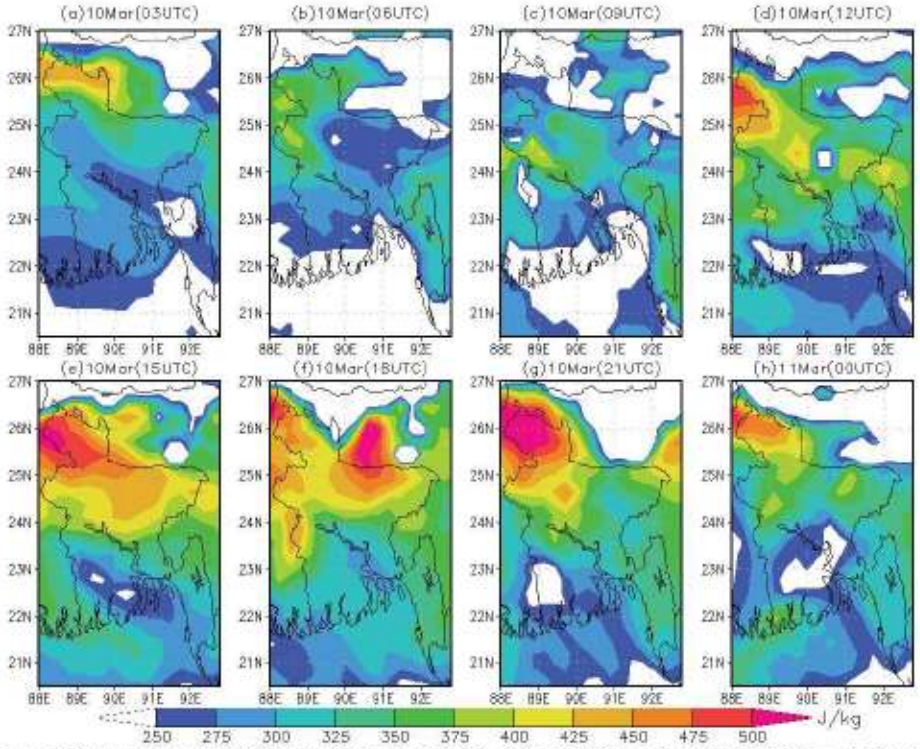

Fig. 10: Simulated SWEAT at (a) 0300, (b) 0600, (c) 0900, (d) 1200, (e) 1500, (f) 1800 (g) 2100 of 10 March 2017 and (h) 0000 of 11 March 2017

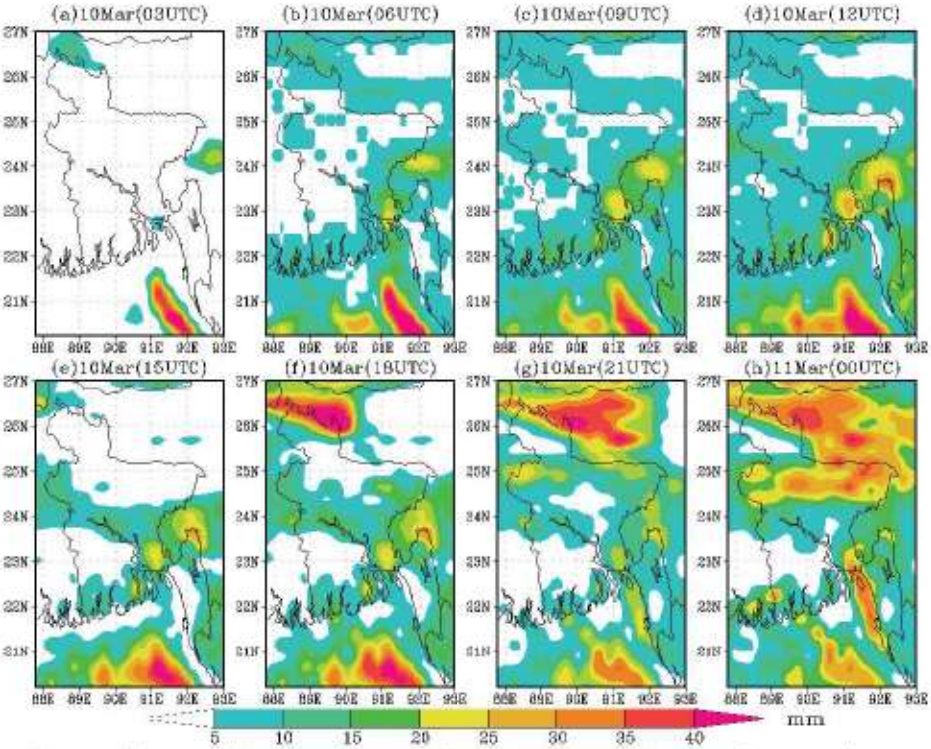

Fig. 11: PW at (a) 0300, (b) 0600, (c) 0900, (d) 1200, (e) 1500, (f) 1800 (g) 2100 of 10 March 2017 and (h) 0000 of 11 March 2017

3.3.3 Simulated rainfall

Model simulates strong signature of rainfall over Rajshahi, Mymensingh, Sylhet and coastal area of Chattogram divisions for both the domains D1 and D2 (Fig. 12). Location specific rainfalls for 42 rain gauge locations of BMD are collected from the simulation and found that RMSE are 19.9 and 21.3 mm for D1 and D2. But RMSE for the location specific model rainfall with the observed rainfall of 30 mm or more are 29.2 and 29.3 mm. Spatial distribution of deviation of rainfall shows that model rainfall is higher than observation over central to southern part of Bangladesh with the maximum deviation over central part for D1 (Fig. 13a). On the other hand simulated rainfalls are lower than observation over northwestern and adjoining northern part of Bangladesh (Fig. 13b). Similar pattern is found for D2 with slightly different deviation distribution.

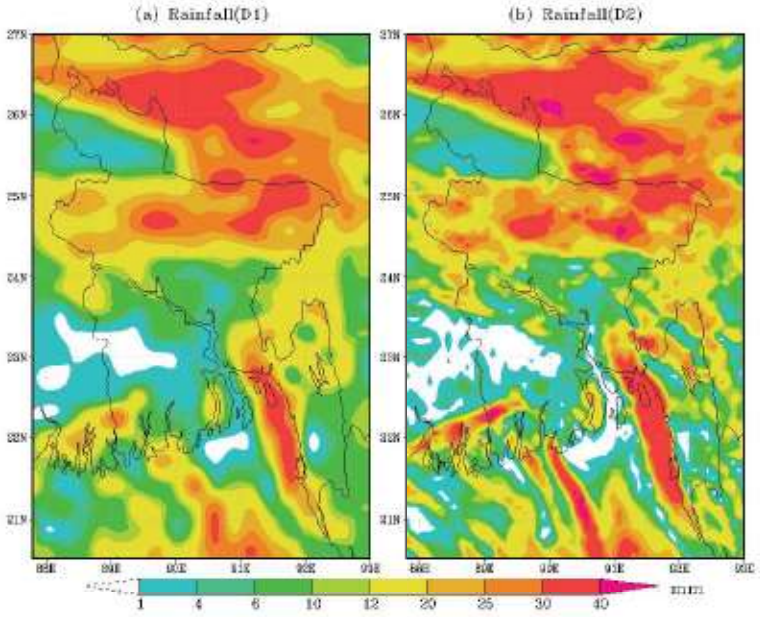

Fig. 12: Simulated rainfall for (a) D1 and (b) D2 during 10 March 2017

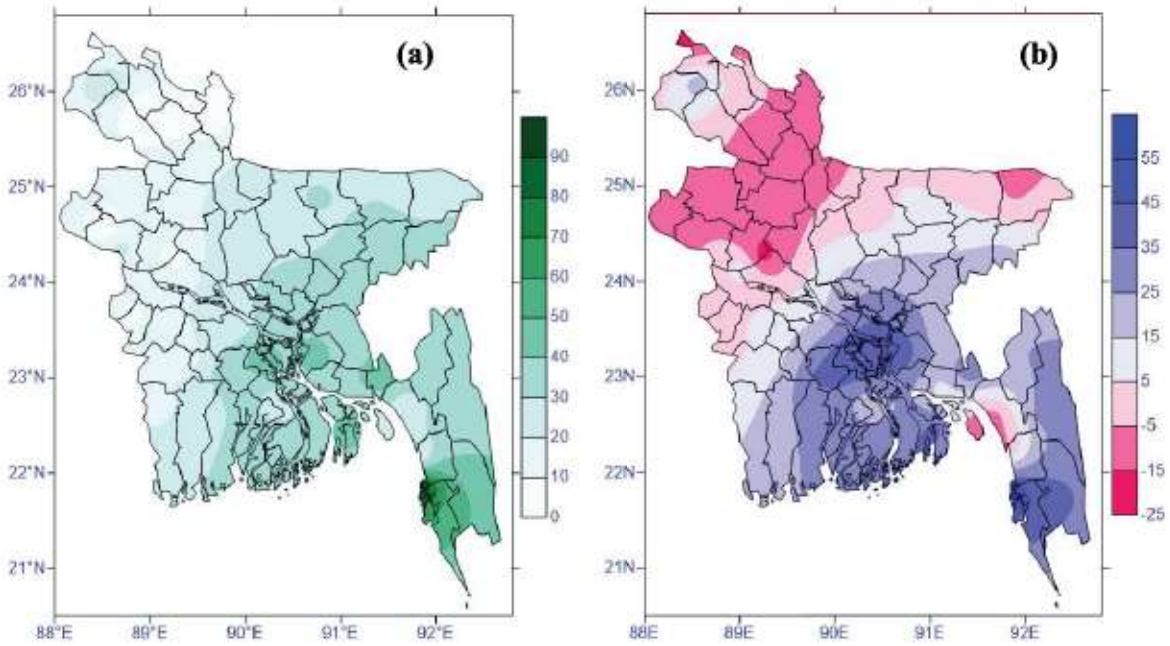

Fig. 13: Deviation of simulated rainfall for (a) D1 and (b) D2 domains during 10 March 2017

4. Conclusion

From this study the following conclusions can be drawn:

i. Atmospheric condition was stable in the morning hours but it became unstable in the afternoon period in the dates when TS occurs in the late hours of the day.

ii. The magnitude of LI, SI, KI were higher than average value though CAPE and CINE values were lower than average during the observed days in the afternoon. The magnitudes of PW were above 30 mm and accordingly high amounts of rainfall were recorded on the selected dates.

iii. The magnitudes of the thermodynamic indices recorded at 0000UTC are not always representing the instability condition of the day. They are sometimes limited with the time and location. The indices of LI, SI, KI, SWEAT, CAPE, CINE and PW are sometimes not representing signature of the occurrence of the events. Forecasters may miss the events following the magnitudes of the indices available at 0000UTC only. This situation may overcome following the evolvement of the indices further through numerical simulation.

iv. Model simulates the evolution of CAPE, KI, TTI, SWI and PW on 10 March 2017, which indicates that with the progress of the day all of these parameters evolved and became the favourable for TS occurrence with high amounts of rainfall.

v. Model simulates more rainfall than observation over central and southeastern part of Bangladesh but less rainfall than observation over northwestern part of Bangladesh. RMSEs of simulated rainfall at BMD station locations for D1 and D2 are 19.9 and 21.3 mm. But RMSEs of model rainfall with station rainfall of 30 mm or more are 29.2 and 29.3 mm.

References

Ali A, 1999: Climate change impacts and adaptation assessment in Bangladesh. Space Research and Remote Sensing Organization (SPARRSO), Agargaon, Sher-e Bangla Nagar, Dhaka 1207, Bangladesh, 12: 109–116.

Ferdousi N, Debsarma SK, Mannan M A and Sarker M. A., 2014: Impact of data assimilation in simulation of TS event over Bangladesh using WRF model, High impact weather events over the SAARC region, P35-48.

Gomes C, Kithil R, Ahmed M, 2006: Developing a lightning awareness program model third world based on American experience, Proc. of the 28thInt. Conference on Lightning Protection (ICLP), Kanasawa, Japan.

Gomes, C., M. A. F. Hussain, and K.R. Abeysinghe, 2006: Lightning accidents and awareness in South Asia: Experience in Sri Lanka and Bangladesh. 28th Intl. Conf. on Lightning Protection, Kanazawa, Japan, 1240-1243.

Karmaker, S., 2001: Climatology of thunderstorm days over Bangladesh during the pre-monsoon season, Bangladesh J. Sci. & Tech. 3(1), pp.103-122.

Mannan M. A., Chowdhury M. A. M, Karmakar, S., Ahmed, S. and Rahman, A. and Mondal, M. S. H., 2016b: Prediction of Heavy Rainfall in association with Severe Thunderstorm in Bangladesh during pre-monsoon Season, The Atmosphere, Bangladesh Meteorological Department, Dhaka, Bangladesh 6(1): 64-76.

Mannan M. A., Chowdhury M. A. M, Karmakar, S., Ahmed, S., 2017: Simulation of Heavy Rainfall in association with Severe Thunderstorm in Bangladesh during pre-monsoon season, The Journal of NOAMI, 34(1), 69-85, June 2017.

Yamane, Y., Hayashi, T., Dewan. A. M., and Akter, F, 2010: Severe local convective storms in Bangladesh: Part II. Environmental conditions, Atmospheric Research 95, pp. 407-418.

ISSN 2414-6056

DEW-DROP

Contents

Volume 5, Number 1, June 2018

Articles: